UNIVERSITÀ DEGLI STUDI DI TORINO

DIPARTIMENTO DI FISICA GENERALE "A. AVOGADRO"

DOTTORATO DI RICERCA IN FISICA

CICLO XVI

EFFECTS OF FRICTION AND POLYMERS ON 2D TURBULENCE

Tesi presentata da:

Dott. **Stefano Musacchio**

Tutor:

Prof. **Guido Boffetta**

Coordinatore del ciclo:

Prof. **Ezio Menichetti**

ANNI ACCADEMICI 2000/01 2001/02 2002/03

Contents

Introduction **7**

1 Introduction to turbulence **9**
1.1 Navier-Stokes equation 10
1.1.1 Reynolds number 11
1.1.2 Energy balance 12
1.1.3 Energy transfer 13
1.2 Phenomenology of the turbulent cascade 17
1.2.1 Kolmogorov K41 18
1.2.2 Intermittency 20
1.3 Two-dimensional turbulence 22
1.3.1 Vorticity equation in two dimensions 22
1.3.2 Conservation laws 23
1.3.3 Inverse energy cascade 25
1.3.4 Direct enstrophy cascade 27
1.3.5 Coherent vortices 28

2 Effects of friction in two-dimensional turbulence **29**
2.1 Origin of the friction term 30
2.2 Steepening of the energy spectrum 31
2.3 Analogies with the passive scalar problem 32
2.4 Passive scalar with finite lifetime 34
2.4.1 Chaotic advection 34
2.4.2 Chaotic advection and linear damping 36
2.4.3 Intermittency 37
2.4.4 Smooth-filamental transition 38
2.5 Lagrangian description of the vorticity cascade 39
2.5.1 Fluid trajectories and exit-times 39
2.5.2 Structure functions and scaling exponents 42
2.5.3 From active to passive problem 43
2.6 Numerical results 44

2.6.1 Steepening of the vorticity spectrum 45
2.6.2 Intermittency 45
2.6.3 Vorticity vs. passive scalar statistics 46
2.6.4 Scaling exponents and exit-time statistics 48
2.7 Summary 50

3 Polymer solutions: a brief introduction 53
3.1 Polymer dynamics in fluids 54
3.2 Dumbbell model 57
3.2.1 Coil-Stretch transition 59
3.3 Oldroyd-B model 60
3.3.1 Newtonian limit: viscosity renormalization 62
3.3.2 Energy balance 62
3.4 Fene-p 64
3.5 Drag reduction 65
3.6 Elastic turbulence 67

4 Two-dimensional turbulence of dilute polymer solutions 69
4.1 2D Oldroyd-B model 70
4.2 Passive polymers 70
4.2.1 Coiled state 71
4.2.2 Stretched state 74
4.3 Active polymers 75
4.3.1 Depletion of kinetic energy 77
4.3.2 Energy balance 78
4.3.3 Statistics of velocity fluctuations 78
4.3.4 Lagrangian chaos reduction 80
4.3.5 Decaying turbulence 81
4.3.6 Inverse energy cascade 82
4.4 Summary 84

Conclusions 87

A Lagrangian code for polymer dynamics 89
A.0.1 Hyperbolic regions 91
A.0.2 Elliptic regions 92
A.0.3 Neutral regions 93

Acknowledgments 101

Introduzione

In questa tesi viene presentata un'analisi degli effetti indotti dalla presenza di una forza di frizione lineare e dall'aggiunta di piccole quantità di polimeri sulle proprietà statistiche della turbolenza bidimensionale.

La prima parte della tesi riguarda gli effetti di una forza di frizione lineare sulla cascata diretta di enstrofia. Si mostra come la frizione causi un aumento della pendenza dello spettro di energia, e una forte intermittenza nella statistica delle fluttuazioni di vorticità a piccola scala.

Questi effetti possono essere previsti e quantificati per mezzo della statistica lagrangiana. In particolare mostrerò che la forza di frizione lineare riduce le proprietà statistiche della vorticità a piccola scala a coincidere con quelle di un campo scalare passivo con vita media finita trasportato dallo stesso flusso.

Le previsioni teoriche ottenute mediante l'approccio Lagrangiano sono state verificate per mezzo di simulazioni numeriche dell'equazione di Navier-Stokes e dell'equazione di avvezione-reazione per lo scalare passivo.

Nella seconda parte viene affrontato lo studio di soluzioni diluite di polimeri in due dimensioni per mezzo di un modello viscoelastico lineare (Oldroyd-B).

Nel caso passivo, ossia trascurando la reazione dei polimeri sul flusso, si dimostra che la distribuzione di probabilità dell'elongazione dei polimeri ha una coda a legge di potenza, la cui pendenza può essere calcolata a partire dalla statistica dei tempi di uscita lagrangiani.

Nel caso attivo mostrerò che l'energia cinetica del fluido è fortemente ridotta dalla reazione dei polimeri. Questo fenomeno va confontato con il caso tridimensionale, in cui viceversa l'energia cinetica del flusso medio risulta aumentata dalla presenza dei polimeri.

Il modello viscoelastico adottato fornisce una chiara spiegazione dell'origine della riduzione dell energia, che è stata osservata anche in esperimenti su pellicole di sapone.

Inoltre mostrerò che la presenza dei polimeri causa una forte riduzione del caos lagrangiano, e influenza il decadimento della turbolenza bidimensionale così come la cascata inversa di energia, che può venire completamente soppressa qualora l'elasticità dei polimeri sia sufficientemente elevata.

Le due parti della tesi sono strettamente collegate dai metodi utilizzati per studiare due differenti situazioni fisiche, che sono entrambe ricondotte al problema generale del trasporto di campi attivi, scalari o tensoriali. La descrizione lagrangiana del trasporto turbolento, che si è rivelata essere il più potente strumento per la comprensione del problema passivo, viene qui utilizzata per studiare due casi in cui le quantità trasportate sono attive, ossia hanno delle ripercussioni sul campo di velocità.

La tesi è organizzata in quattro capitoli. Il primo capitolo vuole essere una breve introduzione alla turbolenza pienamente sviluppata in due dimensioni. Riassumerò la fenomenologia di base, introducendo i concetti e la terminologia che verrano utilizzati nella tesi e sottolineando le principali differenze rispetto al caso tridimensionale.

Il secondo capitolo tratta degli effetti della frizione in turbolenza bidimensionale. Mostrerò l'analogia con il problema del trasporto di un campo scalare passivo con vita media finita, fornando una breve rassegna di recenti risultati ottenuti per questo problema, e mostrando come e sotto quali condizioni essi possano essere applicati al caso della vorticità in turbolenza bidimensionale in presenza di frizione. Presenterò quindi un confronto fra i risultati ottenuti per mezzo di simulazioni numeriche e le previsioni basate sulla statistica lagrangiana.

Nel terzo capitolo presento una breve introduzione alla fisica delle soluzioni diluite di polimeri, descrivendo alcuni dei fenomeni osservati negli esperimenti e introducendo il modello viscoelastico utilizzato nella tesi.

Il quarto capitolo contiene i risultati dello studio teorico e numerico delle soluzioni diluite di polimeri in due dimensioni.

Introduction

In this thesis I present an analysis of the effects induced by the presence of a linear friction force and by the addition of small quantities of polymers on the statistical properties of two-dimensional turbulence.

The first part of the thesis deals with the effects of a linear friction force on the direct enstrophy cascade. It is shown that friction produces a steepening of the energy spectrum, and a strong intermittency in the statistics of small-scale fluctuations of vorticity.

These effects can be predicted and quantified by means of Lagrangian statistics. In particular I will show that a linear friction force reduces the statistical properties of vorticity at small scale to coincide with those of a passive scalar field with finite lifetime transported by the same flow.

Theoretical predictions obtained within the Lagrangian approach are validated by the results of numerical simulations of Navier-Stoker equation and the advection-reaction equation for the passive scalar.

In the second part the study of two-dimensional dilute polymer solutions is addressed by means of a linear viscoelastic model (Oldroyd-B).

In the passive case, i.e. neglecting the feedback of polymers on the flow, it is shown that the probability distribution function of polymer elongation has a power law tail, whose slope can be predicted in terms of Lagrangian exit-time statistics.

In the active case I will show that the kinetic energy of the fluid is drastically reduced by the polymer back-reaction. This phenomenon should be contrasted with the three-dimensional case where, on the opposite, kinetic energy of the mean flow is enhanced by the presence of polymers.

The viscoelastic model adopted provides a clear explanation for the origin of energy suppression which has been observed also in soap-film experiments.

Moreover I will show that the presence of polymers causes a strong reduction of Lagrangian chaos, and influences the decay of two-dimensional turbulence as well as the inverse energy cascade, which can be completely

depleted for large enough polymer elasticity.

The two parts of the thesis are strictly connected by the methods used for studying the two different physical situations, which are both reduced to the general problem of transport of active scalar or tensorial fields. The Lagrangian description of turbulence transport, which has revealed as the most powerful tool for the comprehension of the passive problem is here used to study two cases where the transported quantities are active, i.e. they have a feedback on the velocity field.

The thesis is organized in four chapter. The first chapter is intended as a short introduction to fully developed turbulence in two dimensions. I will summarize the basic phenomenology, introducing the concepts and terminology that will be used in the thesis, and stressing the main differences with the three-dimensional case.

The second chapter deals with the effects of friction in two-dimensional turbulence. I will show the analogy with the problem of transport of a passive scalar field with finite lifetime, giving a short review of recent results for this problem, and showing how and under which condition they can be applied to the case of vorticity in two-dimensional turbulence with friction. Then I will present a comparison between the results obtained by means of numerical simulations and the prediction based on the Lagrangian statistics.

In the third chapter I provide a brief introduction to the physics of dilute polymer solution, describing some of the phenomena which have been observed in experiments and introducing the viscoelastic model adopted in this thesis.

The fourth chapter contains the results of the theoretical and numerical study of two-dimensional dilute polymers solutions.

Chapter 1

Introduction to turbulence

The complexity of turbulence has attracted for centuries the interest of scientists, philosophers and poets. Images and metaphors of turbulence of impetuous rivers and stormy seas are ubiquitous in literature, and the drawings and scripts of Leonardo da Vinci can be considered the earliest scientific studies on turbulence, which grasped some realistic details of the problem.

On the other hands, the interest for turbulence is clearly understandable because of its practical relevance in applications ranging from naval and aeronautical engineering to climate studies and weather forecast.

In the last century the works of L. Euler, L. M. H. Navier, G. G. Stokes, O. Reynolds, has given the basis of a research field which is still open nowadays. Even if the equations which rule the turbulent behavior are well known, a complete understanding of the matter is still lacking.

In this chapter I will present a short introduction to the basic concepts and phenomenology of the classical theory of turbulence, with a particular attention to the case of two-dimensional turbulence, stressing the differences and similarities with the three-dimensional case. The aim is not to provide a review of the matter which can be found in [1, 2, 3, 4, 5, 6], but just to introduce, for the sake of self-consistency, the terms and concepts that will be used in the thesis.

1.1 Navier-Stokes equation

The dynamics of an incompressible Newtonian fluid is determined by the celebrated Navier-Stokes equations (1823), supplemented by the incompressibility condition:

$$\partial_t \boldsymbol{u} + \boldsymbol{u} \cdot \nabla \boldsymbol{u} = -\frac{\nabla P}{\rho} + \nu \Delta \boldsymbol{u} + \boldsymbol{f} \tag{1.1}$$

$$\nabla \cdot \boldsymbol{u} = 0 \tag{1.2}$$

where P is the pressure, ρ is the density of the fluid, $\nu = \frac{\mu}{\rho}$ is its kinematic viscosity, and $\boldsymbol{f}$ represents the sum of the external forces per unit mass which sustain the motion.

Let us briefly describe the different terms in Navier-Stokes equation:

- $\boldsymbol{u} \cdot \nabla \boldsymbol{u}$ the inertial, or non-linear term which characterizes Navier Stokes equation, and is responsible for the transfer of kinetic energy in the turbulent cascade.

- $-\nabla P/\rho$ the pressure gradients which guarantee the incompressibility of the flow. In absence of external forces they are determined by the Poisson equation
$$\Delta p = -\rho \partial_i \partial_j u_i u_j \tag{1.3}$$
which is obtained taking the divergence of Eq. (1.1).

- $\nu \Delta \boldsymbol{u}$ the dissipative viscous term. It is originated by the Reynolds stresses of the Newtonian fluid, and it is proportional to the viscosity. It is the dominant term in the laminar regime.

The origin of Eqs. (1.1,1.2) is just the conservation of mass and momentum per unit volume:

$$\frac{\partial \rho}{\partial t} + \nabla \cdot (\rho \boldsymbol{u}) = 0 \tag{1.4}$$

$$\rho \frac{Du_i}{Dt} = f_i + \frac{\partial \mathbb{T}_{ij}}{\partial x_j} \tag{1.5}$$

where $\mathbb{T}$ is the stress tensor of the fluid, which for a Newtonian fluid is linear in the deformation tensor $e_{ij} = 1/2(\nabla_j u_i + \nabla_i u_j)$, and is given by [4]:

$$\mathbb{T}^N_{ij} = -P\delta_{ij} + \mu \left[(\nabla_j u_i + \nabla_i u_j) - \frac{2}{3} \nabla_k u_k \delta_{ij} \right] . \tag{1.6}$$

The incompressibility assumption is consistent until velocities smaller than speed of sound c_s in the fluid are considered. Since eventual density

fluctuations are swept away exactly as sound waves, for small value of the Mach number which measures the ratio between the typical velocities and the speed of sound in the considered fluid, the density can be assumed to be constant in time and space $\rho(\boldsymbol{x}, t) = \rho$ and the mass conservation (1.4) leads to the divergence-less condition on the velocity field $\nabla \cdot \boldsymbol{u} = 0$. It is common to assume the constant density to be equal to unity, or equivalently to consider dynamical quantities per unit mass of fluid. As an example we will often refer to the square modulus of velocity as kinetic energy.

Because of the presence of a non-linear term in Navier-Stokes equation, the space of its solutions does not have an affine structure, and consequently a generic solution can not be obtained as linear superposition of basic solutions. Moreover, a typical feature of turbulence is the presence of chaos, i.e. the Navier-Stokes equations display a strong sensitivity to initial conditions, which drastically reduces the interest for their exact solutions. For this reason the theory of turbulence has a statistical approach, trying to predict the statistical properties of the flow instead of searching a peculiar analytic solution.

1.1.1 Reynolds number

A measure of the non-linearity of Navier-Stokes equations is given by the Reynolds number

$$Re = \frac{UL}{\nu} \tag{1.7}$$

where L and U are respectively the typical length scale and velocity of the fluid, e.g. in a pipe flow L is the diameter of the pipe and U the mean velocity. It was introduced by Osborne Reynolds, who showed that a transition between laminar and turbulent flow occurs when the Re number reaches a critical value. Different geometries of the flow may change the critical Re number, but the transition is universally controlled by this adimensional parameter. The Reynolds number plays a fundamental role in turbulence, since it gives a dimensional estimate of the relative weight between the inertial term $\mathbf{u} \cdot \nabla \mathbf{u}$ and the viscous term $\nu \Delta \mathbf{u}$:

$$\frac{[\boldsymbol{u} \cdot \nabla \boldsymbol{u}]}{[\nu \Delta \boldsymbol{u}]} \sim \frac{UL}{\nu} \tag{1.8}$$

Because of its definition, the limit $Re \to \infty$ in which fully developed turbulence is achieved, can be rephrased as the zero-viscosity limit $\nu \to 0$.

1.1.2 Energy balance

The energy balance in absence of external forcing for Navier-Stokes equation follows from Eqs. (1.1,1.2). The total kinetic energy of the fluid is

$$E = \int d^3r \frac{1}{2}\rho|\boldsymbol{u}|^2 \tag{1.9}$$

and its temporal variation is

$$\begin{aligned} \frac{dE}{dt} &= \int d^3r \boldsymbol{u} \cdot \frac{\partial \boldsymbol{u}}{\partial t} \\ &= \int d\boldsymbol{r} \left[-u_i u_j \partial_j u_i - u_i \partial_i p + \nu u_i \partial_j \partial_j u_i\right] \end{aligned} \tag{1.10}$$

Assuming periodic boundary condition on a cubic volume of size L

$$\boldsymbol{u}(x+nL, y+mL, z+qL) = \boldsymbol{u}(x,y,z) \quad \forall x,y,z \in \mathbb{R} \forall n,m,q \in \mathbb{Z} \tag{1.11}$$

or null boundary condition on a volume V

$$\boldsymbol{u}|_{\partial V} = 0 \tag{1.12}$$

the first two terms in the integral vanishes and using the identity

$$\begin{aligned} (\nabla \times \mathbf{u}) \cdot (\nabla \times \mathbf{u}) &= (\epsilon_{ijk}\partial_j u_k)(\epsilon_{ilm}\partial_l u_m) \\ &= \partial_j(u_k \partial_j u_k) - \partial_j \partial_k (u_j u_k) - u_k \partial_j \partial_j u_k \end{aligned} \tag{1.13}$$

one gets

$$\frac{dE}{dt} = \nu \int d^3r \rho \boldsymbol{u} \Delta \boldsymbol{u} = -\nu \int d^3r \rho (\nabla \times \boldsymbol{u})^2 = -\nu \int d^3r \rho |\boldsymbol{\omega}|^2 \tag{1.14}$$

where we have have introduced the *vorticity* of the fluid $\boldsymbol{\omega} = \nabla \times \boldsymbol{u}$. Defining the total *enstrophy* as

$$Z = \int d^3r \frac{1}{2}\rho |\nabla \times \boldsymbol{u}|^2 \tag{1.15}$$

the energy balance reads:

$$\frac{dE}{dt} = -2\nu Z \tag{1.16}$$

which shows that in absence of external forcing and for $\nu = 0$ the kinetic energy is conserved by the dynamics, i.e. it is an inviscid invariant. On the contrary in the limit $\nu \to 0$ the energy dissipation rate does not vanish, but reaches a constant value [7]:

$$\lim_{\nu \to 0} 2\nu Z \equiv \epsilon \tag{1.17}$$

This phenomenon is known as *dissipative anomaly*, and implies that in the limit $\nu \to 0$ the total enstrophy must grow as $Z \sim \nu^{-1}$ to compensate the decreasing viscosity. The unbounded growth of enstrophy in three dimensions is the physical origin of the dissipative anomaly, and it is possible because of the *vortex stretching*, which produces diverging velocity gradient in the limit $Re \to \infty$.

1.1.3 Energy transfer

As shown by the global energy balance (Eq. 1.16) the non-linear term in Navier-Stokes equation does not change the total kinetic energy. Nevertheless it plays a fundamental role in turbulence, because it is responsible for the energy transfer between different modes which is the origin of the turbulent cascade. To describe how it is involved in the energy transfer it is worthwhile to consider the energy balance in Fourier space. For the sake of simplicity we will consider the infinite volume limit, in which the fluid is supposed to fill the entire space, and the Fourier transform reads

$$u_\alpha(\boldsymbol{k}) = \frac{1}{(2\pi)^3} \int d^3x e^{-i\boldsymbol{k}\cdot\boldsymbol{x}} u_\alpha(\boldsymbol{x}) \tag{1.18}$$

and its inverse is

$$u_\alpha(\boldsymbol{x}) = \int d^3k e^{i\boldsymbol{k}\cdot\boldsymbol{x}} u_\alpha(\boldsymbol{k}) \tag{1.19}$$

The reality condition on the velocity fields $u^*_\alpha(\boldsymbol{x}) = u_\alpha(\boldsymbol{x})$ in Fourier space reads $u^*_\alpha(\boldsymbol{k}) = u_\alpha(-\boldsymbol{k})$, and the derivatives became multiplicative operators ($\nabla \to i\boldsymbol{k}$), thus the incompressibility assumption is written as $\boldsymbol{k}\cdot\boldsymbol{u} = 0$. In Fourier space Navier-Stokes equation has the form:

$$\begin{aligned} \frac{\partial u_\alpha(\boldsymbol{k})}{\partial t} &= -i \int d^3p \; (k_\beta - p_\beta) u_\beta(\boldsymbol{p}) u_\alpha(\boldsymbol{k}-\boldsymbol{p}) + \\ &\quad + i\frac{k_\alpha}{k^2} \int d^3p \; p_\gamma (k_\beta - p_\beta) u_\beta(\boldsymbol{p}) u_\gamma(\boldsymbol{k}-\boldsymbol{p}) + \\ &\quad - \nu k^2 u_\alpha(\boldsymbol{k}) \end{aligned} \tag{1.20}$$

where it is still possible to distinguish the inertial term, the pressure term and dissipative term, while the forcing has been omitted. The constant density has been fixed to $\rho = 1$.

Using the incompressibility and the symmetry of the integrals for $(\boldsymbol{p}, \boldsymbol{k}-\boldsymbol{p}) \to (\boldsymbol{p}-\boldsymbol{k}, \boldsymbol{p})$ it is possible to rewrite Eq. (1.20) as

$$\left(\frac{\partial}{\partial t} + \nu k^2\right) u_\alpha(\boldsymbol{k}) = -i\left(k_\beta \delta_{\alpha\gamma} - \frac{k_\alpha k_\beta k_\gamma}{k^2}\right) \int d^3p \; u_\beta(\boldsymbol{p}) u_\gamma(\boldsymbol{k}-\boldsymbol{p}) \tag{1.21}$$

Introducing the tensors

$$P_{\alpha\beta}(\boldsymbol{k}) = \delta_{\alpha\beta} - \frac{k_\alpha k_\beta}{k^2} \tag{1.22}$$

$$P_{\alpha\beta\gamma}(\boldsymbol{k}) = k_\beta P_{\alpha\gamma}(\boldsymbol{k}) + k_\gamma P_{\alpha\beta}(\boldsymbol{k}) \tag{1.23}$$

Navier-Stokes equation can be written in Fourier space as:

$$\left(\frac{\partial}{\partial t} + \nu k^2\right) u_\alpha(\boldsymbol{k}) = -\frac{i}{2} P_{\alpha\beta\gamma}(\boldsymbol{k}) \int d^3p \; u_\beta(\boldsymbol{p}) u_\gamma(\boldsymbol{k}-\boldsymbol{p}) \tag{1.24}$$

Let's now introduce some notations. The two-point correlation function is defined as

$$Q_{\alpha\beta}(\boldsymbol{r}) = \langle u_\alpha(\boldsymbol{x}) u_\beta(\boldsymbol{x}+\boldsymbol{r}) \rangle \tag{1.25}$$

where $\langle \ldots \rangle$ stands for the average over the volume V $\langle f(\boldsymbol{x}) \rangle = \frac{1}{V} \int_V d^3x f(\boldsymbol{x})$. Its Fourier transform is

$$S_{\alpha\beta}(\boldsymbol{k}) = \frac{1}{(2\pi)^3} \int d^3x e^{-i\boldsymbol{k}\cdot\boldsymbol{x}} Q_{\alpha\beta}(\boldsymbol{r}) \tag{1.26}$$

and the correlation function in Fourier space reads

$$\langle u_\alpha(\boldsymbol{k}) u_\beta(\boldsymbol{k}') \rangle = \delta(\boldsymbol{k}+\boldsymbol{k}') S_{\alpha\beta}(\boldsymbol{k}) \tag{1.27}$$

The assumption of isotropy imposes for the tensor $S_{\alpha\beta}$ the form

$$S_{\alpha\beta}(\boldsymbol{k}) = A(k) k_\alpha k_\beta + B(k) \delta_{\alpha\beta} \tag{1.28}$$

where A and B are function of the modulus $k = |\boldsymbol{k}|$. Multiplying Eq. (1.27) by k_β and using incompressibility one gets $B(k) = -k^2 A(k)$, which substituted in Eq. (1.28) leads to

$$S_{\alpha\beta}(\boldsymbol{k}) = P_{\alpha\beta}(\boldsymbol{k}) B(k) \tag{1.29}$$

The energy spectrum is defined as the integral of the square modulus of velocity over a shell with fixed modulus k in Fourier space:

$$E(k) = \frac{1}{2} \int k^2 d\Omega_k |\boldsymbol{u}(\boldsymbol{k})|^2 \tag{1.30}$$

and the total energy is its integral $E = \int_0^\infty dk \; E(k)$. By definition $S_{\alpha\alpha}(\boldsymbol{k}) = \langle |\boldsymbol{u}(\boldsymbol{k})|^2 \rangle$, but from Eq. (1.29) $S_{\alpha\alpha}(\boldsymbol{k}) = 2B(k)$, thus the following relation holds

$$B(k) = \frac{1}{4\pi k^2} E(k) \tag{1.31}$$

which gives the relation between the energy spectrum and the Fourier transform of two-point correlation function:

$$S_{\alpha\beta}(\boldsymbol{k}) = \frac{E(k)}{4\pi k^2} P_{\alpha\beta}(\boldsymbol{k}) \tag{1.32}$$

The temporal derivative of the two-point correlation function is obtained from Navier-Stokes equation as

$$\begin{aligned}\left(\frac{\partial}{\partial t} + 2\nu k^2\right) S_{\alpha\beta}(\boldsymbol{k}) &= -\frac{i}{2} P_{\alpha\rho\sigma}(\boldsymbol{k}) \int d^3p\; T_{\beta\rho\sigma}(-\boldsymbol{k}, \boldsymbol{p}) \\ &\quad -\frac{i}{2} P_{\beta\rho\sigma}(-\boldsymbol{k}) \int d^3p\; T_{\alpha\rho\sigma}(\boldsymbol{k}, \boldsymbol{p})\end{aligned} \tag{1.33}$$

where has been introduced the three-point correlation function

$$\langle u_\alpha(\boldsymbol{k}) u_\beta(\boldsymbol{k}') u_\gamma(\boldsymbol{k}'') = \delta(\boldsymbol{k} + \boldsymbol{k}' + \boldsymbol{k}'') T_{\alpha\beta\gamma}(\boldsymbol{k}, \boldsymbol{k}') \tag{1.34}$$

The energy balance is obtained from Eq. (1.33) remembering the relation (1.32) between the energy spectrum and the two-point correlation function. Using the antisymmetry $P_{\alpha\beta\gamma}(-\boldsymbol{k}) = -P_{\alpha\beta\gamma}(\boldsymbol{k})$ and the reality condition $T_{\alpha\beta\gamma}(-\boldsymbol{k}, \boldsymbol{p}) = T^*_{\alpha\beta\gamma}(\boldsymbol{k}, -\boldsymbol{p})$ on gets

$$\left(\frac{\partial}{\partial t} + 2\nu k^2\right) E(k) = T(k) \tag{1.35}$$

where has been introduced the *energy transfer* $T(k)$:

$$T(k) = -4\pi k^2 k_\rho Im \left\{ \int d^3p\; T_{\sigma\rho\sigma}(\boldsymbol{k}, \boldsymbol{p}) \right\} \tag{1.36}$$

Defining the *enstrophy spectrum* as:

$$Z(k) = \frac{1}{2} \int k^2 d\Omega_k |\boldsymbol{\omega}(\boldsymbol{k})|^2 = k^2 E(k) \tag{1.37}$$

and restoring the external force $\boldsymbol{f}$ in Navier-Stoked equation, the energy balance can be rewritten as

$$\partial_t E(k) = -2\nu Z(k) + T(k) + F(k) \tag{1.38}$$

where $F(k)$ is the injection energy spectrum:

$$F(k) = \int k^2 d\Omega_k \boldsymbol{u}(\boldsymbol{k}) \cdot \boldsymbol{f}(\boldsymbol{k}) \tag{1.39}$$

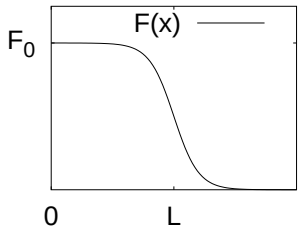

If the external forcing is a Gaussian process δ-correlated in time, whose statistic is determined by the correlation $\langle f_i(\boldsymbol{x},t)f_j(\boldsymbol{x'},t')\rangle = F(|\boldsymbol{x}-\boldsymbol{x'}|)\delta_{ij}\delta(t-t')$, the input of energy is flow-independent, i.e, the injection energy spectrum $F(k)$ is uniquely determined by the statistics of the forcing. In the case of a large scale forcing, with a forcing correlation length L such that

$$F(x) \simeq F_0 \quad for \quad x < L \tag{1.40}$$

$$F(x) \simeq 0 \quad for \quad x > L \tag{1.41}$$

the injection spectrum will dominate the energy balance at small wave-numbers $k \sim k_f \sim 1/L$. On the contrary the viscous dissipation, being proportional to $\nu Z(k) = \nu k^2 E(k)$ will give strong contribution at large wave-numbers, where k^2 is large. In the intermediate range of wave-numbers, where both injection and dissipation of energy are negligible, the dominant term in Eq. (1.38) is the energy transfer $T(k)$. In this *inertial range* the energy is conserved and transferred by triadic interaction between modes with wave-numbers such that $\boldsymbol{k}+\boldsymbol{k'}+\boldsymbol{k''} \simeq 0$.

Equation (1.24) for velocity involves the two-point correlation function, and Equation (1.33) for the two-point correlation function requires the tree-point one. It is easy to understand that the presence of a quadratic term in Navier-Stokes equation reproduces this *closure problem* at every order, i.e. the equation for the n-point correlation function will require the $n+1$ one. During the last fifty years several closures have been proposed, i.e. assumptions on the statistics of velocity which allow to obtain a closed set of equations for the correlation functions, from the simplest Quasi-Normal closure in which the fourth-order moments of velocity distribution are expressed in term of the second-order ones, in the same way of what happens for a Gaussian variable, to the Eddy-Damped-Quasi-Normal closure proposed by Orszag [8].

1.2 Phenomenology of the turbulent cascade

The basic phenomenology of turbulence can be recovered from a simple dimensional analysis of Navier-Stokes equations, using the image of the *turbulent cascade* proposed by Richardson [9].

The kinetic energy is supposed to be injected by an external forcing which sustains the motion of large scale eddies. This structures are deformed and stretched by the fluid dynamics, until they break into smaller eddies, and the process is repeated such that energy is transported to smaller and smaller structures. Finally at small scales the kinetic energy is dissipated by the viscosity of the fluid. The whole process of transport of energy from the large scale of injection to the small dissipative scale, through the hierarchy of eddies is known as turbulent cascade. It is worthwhile to remember that the eddies must not be thought as real vortices, but just as a metaphoric description of the triadic interaction between modes which has been formally presented in the previous section.

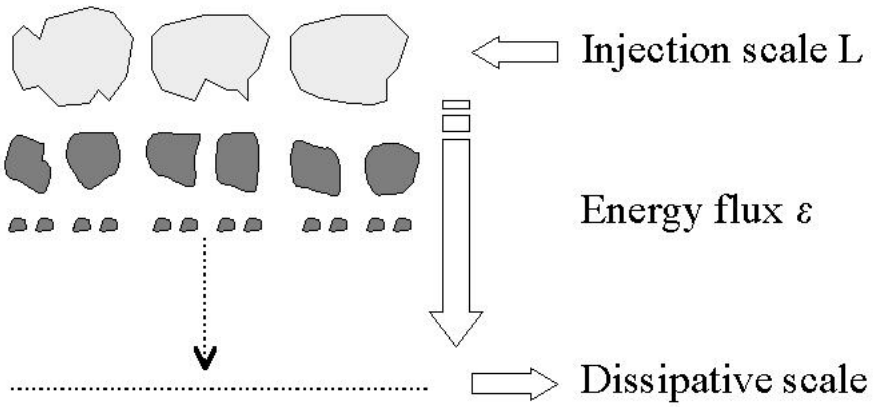

A dimensional analysis of the different terms of Navier-Stokes equation provides an estimate for the time required to transfer energy from an eddy of size ℓ to smaller eddies $\tau_\ell \sim \ell/u_\ell$, where u_ℓ is the rms velocity fluctuation on the scale ℓ, and the time required to dissipate the energy contained in the same eddy by the viscous term: $\tau_\ell^{diss} \sim \ell^2/\nu$.

Three different range of scales can thus be identified:

Injective range which corresponds to the large scales where the forcing injects the energy.

Inertial range where the time required for energy transfer is shorter than the dissipative time $\tau_\ell << \tau_\ell^{diss}$ and the energy is thus conserved and transported to smaller scales.

Dissipative range where the energy dissipation overcomes the transfer and the cascade is stopped.

The hypothesis of a statistically steady state for the turbulent cascade requires a constant energy flux $\Pi(\ell)$ in the inertial range, i.e. a constant rate of energy transfer that must be equal to the energy dissipation rate ϵ:

$$\Pi(\ell) \sim \frac{E(\ell)}{\tau_\ell} \sim u_\ell^2 \frac{u_\ell}{\ell} = \epsilon \, . \tag{1.42}$$

The above relation determines the Kolmogorov scaling for velocities and characteristic times:

$$u_\ell \sim \epsilon^{1/3} \ell^{1/3} \tag{1.43}$$

$$\tau_\ell \sim \epsilon^{-1/3} \ell^{2/3} \tag{1.44}$$

The border between the inertial and dissipative range is identified by the *Kolmogorov scale* η, where the dissipative and transfer times are equal $\tau_\ell = \tau_\ell^{diss}$:

$$\eta \sim \epsilon^{-1/4} \nu^{3/4} \tag{1.45}$$

Below the Kolmogorov scale, the viscous linear term dominates the evolution of the fluid, and the resulting velocity field is smooth and differentiable.

1.2.1 Kolmogorov K41

The naive picture drawn above can be formally stated within the $K41$ theory in term of the scaling properties of the *Structure functions*:

$$S_p(\ell) \equiv \langle (\delta u_\ell)^p \rangle \tag{1.46}$$

which are defined as the moments of the distribution of longitudinal velocity increments $\delta u_\ell(\boldsymbol{x}) \equiv [\boldsymbol{u}(\boldsymbol{x}+\boldsymbol{\ell}) - \boldsymbol{u}(\boldsymbol{\ell})] \cdot \boldsymbol{\ell}$.

The longitudinal velocity increments are easily achievable in experiments, e.g with hot wire anemometry. Let's suppose to have a velocity field $\boldsymbol{u}$ which can be decomposed in a mean flow $\boldsymbol{U} = (U, 0, 0)$ and a turbulent fluctuating part $\boldsymbol{u}$' = $\boldsymbol{u}$ - $\boldsymbol{U}$ whose intensity is assumed to be small compared with the mean flow $\langle |\boldsymbol{u}'|^2 \rangle^{1/2} \ll U$. By putting an hot wire perpendicular to the mean flow, let's say in the z direction, and measuring its resistance which is reduced because of the cooling due to the flow, it is possible to obtain the time series of the velocity integrated in the direction of the wire, i.e.

$$u_N = [(u_x' + U)^2 + u_y'^2]^{1/2} = U[1 + \frac{u_x'}{U} + O(\frac{u'^2}{U^2})] \tag{1.47}$$

where it has been supposed that amplitudes of fluctuations in the two direction perpendicular to the wire are of the same order $u'_y \sim u'_x$. Within Taylor's hypothesis, i.e. assuming that the turbulent velocity field for short time delay τ is almost frozen and it is simply transported through the wire by the fast mean flow $\boldsymbol{U}$, the time series $u'_x(t)$ can be considered as a space series

$$u'_x(x, t+\tau) = u'_x(x - U/\tau, t) \tag{1.48}$$

allowing to obtain the longitudinal structure function.

The basic assumption of the Kolmogorov theory is the *Similarity Hypothesis*. Kolmogorov's hypothesis assumes that if the inertial range is large enough, the influence of the large scale forcing and the small scale viscous dissipation can be neglected, and the scale invariance of Navier-Stokes equation in the inviscid limit:

$$t, \boldsymbol{r}, \boldsymbol{u} \mapsto \lambda^{1-h} t, \lambda \boldsymbol{r}, \lambda^h \boldsymbol{u} \quad \lambda \in \mathbb{R}_+, h \in \mathbb{R} \tag{1.49}$$

is recovered by the turbulent velocity field in a statistical sense. The velocity fluctuations on scale ℓ within the inertial range are supposed to be self-similar

$$\delta u_{\lambda \ell} \sim \lambda^h \delta u_\ell \tag{1.50}$$

i.e. their probability distribution are supposed to be identical once they are rescaled according to the scaling exponent h, and the structure functions in the limit $Re \to \infty$ are expected to display a power law behavior

$$S_p(\ell) = \langle (\delta u_\ell)^p \rangle \sim \ell^{hp} \tag{1.51}$$

Starting from the Karman-Howarth-Monin relation [1] Kolmogorov derived an exact result for the third order structure function, the famous

Kolmogorov's four-fifths law *In the limit of infinite Reynolds number the third order (longitudinal) structure function of homogeneous isotropic turbulence, evaluated for increments ℓ small compared to the integral scale, is given in terms of the mean energy dissipation per unit mass ϵ by*

$$S_3(\ell) \equiv \langle (\delta u_\ell)^3 \rangle = -\frac{4}{5} \epsilon \ell \tag{1.52}$$

The four-fifths law allows to fix the value of the scaling exponent $h = 1/3$ and together with the scaling hypothesis for the structure functions leads to the Kolmogorov scaling law:

$$S_p(\ell) \sim C_p \epsilon^{p/3} \ell^{p/3} \tag{1.53}$$

and to the Kolmogorov energy spectrum

$$E(k) \equiv 2\pi k \langle |\hat{\boldsymbol{u}}(\boldsymbol{k})|^2 \rangle = C\epsilon^{2/3} k^{5/3} \, . \tag{1.54}$$

A Kolmogorov energy spectrum has been observed in many different physical situations, from the experiments in tidal channel [10] which gave the first confirmations of Kolmogorov's theory, to recent measurements in wind-tunnel experiments[11].

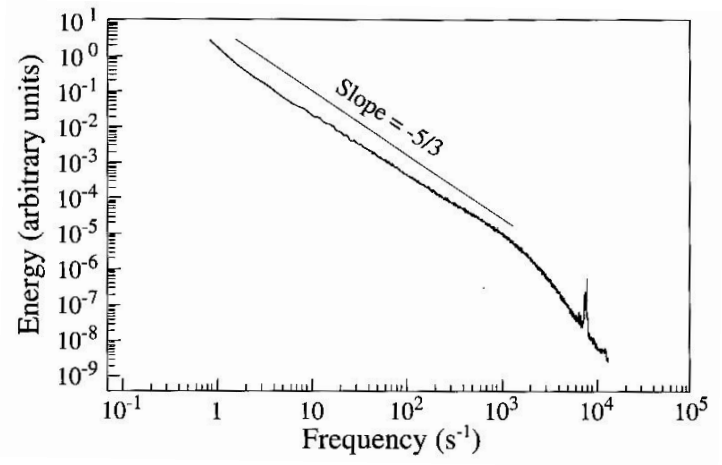

Figure 1.1: Kolmogorov's energy spectrum in the S1 wind tunnel ONERA [11]

1.2.2 Intermittency

The basic assumption of Kolmogorov K41 theory is the self-similarity of turbulent flow. Indeed experimental data [12, 13] shows that the probability distribution function (pfd) of velocity increments are roughly Gaussian at large scales, but when small scales are considered, the tails of the distributions depart from the Gaussian behavior, and events larger than the standard deviation have a larger probability to occur than in the Gaussian case.

This anomaly is confirmed by time series of turbulent velocities, which appear to be roughly self similar, but once they are high-pass filtered reveals an intermittent behavior, i.e. there is an alternation of periods of quiescence and periods of intense fluctuations [5]. Within the Taylor's hypothesis this is equivalent to state that on small scales the statistic of velocity fluctuations is strongly intermittent.

A measure of the intermittency is given by the *flatness*:

$$F(\ell) = \frac{S_4(\ell)}{(S_2(\ell))^2} = \frac{\langle (\delta u_\ell)^4 \rangle}{\langle (\delta u_\ell)^2 \rangle^2} \tag{1.55}$$

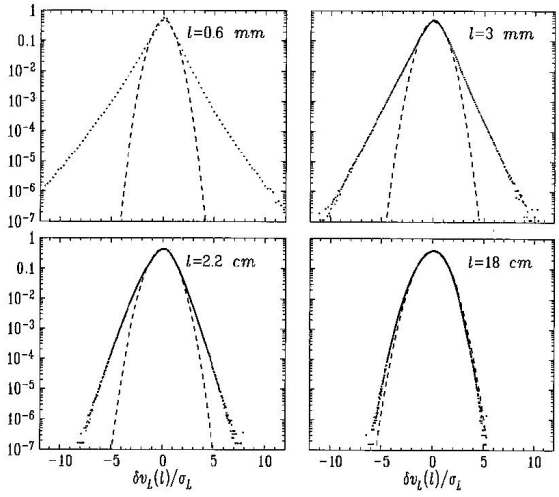

Figure 1.2: Probability distribution function $\sigma_\ell P(\delta u_\ell)$ of longitudinal velocity increments at different scales ℓ normalized with their standard deviations $\sigma_\ell = \langle \delta u_\ell^2 \rangle^{1/2}$. Experiments by Herweijer and Van de Water [1995]

Since the fourth order moment receives contributions from the tails of the pdf, the flatness gives a measure of how frequent are the events larger than the standard deviation. While the flatness of turbulent velocity fluctuations on large scale is close to the Gaussian value $F = 3$, it grows on small scale, as a consequence of the non-similarity of pdf's of fluctuations at different scales.

Measurements of the high order structure function[11] have shown that a power law behavior is indeed observable,

$$S_p(\ell) = \langle (\delta u_\ell)^p \rangle \ell^{\zeta_p} \tag{1.56}$$

but the scaling exponents differ from the dimensional $K41$ prediction $\zeta_p = p/3$.

In the multifractal approach [14], instead of a global scale-invariance, a local scale-invariance is assumed, so that the scaling exponent h of the velocity field can assume a whole range of different values, with a probability determined by the dimension $D(h)$ of the fractal set with a given exponent h. The scaling exponents of the structure function of order p are obtained as Legendre transform of the fractal dimension $D(h)$:

$$\zeta_p = \inf_h [ph + 3 - D(h)] \tag{1.57}$$

1.3 Two-dimensional turbulence

The study of two-dimensional incompressible flows at high Reynolds numbers presents several reasons of interest. A principal reason is provided by its relevance for geophysics. Indeed, the intermediate-scale dynamics of oceans and atmosphere, because of the combined effects of their stratification and the earth's rotation, can be roughly described as a two-dimensional flow. An other reason comes from plasma physics, where the presence of a strong mean magnetic field can confine the turbulent motions of plasma in the plane perpendicular to the magnetic field, and again the dynamics can be described by two-dimensional magneto-hydrodynamics (2D MHD) [15].

The classical theory of two-dimensional turbulence originates from the works of Batchelor, Kraichnan and Leith [16, 17, 18], which showed that the conservation of vorticity along the streamlines which occurs in two dimensions, produces radical changes in the behavior of turbulence.

Far from being a simplified version of the three-dimensional problem, two-dimensional turbulence presents a rich panorama of new phenomena, like the formation of coherent vortices from an initially disordered "sea" of vorticity which have attracted a large interest.

Finally, Navier-Stokes equation in two dimensions has the appealing feature to be less demanding on a computational level than the three-dimensional case, allowing to reach relatively high Re numbers in direct numerical simulation (DNS).

1.3.1 Vorticity equation in two dimensions

In two dimensions, the incompressible velocity field $\boldsymbol{u}$ can be expressed in terms of the *stream-function* ψ as:

$$\boldsymbol{u} = (\partial_y \psi, -\partial_x \psi) \tag{1.58}$$

The vorticity field, defined as the curl of velocity, $\boldsymbol{\omega} = \nabla \times \boldsymbol{u}$, in two dimensions has only one non-zero component which is orthogonal to the plane of velocity and is related to the stream-function by

$$\omega = -\Delta \psi \tag{1.59}$$

Thus instead of giving a description of the flow in term of the two components of velocity, which are not independent because of the incompressibility condition, it is convenient to rewrite the two-dimensional Navier-Stokes equations in terms of the vorticity scalar field:

$$\frac{\partial \omega}{\partial t} + \boldsymbol{u} \cdot \nabla \omega = \nu \nabla^2 \omega - \alpha \boldsymbol{u} + f_\omega \ , \tag{1.60}$$

The linear dissipative term accounts for friction between the thin layer of fluid which is considered, and the rest of the three dimensional environment. Its effects will be discussed in the following chapter. The term f_ω represents the external source of energy acting on the largest scales – e.g. stirring. This term counteracts the dissipation by viscosity ν and friction α and allows to obtain a statistically steady state.

To solve Eq. (1.60) it is necessary to specify a set of boundary conditions which are required to solve the Poisson equation (1.59) for the stream function. In most studies on 2D turbulence, periodic boundary conditions are assumed in both the two directions. The presence of realistic no-slip boundaries gives origin to a source of vorticity fluctuations.

1.3.2 Conservation laws

The main difference with the three-dimensional case is the conservation of vorticity along fluid trajectories when viscosity, friction and external forcing are ignored.

The origin of this phenomenon is due to the vanishing in two dimensions of the so called "vortex stretching term" $(\boldsymbol{\omega} \cdot \nabla)\boldsymbol{v}$ that appears as a forcing term in the evolution equation for vorticity in the three-dimensional case where it is responsible for the unbounded growth of enstrophy in the limit $Re \to \infty$.

In the inviscid limit $\nu = 0$ and in absence of external forcing and friction, the vorticity equations simply states that the derivative of the vorticity along the fluid trajectories vanishes

$$\frac{D\omega}{Dt} = \frac{\partial \omega}{\partial t} + \boldsymbol{u} \cdot \nabla \omega = 0 \tag{1.61}$$

which means that since the vortex stretching is absent the vorticity of a fluid parcel is conserved. Thus all the integrals of the form $\int f(\omega) d\boldsymbol{r}$ are inviscid invariants of the flow. In particular this properties yields to the conservation of the *circulation* Γ defined as

$$\Gamma = \int_D \omega d^2 r = \oint_{\partial D} \boldsymbol{u}(\boldsymbol{r}, t) \cdot d\boldsymbol{s} \tag{1.62}$$

where $d\boldsymbol{s}$ denotes the length of an infinitesimal element of the boundary ∂D, and the total enstrophy

$$Z = \int d^2 r \frac{1}{2} \rho |\omega|^2 \tag{1.63}$$

In two dimension the enstrophy is bounded by the energy balance equation, which is obtained from Eq. (1.60) in absence of external forcing $f = 0$

and friction $\alpha = 0$, and assuming periodic boundary conditions:

$$\frac{dZ}{dt} = -\nu \int d^2 r \rho |\boldsymbol{\nabla}\omega|^2 \tag{1.64}$$

Therefore, at variance with the three-dimensional case, in two-dimensional turbulence the viscous dissipation of energy vanishes in the limit $\nu \to 0$

$$\lim_{\nu \to 0} \frac{dE}{dt} = \lim_{\nu \to 0} -2\nu Z = 0 \tag{1.65}$$

whereas there is dissipative anomaly for enstrophy when friction is not considered. One of the effects of friction that will be discussed in next chapter is the regularization of the vorticity field: in presence of friction also the enstrophy dissipation vanishes in the limit of vanishingly small viscosity [19].

Since the viscous energy dissipation vanishes it the limit $Re \to \infty$, in fully developed two-dimensional turbulence it is impossible to have a cascade of energy with constant flux toward small scales.

Moreover, the presence of two quadratic inviscid invariant, the energy and the enstrophy, modifies the picture of the turbulent cascade. Dividing the wavenumber space into shells of modulus $k_n = k_0 2^n$ the triad interactions between wavenumbers which produce the energy cascade in three dimensions can be thought of as pair interactions between the n-th shell and the $(n+1)$-th one. This is inadmissible in two dimensions because pair interaction between two neighbor shells cannot transfer both energy and enstrophy conservatively between equal wave-numbers. In order for both energy and vorticity to be conserved the net transfer by each triad interaction must be out of the middle wavenumber into both smallest and largest wave-numbers. Starting from the

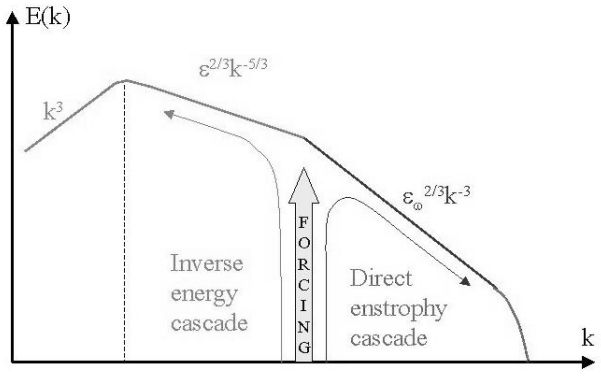

Figure 1.3: Schematic double cascading spectrum of forced two-dimensional turbulence

hint that the interactions should act toward producing equilibrium, a state which is never reached because of the viscous dissipation, Kraichnan showed that in two-dimensional turbulence the enstrophy is mainly transferred to high wave-numbers where it is dissipated by viscosity, giving rise to the *direct enstrophy cascade*. On the contrary, the energy is transported to lower wave-numbers in the *inverse energy cascade*.

1.3.3 Inverse energy cascade

The scaling laws in both cascades can be obtained from dimensional analysis of Navier-Stokes equation as well as in the three-dimensional case.

For the inverse energy cascade, the assumption of a constant flux of energy $\Pi(\ell) = -\epsilon$ toward large scales reproduces 3d-like scaling laws for velocities and characteristic times:

$$u_\ell \sim \epsilon^{1/3} \ell^{1/3} \tag{1.66}$$

$$\tau_\ell \sim \epsilon^{-1/3} \ell^{2/3} \tag{1.67}$$

This means that the velocity field in the inverse cascade is rough, with scaling exponent $h = 1/3$, exactly as in the three-dimensional case. The prediction for the energy spectrum reads

$$E(k) = C\epsilon^{2/3} k^{-5/3} \tag{1.68}$$

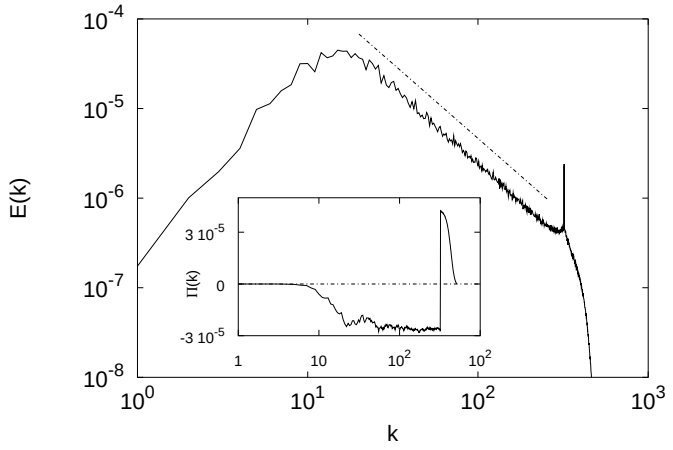

Figure 1.4: Energy spectrum of the inverse energy cascade $E(k) \sim k^{-5/3}$. In the scaling range the energy flux (shown in the inset) is constant and negative.

The hypothesis of locality of triadic interactions in the inverse cascade is consistent with the $k^{-3/5}$ spectrum. The transfer is associated with the distortion of the velocity field by its own shear. The effective shear at given wavenumber k is expected to be negligibly affected by wave-numbers $\ll k$ because the integral $\int_0^\infty k^2 E(k) dk$, which measure the mean-square shear, converges at $k = 0$. Also the contribution by high wavenumber $\gg k$ is negligible because vorticity associated with those wave-numbers fluctuates rapidly in space and times and gives a small effective shear across distances of order k^{-1}.

In absence of a large-scale sink of energy the inverse cascade can only be quasi-steady because the peak k_E of the energy spectrum keeps moving down to ever-lower wave-numbers as

$$k_E(t) \sim \epsilon^{-1/2} t^{-3/2} \tag{1.69}$$

while the total energy grows linearly in time $E(t) = \epsilon t$. If the input of energy continues for a sufficiently long time, the cascade can eventually reach the integral scale and energy begins to accumulate in the lowest mode, a phenomenon which is the analogous of Bose-Einstein condensation [20] of a finite two-dimensional quantum gas. This pile up of energy can produce a large scale spectrum steeper than k^{-3} which violates the hypothesis of locality of interactions.

The presence of friction stops the energy cascade at wavenumber

$$k_E \sim \epsilon^{-1/2} \alpha^{3/2} \tag{1.70}$$

where the energy dissipation balances the energy transfer $2\alpha E_{eq} = \epsilon$.

In two-dimensional turbulence it is possible to demonstrate the analogous of the Kolmogorov's *four-fifths law*. In the limit of infinite Reynolds number the third order (longitudinal) structure function of two-dimensional homogeneous isotropic turbulence, evaluated for increments ℓ small compared to the integral scale, and larger than the forcing correlation length, is given in terms of the mean energy flux per unit mass ϵ by

$$S_3(\ell) \equiv \langle (\delta u_\ell)^3 \rangle = \frac{3}{2} \epsilon \ell \tag{1.71}$$

Together with the scaling hypothesis for the structure functions $S_P(\ell) \sim \ell^{\zeta_p}$ the *three-half law* allows to obtain the equivalent of $K41$ theory for the inverse energy cascade in two-dimensional turbulence.

At variance with the three-dimensional case, where the dimensional prediction for the scaling exponents is modified by the presence of small scale intermittency, the statistics of velocity fluctuations at different scale ℓ in the scaling range of the inverse energy cascade are found to be roughly self-similar [21], with small deviations from gaussianity.

1.3.4 Direct enstrophy cascade

On scales smaller than the forcing correlation length, the hypothesis of a constant enstrophy flux $\Pi_\omega(\ell) = \epsilon_\omega$ leads to a different scaling. The enstrophy contained in the eddies of size ℓ can be estimated as $Z(\ell) \sim E(\ell)/\ell^2 \sim u_\ell^2 \ell^2$, and its flux

$$\Pi_\omega(\ell) \sim \frac{Z(\ell)}{\tau_\ell} \sim \frac{u_\ell^2}{\ell^2}\frac{u_\ell}{\ell} = \epsilon_\omega \ . \tag{1.72}$$

gives the following scaling for velocities:

$$u_\ell \sim \epsilon_\omega^{1/3} \ell \tag{1.73}$$

Therefore the velocity field in the enstrophy cascade is smooth, at variance with the velocity field in the inverse cascade. The dimensional prediction for characteristic times simply tells that there is essentially one single time scale in the direct energy cascade $\tau \sim \epsilon_\omega^{-1/3}$, which provides an estimate of the inverse of the Lyapunov exponent of the flow. The prediction for the energy spectrum reads

$$E(k) = C' \epsilon_\omega^{2/3} k^{-3} \tag{1.74}$$

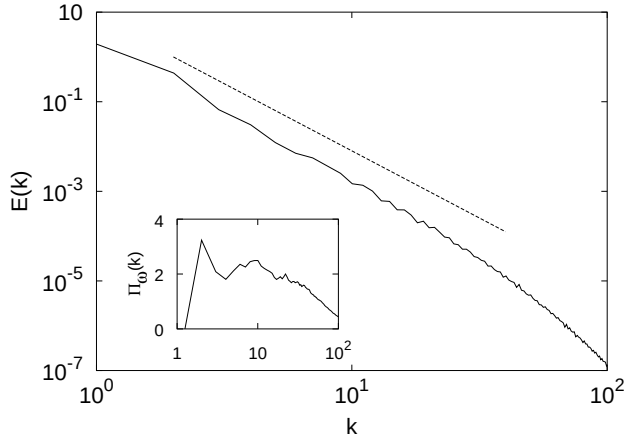

Figure 1.5: Energy spectrum of the direct enstrophy cascade $E(k) \sim k^{-3}$. In the scaling range the enstrophy flux (shown in the inset) is almost constant.

A spectrum k^{-3} means that the integral $\int_0^\infty k^2 E(k) dk$, which measure the mean-square shear has a logarithmic divergence in the infrared cutoff. Thus the hypothesis of locality of interactions in the cascade can be violated in the direct enstrophy cascade.

In next chapter I will discuss how the presence of a linear drag modifies this picture. We will show the presence of small-scale intermittency for the statistics of vorticity fluctuations and its dependence on the friction intensity.

1.3.5 Coherent vortices

The decay of two-dimensional turbulence has the fascinating property of organizing into coherent structures from a disordered background. This feature has been observed in laboratory experiments [22] as well as in numerical simulations [23, 24]. In a first stage the system self-organizes into a set of coherent vortices containing most of the flow vorticity, surrounded by an incoherent sea of small scale vorticity. The vortices mutually advect each other and their dynamics is well represented by the Hamiltonian point-vortex model. When two vortices of the same sign come close to each other they can merge in a bigger one, and the total number of vortices decay algebraically [25, 26] as $n(t) \sim t^{-\xi}$. In the final state remains only a survivor dipole, which decay diffusively.

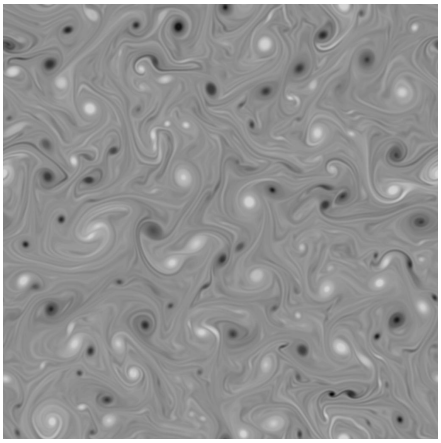

Figure 1.6: The formation of coherent structures in decaying two-dimensional turbulence.

The interest for this process is clearly motivated by its relation with the formation of large vortices in atmosphere, which play a fundamental role in our weather and our climate. As I will show, the presence of friction or polymers strongly modifies the classical picture of decaying turbulence, and may completely suppress the self-organization into large scale vortices.

Chapter 2

Effects of friction in two-dimensional turbulence

In order to study the properties of fully developed three-dimensional turbulence, it can be interesting to consider a portion of the fluid far from the boundaries, such that their interaction with the fluid can be neglected. On the contrary, when a thin layer of fluid is considered, it is important to include the effects of the friction between the two surfaces of the layer and the surrounding three-dimensional environment.

In many physical situations, the incompressible flow of a shallow layer of fluid can be described by the two-dimensional Navier-Stokes equations supplemented by a linear damping term which accounts for friction. An important instance, among others, relevant to geophysical applications is the rotating flow subject to Ekman friction [27]. Other well known examples are the Rayleigh friction in stratified fluids, the Hartmann friction in Magneto-Hydro-Dynamics [28] and the friction induced by surrounding air in soap films [29].

Understanding the effects of the friction term is thus a fundamental issue because of their physical relevance. Moreover, in numerical study of forced two-dimensional turbulence, in order to obtain a statistically steady state, it is necessary to introduce a large scale sink of energy to stop the inverse cascade and to prevent the Bose-Einstein condensation phenomenon [20]. The linear friction term is a natural candidate for this purpose, but its presence can produce strong effects not only on the large scales, but also on scales smaller than forcing correlation length, in the inner core of the direct enstrophy cascade.

In this chapter I will study these effects focusing on the influence of friction on the statistical properties of small-scale vorticity fluctuations.

I will first show the analogies and differences between this problem and

the transport of a passive scalar with finite lifetime [30], presenting some results recently obtained for the passive scalar statistics.

Using a Lagrangian description of the vorticity cascade I will then obtain the condition for the equivalence between small-scale vorticity and passive scalar statistics, which allows to extend to vorticity the results of the passive case.

Finally I will present the results of direct numerical simulations which confirms the predictions obtained using the Lagrangian approach. In particular I will show that the statistics of small-scale vorticity fluctuations is intermittent and that intermittency arises from the competition between the stretching properties of the flow and the exponential decay induced by friction.

2.1 Origin of the friction term

A linear friction term naturally arises in a wide range of different physical situations, and its origin should be considered within each specific context. Here we will briefly consider the case of thin stratified layers of fluids electromagnetically forced [31, 32], in which the origin of the friction term can be easily understood starting from the classical three-dimensional Navier-Stokes equations.

The dynamics of a shallow layer of incompressible fluid, with a thickness h much smaller than its extension L is described by Navier-Stokes equations:

$$\partial_t \boldsymbol{u} + \boldsymbol{u} \cdot \nabla \boldsymbol{u} = -\frac{\nabla P}{\rho} + \nu \Delta \boldsymbol{u} + \boldsymbol{f} \tag{2.1}$$

where P is the pressure, ρ is the density of the fluid, ν is its kinematic viscosity, and $\boldsymbol{f}$ the external forcing.

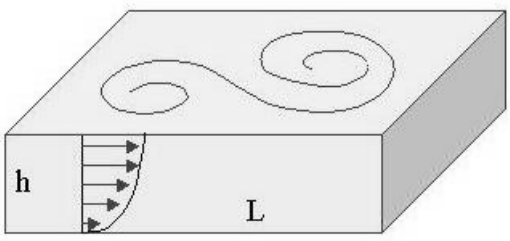

In the passage from a three-dimensional to a two-dimensional description the vertical components of velocity u_z are neglected, since their magnitude

with respect to the horizontal ones u_H is assumed to be of the same order of the aspect ratio:

$$\frac{(u_z)_{rms}}{(u_H)_{rms}} \sim \frac{h}{L} \tag{2.2}$$

Then we need to parameterize the vertical dependence of horizontal velocities. Experimental results [31] suggest that the flow structure within the layer is close to a Poiseuille flow, so we can assume a laminar viscous profile of velocities in the z-direction: $u(z) - u(h) \sim (z-h)^2$. With this assumption the three dimensional viscous term in eq.(2.1) gives origin to a two dimensional viscous term plus an additional linear damping term, which represent the effects of the bottom friction of the fluid:

$$\nu(\partial_x\partial_x + \partial_y\partial_y + \partial_z\partial_z)\boldsymbol{u} \rightarrow \nu(\partial_x\partial_x + \partial_y\partial_y)\boldsymbol{u} - \alpha\boldsymbol{u} \tag{2.3}$$

The resulting friction coefficient α is proportional to the inverse of the square of the total thickness of the layer h:

$$\alpha \sim \frac{\nu}{h^2} \tag{2.4}$$

according to the intuitive idea that the thinner is the layer, the stronger it feels the bottom friction.

2.2 Steepening of the energy spectrum

In absence of friction the requirement of a constant enstrophy flux in the direct cascade allows to obtain a dimensional prediction for the energy spectrum $E(k) = C'\epsilon_\omega^{2/3}k^{-3}$ (see Chapter 1). As already shown by Bernard [33] and Nam *et al* [30], a non-vanishing friction regularizes the flow depleting the formation of small-size structures and results in a steeper spectrum [30]

$$E(k) \sim k^{-3-\xi} \tag{2.5}$$

In the range $0 < \xi < 2$ the exponent ξ coincides with the scaling exponent ζ_2 of the second-order moment of vorticity fluctuations $S_2^\omega(r) = \langle(\delta_r\omega)^2\rangle \sim r^{\zeta_2}$. An explicit expression for the correction ξ to the spectral slope will be given in Section. 2.4.

The physical origin of the steepening of the spectrum is clear: part of the enstrophy which is transported to small scales is removed by the friction during the cascade process, thus the amplitude of fluctuations which reach the small scales is reduced. Since the energy spectrum is steeper than $E(k) \sim$

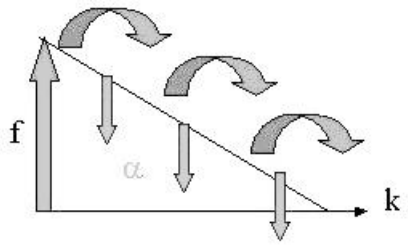

k^{-3}, the second-order velocity structure function $S_2(\ell) = \langle \delta u_\ell^2 \rangle$ is dominated by the IR contribution of the spectrum and trivially displays smooth scaling independently of the value of ξ. Thus the presence of a non-vanishing friction term ensures that the velocity fields in the direct enstrophy cascade is smooth.

2.3 Analogies with the passive scalar problem

The problem of two-dimensional turbulence with a linear friction can be considered as the active version of the transport of a passive scalar field with finite lifetime.

Indeed, there is a formal analogy between two-dimensional Navier-Stokes equation for the scalar vorticity $\omega = \nabla \times \boldsymbol{u}$, supplemented by the linear friction term

$$\frac{\partial \omega}{\partial t} + \boldsymbol{u} \cdot \nabla \omega = \nu \nabla^2 \omega - \alpha \omega + f_\omega \, . \tag{2.6}$$

and the dynamics of a concentration field $\theta(\boldsymbol{x}, t)$ with a finite lifetime τ, transported by the velocity field $\boldsymbol{u}(\boldsymbol{x}, t)$, which is described by the reaction-diffusion-advection equation

$$\frac{\partial \theta}{\partial t} + \boldsymbol{u} \cdot \nabla \theta = \kappa \nabla^2 \theta - \frac{1}{\tau} \theta + f_\theta \, . \tag{2.7}$$

where κ is the molecular diffusivity and f_θ is the source of scalar fluctuations.

It is clear that the analogy is just apparent: while Eq. (2.7) is a linear equation for the field $\theta(\boldsymbol{x}, t)$, Eq. (2.6) is strongly non-linear, because vorticity is the curl of velocity. Moreover while the equation for the passive scalar needs to be supplemented by an equation for the evolution of the advecting velocity field $\boldsymbol{u}(\boldsymbol{x}, t)$, the equation for vorticity determines also the evolution of velocity. Indeed the incompressible velocity field can be expressed in terms of the stream-function ψ as $\boldsymbol{u} = (\partial_y \psi, -\partial_x \psi)$, and the stream-function can be obtained from the vorticity solving the Poisson equation $\omega = -\Delta \psi$.

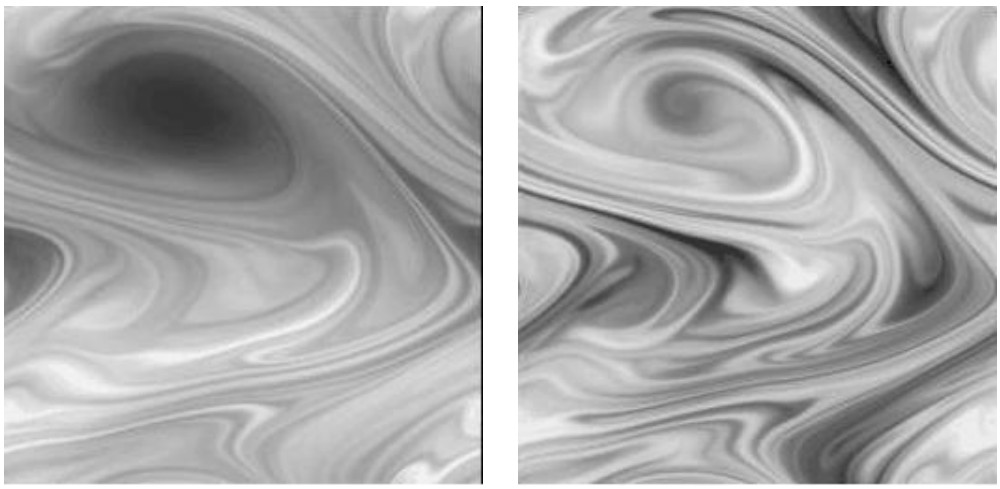

Figure 2.1: Snapshots of the vorticity field (left) and passive scalar field with finite lifetime (right) resulting from the simultaneous integration of Eq. (2.7) and Eq. (2.6). Detail of the simulation are reported in Sec. (2.5)

Nevertheless comparing a snapshot of the vorticity field obtained from numerical integration of Eq. (2.6), with a simultaneous snapshot of the passive scalar (see Fig. 2.1) obtained by the parallel integration of Eq. (2.7), using identical parameters $\kappa = \nu$ and $\alpha = 1/\tau$, it is evident that many similarities exist between the passive and the active field. Both vorticity and passive scalar fields are characterized by filamental structures, whose thickness can be as small as the smallest active length-scales. These "active" regions, where the vorticity experiences relatively strong excursions, are alternated to "quiescent" areas, the patches, where vorticity changes smoothly. This is the visual counterpart of the intermittency phenomenon, which is originated by the identical mechanism for vorticity and passive scalar.

It is interesting to notice that the forcings f_ω and f_θ used in our simulations are chosen as independent stochastic processes with the same statistics. Were the two forcings identical $f_\omega \equiv f_\theta$ they would cancel each other in the equation for the difference field $\theta(\boldsymbol{x}, t) - \omega(\boldsymbol{x}, t)$ which consequently would decay to 0 in a finite time. This means that if the passive field is forced exactly in the same way of the vorticity field, after some time it becomes identical to the active one, although it has no feedback on the fluid. This trivial observation is revealing of the crucial role played by the correlation between forcing and fluid trajectories in the passage from the passive to the active problem.

2.4 Passive scalar with finite lifetime

The problem of transport of a passive scalar with finite lifetime has seen in the last years a renewed interest [19, 34, 35, 36] because it is the prototype of a wide class of physical problems, ranging from biological processes like plankton dynamics, to chemical reactions in chaotic flows. It grasps the basic relevant features of the general problem of transport by a fluid environment of substance with an intrinsic dynamics, with the appealing feature of its simplicity, which in some specific situation allows to obtain analytical solutions.

In this section I will introduce the passive scalar problem following the works of M. Chertkov, E. Hernandez-Garcia, Z. Neufeld *et al.*, showing how the interaction between chaotic advection and linear damping can originates intermittency and smooth-filamental transition for the scalar field. These results will be extended in Section (2.5) to the active case.

2.4.1 Chaotic advection

Studying the advection of a passive scalar field is the basic approach for understanding the general problem of mixing in fluids.

The evolution of a scalar field $\theta(\boldsymbol{x}, t)$ diffusing and transported by a given velocity field $\boldsymbol{u}(\boldsymbol{x}, t)$ is given by the advection-diffusion equation

$$\frac{\partial \theta}{\partial t} + \boldsymbol{u} \cdot \nabla \theta = \kappa \nabla^2 \theta \, . \tag{2.8}$$

In the passive approach one assumes that it is possible to neglect all the possible kind of feedback of the transported field on the flow, e.g. the buoyancy force in the case of temperature field. Moreover Equation (2.8) is obtained assuming that the trajectories of the advected field coincide with those of the fluid particle, i.e. neglecting inertial effects [37] which are originated by difference of density between the solution and the solute or by finite size of the particle in suspension.

This clearly means that one is just giving an approximate description of fluid transport, but on the other side this approach has the great advantage that the behavior of a blob of passive scalar injected in the fluid can be understood in term of the statistical properties of fluid trajectories, which is the essence of the Lagrangian description of transport.

Fluid trajectories in realistic flows are typically chaotic, i.e they show a sensible dependence on initial conditions, thus also the advection of a scalar field will be chaotic. Chaotic advection contains the essence of the mixing

properties of fluid transport, that is the characteristic mechanism of stretching and folding of material elements.

Here we will focus on chaotic advection by a smooth, two-dimensional, time-dependent, incompressible velocity field, which is the case of the velocity field in the direct enstrophy cascade in presence of friction, as discussed in the previous section.

Because of the presence of chaos, nearby fluid trajectories typically separate with an exponential rate given by the leading Lyapunov exponent [38]:

$$\lambda = \lim_{t\to\infty} \lim_{\delta_0\to 0} \frac{1}{t} \ln \frac{\delta(t)}{\delta_0} \tag{2.9}$$

where δ_0 and $\delta(t)$ are respectively the initial separation and the separation

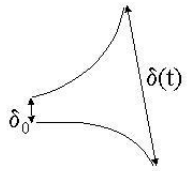

at time t of the two Lagrangian trajectories: $\delta(t) = |\boldsymbol{x}^{(1)}(t) - \boldsymbol{x}^{(2)}(t)|$. As a consequence an element of fluid is elongated exponentially in the direction of the leading Lyapunov vector, resulting in a long filament, which is folded on itself several times. At the same time, because of incompressibility, the area of the two-dimensional fluid element is preserved, and so the thickness in the transverse direction must decrease exponentially fast with the same rate.

Injecting in the fluid a blob of passive tracer with a typical size ℓ_0 it will follow the same evolution, and in a time t it will became a filament of length $L = \ell_0 \exp(\lambda t)$ and thickness $r = \ell_0 \exp(-\lambda t)$. The thinning process is finally stopped by the diffusion process on the diffusive scale $\sqrt{\lambda\kappa}$

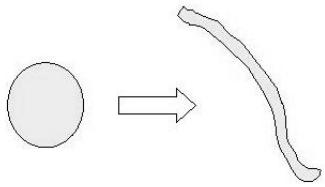

This means that the original fluctuation of passive scalar which was injected at the scale ℓ_0 in a time t has been transported down to the small scale r. This phenomenon is known as the direct cascade of passive scalar, in

which large scale inhomogeneities of the concentration field are transported by the flow to the small scales where they are omogeneized by molecular diffusivity.

Chaotic advection provides a mechanism to transport quickly a large scale fluctuation to small scale, originating the typical filamental pattern which are observed in transported fields. The roughness of the concentration field can be characterized by a Hölder exponent h:

$$|\delta\theta(\boldsymbol{x},\boldsymbol{r})| \equiv |\theta(\boldsymbol{x}+\boldsymbol{r}) - \theta(\boldsymbol{x})| \sim |\boldsymbol{r}|^h, |\boldsymbol{r}| \to 0 \tag{2.10}$$

For a smooth field (i.e differentiable) at $\boldsymbol{x}$ we have $h = 1$ while the range $0 < h < 1$ correspond to an irregular (e.g. filamental) field.

2.4.2 Chaotic advection and linear damping

If the advected field is reactive, e.g. in the case of concentration field of a chemical product, the resulting structure of the concentration field is determined by the competition between the mixing process and the chemical reaction. We are interested in the simplest case of reaction, that is an exponential decay of the concentration field originating form its finite lifetime, because of its analogy with the friction term in the equation for vorticity.

In this case the two processes in competition are the direct cascade of scalar fluctuation produced by the flow, and the exponential decay of the same fluctuation due to the reaction term. The stretching exerted by the incompressible smooth velocity generates small scale features at exponential rate (Lyapunov):

$$r = Le^{\lambda t} \tag{2.11}$$

At the same time fluctuations initially generated by the external forcing at the large scale L decay at exponential rate given by the inverse of finite lifetime $\alpha = 1/\tau$:

$$\delta\theta(\boldsymbol{r},t) = \delta\theta(L,0)e^{\alpha t} \tag{2.12}$$

Combining the two exponential behavior one has:

$$\delta\theta(\boldsymbol{r},t) = \delta\theta(L,0)\left(\frac{r}{L}\right)^{\alpha/\lambda} \tag{2.13}$$

and thus, in stationary conditions one gets the following scaling law for the structure functions:

$$S_p^\theta(r) \equiv \langle(\delta_r\theta)^p\rangle \sim r^{\zeta_p^\theta} \tag{2.14}$$

with the scaling exponents:

$$\zeta_p^\theta = \min\left[p\frac{\alpha}{\lambda}, p\right] \tag{2.15}$$

When the omogeneization produced by the linear damping is stronger than the stirring $\alpha > \lambda$ the resulting field is smooth with Hölder exponent $h = 1$, otherwise one obtains a filamental rough field with $h = \alpha/\lambda$. This phenomenon is known as smooth-filamental transition [36].

In the scaling range the prediction for the power spectrum of passive scalar fluctuations reads:

$$E_\theta = 2\pi k \langle |\hat{\theta}(\boldsymbol{k})|^2 \rangle \sim k^{-1-2\alpha/\lambda} \tag{2.16}$$

The spectral slope shows an explicit dependence on the linear damping coefficient $\alpha = 1/\tau$, and in the limit of infinite lifetime $\alpha \to 0$ the Batchelor's k^{-1} prediction is recovered.

2.4.3 Intermittency

The previous results which has been presented with intuitive but not-rigorous arguments, are formally valid only in a mean field sense, i.e. assuming a constant stretching rate λ. This is not the general case.

While in the limit of infinite time the stretching rate is the same for almost all trajectories in an ergodic region, and is given by the Lyapunov exponent, the stretching rates at a finite time t are given by the *finite time Lyapunov exponents* γ, which are defined as

$$\gamma = \lim_{\delta_0 \to 0} \frac{1}{t} \ln \frac{\delta(t)}{\delta_0} \tag{2.17}$$

Because of their local character they can assume different values depending on the initial positions of the trajectories along which they are measured. For large t their distribution approaches the asymptotic form

$$P(\gamma, t) \sim t^{1/2} \exp[-S(\gamma)t] \tag{2.18}$$

The Cramér function $S(\gamma)$ (also called entropy function) is concave, positive, with a quadratic minimum in λ (the maximum Lyapunov exponent) $S(\lambda) = 0$, and its shape far from the minimum depends on the details of the velocity statistics [38, 39]. The quadratic minimum of $S(\gamma)$ correspond to a Gaussian behavior for the core of the probability distribution of the stretching rate γ, which can be predicted in the general case thanks to the Central Limit Theorem. In the limit $t \to \infty$ the distribution became a δ-distribution with support for $\gamma = \lambda$.

Local fluctuations of the stretching rates are the origin of the intermittent behavior of the passive scalar statistic. Indeed, in order to obtain the correct evaluation of the structure functions of passive scalar fluctuations, it is

necessary to average over the distribution of finite-time Lyapunov exponents:

$$S_p^\theta(r) \equiv \langle (\delta_r \theta)^p \rangle \sim \langle \left(\frac{r}{L}\right)^{p\alpha/\gamma} \rangle \sim \int d\gamma \left(\frac{r}{L}\right)^{[p\alpha + S(\gamma)]/\gamma} \sim \left(\frac{r}{L}\right)^{\zeta_p^\omega} . \quad (2.19)$$

The scaling exponents are evaluated from Eq. (2.20) by a steepest descent argument as:

$$\zeta_p^\theta = \min_\gamma \{p, [p\alpha + S(\gamma)]/\gamma\} . \quad (2.20)$$

Intermittency manifests itself in the nonlinear dependence of the exponents ζ_p^θ on the order p.

In the Gaussian approximation for $P(\gamma)$, which holds near its core, the Cramér function has the quadratic expression:

$$S(\gamma) = \frac{(\gamma - \lambda)^2}{2\Delta} \quad (2.21)$$

and it is possible to obtain an explicit expression for the scaling exponents ζ_p^ω:

$$\zeta_p^\theta = \min \left\{ p, \frac{1}{\Delta} \left(\sqrt{\lambda^2 + 2p\alpha\Delta} - \lambda \right) \right\} \quad (2.22)$$

2.4.4 Smooth-filamental transition

The smooth-filamental transition predicted for $\alpha = \lambda$ in the mean field case, can be recast taking into account the intermittent behavior. According to Eq. (2.20) the exponent of the p-th structure function is the minimum between p, which corresponds to the smooth behavior, and $\min_\gamma \{[p\alpha + S(\gamma)]/\gamma\}$ that describes the rough, filamental field.

In the Gaussian approximation the crossover between the linear and non-linear behavior for the scaling exponent happens for:

$$p^* = \frac{2}{\Delta}(\alpha - \lambda) \quad (2.23)$$

where the curve $1/\Delta(\sqrt{\lambda^2 + 2p\alpha\Delta} - \lambda)$ intersects the line p. Below the smooth-filamental transition, when $\alpha < \lambda$, the intersection is for $p^* < 0$, thus all the positive moments of the distribution of passive scalar fluctuation follow the non-linear behavior. This means that the filamental part of the field is dominant. On the contrary, when $\alpha > \lambda$ there is a crossover between the smooth scaling exponent for the structure functions of order $p \leq p^*$ and the non-linear behavior for $p > p^*$. In this case only the higher moments of the passive scalar statistics are able to detect the filamental structures, while the lower moments are dominated by the smooth behavior of the field.

It is worthwhile to underline that ζ_p^θ in the non-smooth case is determined by the value of $S(\gamma_p^*)$ where γ_p^* is the finite-time Lyapunov exponent which minimizes $[p\alpha+S(\gamma)]/\gamma$. Since γ_p^* is a growing function of p (in the quadratic approximation $\gamma_p^* = \sqrt{\lambda^2 + 2p\alpha\Delta}$) higher moments of passive scalar fluctuations are determined by the tail of the distribution of the stretching rates, where the parabolic approximation for $S(\gamma)$ does not hold in general. Thus the behavior of high order structure functions is extremely dependent on the detail of the velocity field. Nevertheless the presence of a smooth-filamental transition is determined by the asymptotic behavior of the exponents for $p \to 0$ where the Gaussian approximation holds thanks to the Central Limit Theorem, thus the smooth-filamental transition is always present for $\alpha = \lambda$, while for $\alpha > \lambda$ the exact value of the critical moment p^* can deviate from Eq. (2.23).

We notice that relations obtained in the Gaussian approximation are exact for the peculiar case of the Kraichnan-model, that is a smooth velocity field δ-correlated in time, in which the Cramér function $S(\gamma)$ is exactly parabolic.

2.5 Lagrangian description of the vorticity cascade

In this section I will focus on the statistical properties of vorticity fluctuations $\delta_r\omega = \omega(\boldsymbol{x}+\boldsymbol{r},t) - \omega(\boldsymbol{x},t)$ at scales r smaller than the correlation length L of the external forcing. The intuitive arguments presented for the passive scalar will be reformulated in terms of Lagrangian description of the vorticity cascade, which allows to point out the crucial differences between the active and the passive problem.

2.5.1 Fluid trajectories and exit-times

We consider the two-dimensional Navier-Stokes equation for the scalar vorticity $\omega = \nabla \times \boldsymbol{v}$:

$$\frac{\partial \omega}{\partial t} + \boldsymbol{v}\cdot\nabla\omega = \nu\nabla^2\omega - \alpha\omega + f_\omega \,, \tag{2.24}$$

with the additional friction term $-\alpha\omega$.

As already told in Sec. 2.2 the presence of friction regularizes the flow, removing scale by scale part of the enstrophy which is transported to small scales by the cascade process. As a consequence, at variance with the frictionless case where the the flux of enstrophy towards small scale is constant

in the scaling range, in presence of friction it decays as $k^{-\xi}$ (see Figure 2.2). At viscous wave-numbers $k_d \sim \nu^{-1}$ the enstrophy flux is stopped by viscous dissipation, with a dissipation rate $\epsilon_\omega \sim \nu^\xi$ which vanishes in the inviscid limit $\nu \to 0$, since $\xi > 0$. In other words, in the limit of vanishingly small viscosity, there is no dissipative anomaly for enstrophy[19]. The absence of

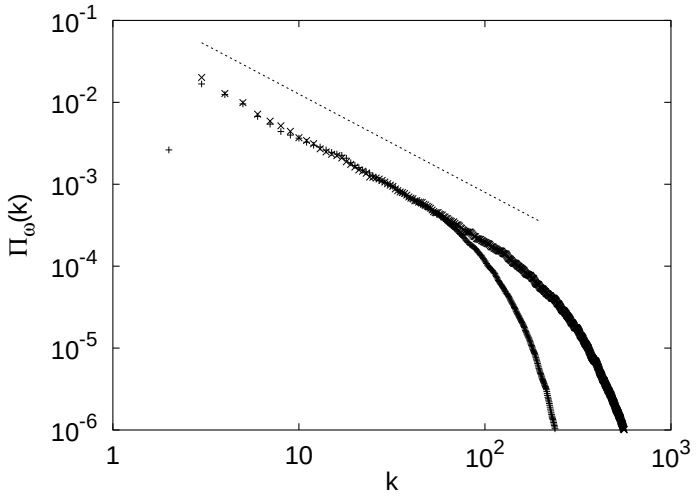

Figure 2.2: Enstrophy flux $\Pi_\omega(k) \sim k^{-\xi}$ for $\nu = 5 \cdot 10^{-5}$ (+) and $\nu = 1.5 \cdot 10^{-5}$ ($\times$). Here $\alpha = 0.15$. Reducing ν the remnant enstrophy flux at small scales tends to zero as ν^ξ, allowing to disregard viscous dissipation.

dissipative anomaly for any α strictly positive allows to disregard the viscous term in Eq. (2.24) as far as we are interested in the statistical properties in the scaling range. In the limit $\nu \to 0$ it is possible to solve Eq. (2.24) by the method of characteristics yielding the expression:

$$\omega(\boldsymbol{x}, t) = \int_{-\infty}^{t} f_\omega(\boldsymbol{X}(s), s) \, \exp[-\alpha(t-s)] \, ds \tag{2.25}$$

where $\boldsymbol{X}(s)$ denotes the trajectory of a particle transported by the flow:

$$\dot{\boldsymbol{X}}(s) = \boldsymbol{v}(\boldsymbol{X}(s), s) \tag{2.26}$$

ending at $\boldsymbol{X}(t) = \boldsymbol{x}$. The uniqueness of the trajectory $\boldsymbol{X}(s)$ in the limit $\nu \to 0$ is ensured by the fact that the velocity field is Lipschitz-continuous [1]

[1] A field f(x) is Lipschitz-continuous of order α if $\exists \epsilon > 0, \exists B finite, \exists 0 < \beta < \alpha : \forall |h| < \epsilon |f(h) - f(0)| \leq B|h|^\beta$.

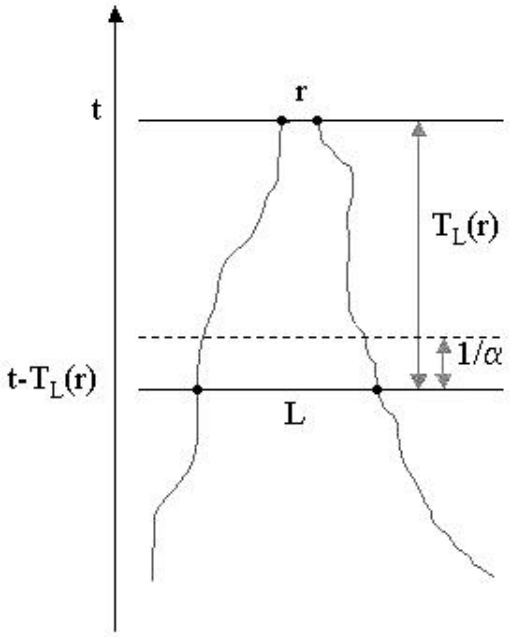

as it can be seen from the velocity spectrum $E(k) \sim k^{-3-\xi}$, always steeper than k^{-3} (see Fig. 2.4).

The physical meaning of Eq. (2.26) is clear: the value of the vorticity field in a certain position $\boldsymbol{x}$ at time t is just the sum of all the contributions given by the forcing along the fluid trajectory which ends in $\boldsymbol{x}$ at time t, depleted by an exponential factor because of the linear damping.

Vorticity differences $\delta_r\omega$ at scale r smaller than the forcing correlation length L are then associated to couples of fluid trajectories which at time t are at distance $|\boldsymbol{X}'(t) - \boldsymbol{X}(t)| = r$

$$\omega(\boldsymbol{x}', t) - \omega(\boldsymbol{x}, t) = \int_{-\infty}^{t} [f_\omega(\boldsymbol{X}'(s), s) - f_\omega(\boldsymbol{X}(s), s)] e^{-\alpha(t-s)}\, ds \qquad (2.27)$$

Inside the time integral, the difference between the value of f_ω at $\boldsymbol{X}'$ and that at $\boldsymbol{X}$ is negligibly small as long as the two fluid particles lie at a distance smaller than L, the correlation length of the forcing; conversely, when the pair is at a distance larger than L, it approximates a Gaussian random variable Ω. One then obtains:

$$\delta_r\omega \sim \Omega \int_{-\infty}^{t-T_L(r)} e^{-\alpha(t-s)}\, ds \sim \Omega e^{-\alpha T_L(r)} \qquad (2.28)$$

where $T_L(r)$ is the time that a couple of particles at distance r at time t takes to reach a separation L backward in time.

Equation (2.28) simply tells that a fluctuation of vorticity is originated by the forcing when the two trajectories are at distance larger than the forcing correlation length, and then it decays exponentially for all the time $T_L(r)$ required to transport by chaotic advection the fluctuation down to the small scale r in the direct cascade process. At a fixed scale r, large vorticity fluctuations arise from couples of particles with relatively short exit-times $T_L(r) \ll \langle T_L(r) \rangle$, whereas small vorticity fluctuations are associated to large exit-times.

2.5.2 Structure functions and scaling exponents

To evaluate the moments of vorticity fluctuations it is necessary to perform an average over the statistics of forcing which generates the fluctuations, and over exit-times statistics:

$$S_p^\omega(r) \equiv \langle (\delta_r \omega)^p \rangle \sim \langle \Omega^p \rangle_f \langle e^{-p\alpha T_L(r)} \rangle_{T_L(r)} \tag{2.29}$$

Since the velocity field is smooth, two-dimensional and incompressible, particles separate exponentially fast and the statistics of exit-times can be replaced by the statistics of finite time Lyapunov exponents, which measure the growth rate of the logarithm of the distance between two particle during a time t. The finite-time Lyapunov exponent and exit-times are thus related in a smooth flow by the condition:

$$L = r e^{\gamma T_L(r)}. \tag{2.30}$$

We remark that this relation does not hold in the case of non-smooth flows, where the relative dispersion follows a power law [40]. In this case the growth of the distance ℓ between two trajectories is dominated by the structure of the flow at the same scale. The scaling law for the intensity of the eddies of size ℓ characterized by the Hölder exponent of the rough velocity field, gives origin to a power law for particle separation. Thus the exit-time $T_L(r)$ value is dominated by the eddy at large scale L and is almost independent from the small initial separation r.

Replacing the average over the statistics of exit-times with the statistics of finite-time Lyapunov exponents, and using the asymptotic behavior for the distribution $P(\gamma, t) \sim t^{1/2} \exp[-S(\gamma)t]$ (see Section (2.4)), one gets the following estimate for moments of vorticity fluctuations

$$S_p^\omega(r) \sim \langle \Omega^p \rangle \int d\gamma P(\gamma) e^{-p\alpha \frac{\ln L/r}{\gamma}} \sim \langle \Omega^p \rangle \int d\gamma \left(\frac{r}{L}\right)^{[p\alpha + S(\gamma)]/\gamma} \sim \left(\frac{r}{L}\right)^{\zeta_p^\omega}. \tag{2.31}$$

The scaling exponents are evaluated from Eq. (2.31) by a steepest descent argument as:

$$\zeta_p^\omega = \min_\gamma \{p, [p\alpha + S(\gamma)]/\gamma\} \ . \tag{2.32}$$

In the range $0 < \zeta_2^\omega < 2$ the scaling exponent of the second order structure function for vorticity is related to the spectral slope of vorticity power spectrum

$$Z(k) = 2\pi k \langle |\hat{\omega}(\boldsymbol{k})|^2 \rangle \sim k^{-1-\xi} \tag{2.33}$$

by the relation $\xi = \zeta_2^\omega$, which gives the explicit dependence on the friction coefficient α of the spectral slope of the energy spectrum:

$$E(k) = Z(k)/k^2 \sim k^{-3-\xi} \tag{2.34}$$

2.5.3 From active to passive problem

It has to be noticed that the active nature of ω has been completely ignored in the above arguments: the prediction for the structure function given by Eq. (2.31) is identical to Eq. (2.29) obtained for the passive scalar with finite life-time. The crucial hypothesis in the derivation of Eq. (2.31) is that we have assumed that the statistics of trajectories is independent of the forcing f_ω:

$$\langle \Omega^p e^{-p\alpha T_L(r)} \rangle_{f,T_L(r)} = \langle \Omega^p \rangle_f \langle e^{-p\alpha T_L(r)} \rangle_{T_L(r)} \tag{2.35}$$

While for the passive scalar this is trivially true, because the forcing of the passive field has no relation with the velocity field, and cannot influence fluid trajectories, in the case of vorticity this is quite a nontrivial assumption, since it is clear that forcing does affect large-scale vorticity and thus influence velocity statistics, but it can be justified by the following argument.

The random variable Ω arises from forcing contributions along the trajectories at times $s < t - T_L(r)$, when the distance between the two fluid particles is larger than the forcing correlation length L, whereas the exit-time T_L is clearly determined by the evolution of the strain at times $t - T_L(r) < s < t$. Since the correlation time of the strain is α^{-1}, for

$$T_L(r) \gg 1/\alpha \tag{2.36}$$

we might expect that Ω and $T_L(r)$ be statistically independent. This condition can be translated in terms of the finite-time Lyapunov exponent as:

$$r \ll L \exp(-\gamma/\alpha) \tag{2.37}$$

and thus at sufficiently small scales it is reasonable to consider ω as a passive field.

We remark that, were the velocity field non-smooth, the exit-times would be independent of r in the limit $r \to 0$ and the above argument would not be relevant. Therefore, the smoothness of the velocity field plays a central role in the equivalence of vorticity and passive scalar statistics.

2.6 Numerical results

To directly check the prediction for the steepening of the enstrophy spectrum and for the statistics of small scale fluctuations of vorticity obtained in the previous section using the analogy with the passive scalar problem, we have performed numerical integration of Navier-Stokes equation for the vorticity field (Eq. (2.6))

The numerical integration is performed by a fully de-aliased pseudo-spectral code with a second-order Runge-Kutta scheme, on a doubly periodic square domain of size $L = 2\pi$ at different resolutions: $N^2 = 512^2, 1024^2, 2048^2$ grid points. Simulations have been partially performed at CINECA on IBM SP3 and SP4 parallel computers.

The vorticity fluctuations are injected by a large-scale forcing f_ω which is Gaussian, δ-correlated in time, and limited to a shell of wave-numbers around $k_f = 2\pi/L$. Forcing amplitude is chosen to provide an enstrophy injection rate $F = 0.16$. At variance with other choices for f_ω commonly used (e.g. large-scale shear) this kind of forcing ensures the statistical isotropy and homogeneity of the vorticity field.

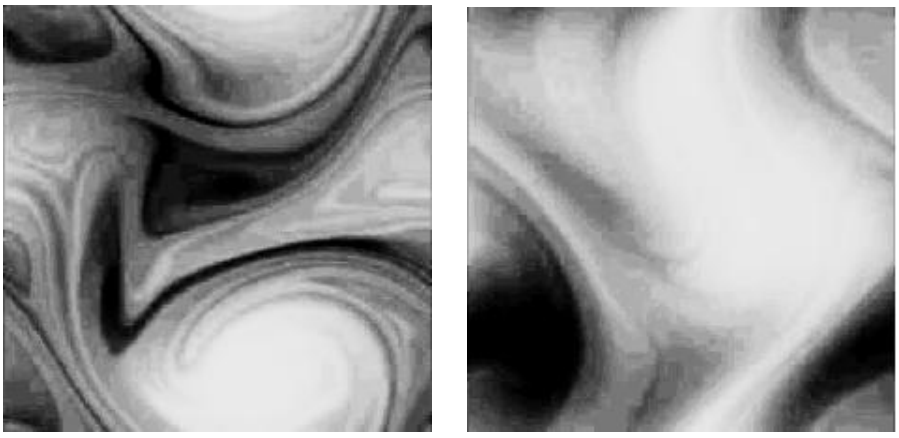

Figure 2.3: Snapshots of the vorticity field obtained from numerical simulations with two different values of friction: $\alpha = 0.15$ (left) and $\alpha = 0.23$ (right).

Different values of the friction $\alpha = 0.15, 0.23, 0.30$ has been tested, and

a small viscosity (see Table (2.7)) is used to remove the remnant enstrophy flux at small scales.

2.6.1 Steepening of the vorticity spectrum

The steepening effect on the vorticity spectrum has been investigated by performing a set of simulations with increasing intensity of the friction $\alpha = 0.15, 0.23, 0.30$.

According to the picture drawn in Section 2.2, at every every step of the cascade process, the friction removes part of the vorticity, thus at higher values of friction the fraction of vorticity which is transported to small scales is reduced, and the resulting filamental structures are less intense, as it can be seen in Figure 2.3. Consequently one observes steeper vorticity spectra at increasing values of friction (see Fig. 2.4), in agreement with Eq. (2.34).

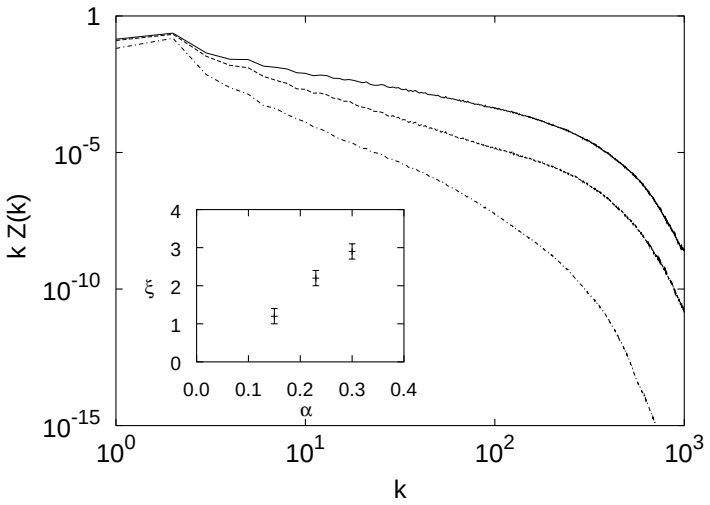

Figure 2.4: The vorticity spectrum $Z(k) \sim k^{-1-\xi}$ steepens by increasing the friction coefficient α. Here $\alpha = 0.15$ (solid line), $\alpha = 0.23$ (dashed line), $\alpha = 0.30$ (dash-dotted line). In the inset, the exponent ξ as a function of α.

2.6.2 Intermittency

In Figure 2.5 are shown the probability density functions of vorticity fluctuations $\delta_r\omega$ at various r, rescaled by their rms value $\langle(\delta_r\omega)^2\rangle^{1/2}$.

As the separation decreases, the probability of observing very weak or very intense vorticity excursions increases at the expense of fluctuations of

average intensity. This phenomenon goes under the name of intermittency. The non-similarity of the probability density functions reflects in the non-linear behavior for the scaling exponents predicted by Eq. (2.33).

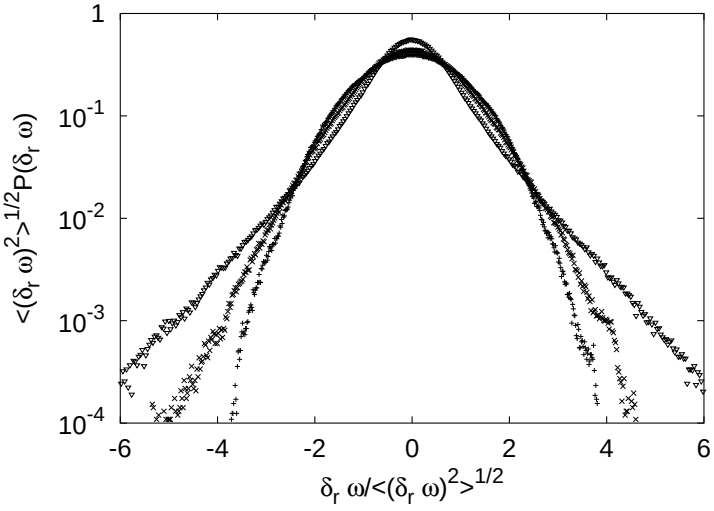

Figure 2.5: Probability density functions of normalized vorticity increments $\delta_r\omega/\langle(\delta_r\omega)^2\rangle^{1/2}$. Here, $r = 0.20$ $(+)$, $r = 0.07$ $(\times)$, $r = 0.02$ $(\bigtriangledown)$. For large separations the statistics is close to Gaussian, becoming increasingly intermittent for smaller r.

2.6.3 Vorticity vs. passive scalar statistics

To directly check whether small-scale vorticity can be considered as passively advected by velocity, we integrated at the same time Navier-Stokes equation for the vorticity field (Eq. (2.6)) and the equation of transport of passive scalar with a finite lifetime (Eq. (2.7)) advected by the velocity fields resulting from parallel integration of Navier-Stokes equation.

The parameters appearing in Eqs. (2.6) and (2.7) are the same ($\nu = \kappa$ and $\alpha = 1/\tau = 0.15$), yet the forcings f_ω and f_θ are independent processes with the same statistics. As already discussed the independence of the two forcings is crucial: were the two fields forced with the identical random process, the difference field $\theta - \omega$ would be free-decaying, and after a short time the passive field would became identical to the active one.

According to the picture drawn in previous section we expect to observe the same statistics for the fluctuations of vorticity $\delta_r\omega$ and passive scalar $\delta_r\theta = \theta(\boldsymbol{x}+\boldsymbol{r},t) - \theta(\boldsymbol{x},t)$ on scales r small enough to ensure that the passive condition (2.37) for vorticity is satisfied.

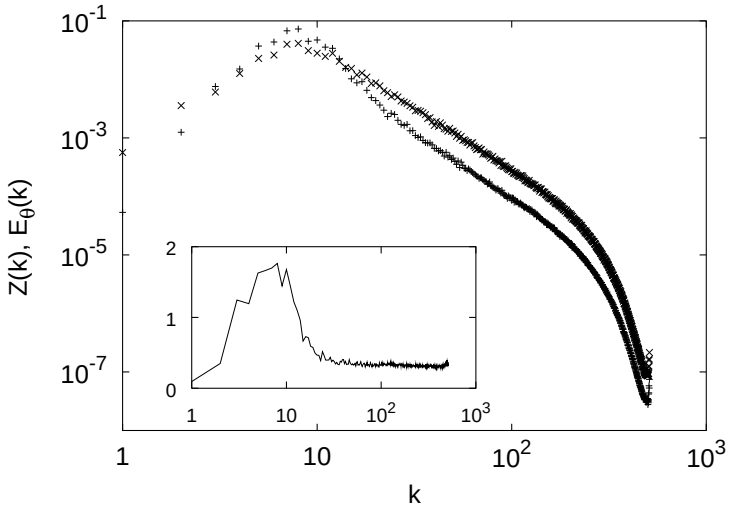

Figure 2.6: Power spectra of passive scalar ($\times$) and vorticity ($+$). Here $\alpha = 0.15$. In the inset we show the ratio $Z(k)/E_\theta(k)$, which approaches a constant for large k

In Figure 2.6 we show the power spectra of vorticity, $Z(k)$, and of passive scalar $E_\theta(k)$. The estimate of the range of wave-numbers at which the statistics of vorticity and passive scalar are expected to be coincident, is $k \gg k^* \simeq k_f \exp(\lambda/\alpha)$. With the actual values $k_f = 8$, $\alpha = 0.15$ and $\lambda = 0.16$ (see Figure 2.9) we have $k^* \simeq 23$. The two curves in Figure 2.6 are indeed parallel at large k ($k \gg k^*$), in agreement with the expectation $\zeta_2^\omega = \zeta_2^\theta$. At smaller wave-numbers we observe a big bump in $Z(k)$ around $k = k_f$ which has no correspondent in $E_\theta(k)$. This deviation is most likely associated to the presence of an inverse energy flux in the Navier-Stokes equation, a phenomenon that has no equivalent in the passive scalar case. Due to this effect, the scaling quality of $S_p^\omega(r)$ is poorer than the $S_p^\theta(r)$ one, and a direct comparison of scaling exponents in physical space is even more difficult.

However, we observe in Figure 2.7 that the probability density functions of vorticity and passive scalar increments, once rescaled by their root-mean-square fluctuation, collapse remarkably well onto each other. That is sufficient to state, along with the result $\zeta_2^\omega = \zeta_2^\theta$ obtained from Fig. 2.6, the equality of scaling exponents of vorticity and passive scalar at any order: $\zeta_p^\omega = \zeta_p^\theta$.

The excellent collapse of the probability distribution of fluctuations confirms that the underlying mechanism which generates intermittency, that is

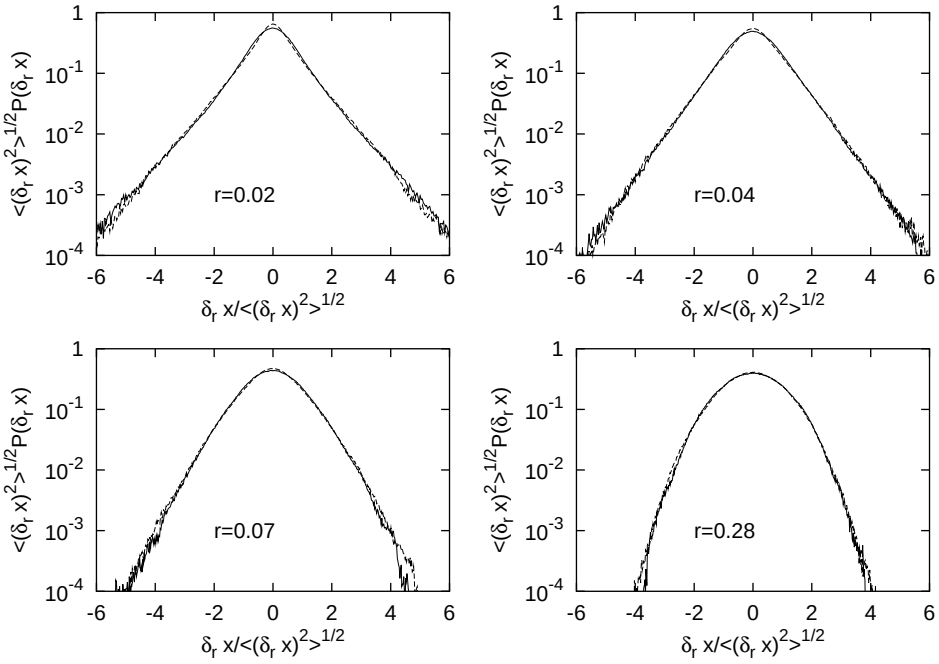

Figure 2.7: Probability density functions of vorticity differences (solid line) and of passive scalar ones (dashed line), normalized by their respective standard deviation, at different scales r within the scaling range.

the competition between exponential separation of Lagrangian trajectories and exponential decay of fluctuations due to the linear damping, is the same both for vorticity and passive scalar.

2.6.4 Scaling exponents and exit-time statistics

The actual values of the scaling exponents can be directly extracted from the statistics of the passive scalar, which is not spoiled by large-scale objects. In Figure 2.8 we plot the exponents ζ_p^θ as obtained by looking at the local slopes of the structure functions $S_p^\theta(r)$, in comparison with the exponents predicted by the Lagrangian exit-time statistics, according to

$$\langle \exp[-\alpha p T_L(r)] \rangle \sim r^{\zeta_p} \tag{2.38}$$

The exit-time statistics has been obtained with the following procedure:

- At time $t = 0$ 2×10^5 couples of Lagrangian particles are located at random position in the periodicity box $(0 < x < L, 0 < y < L)$ of the

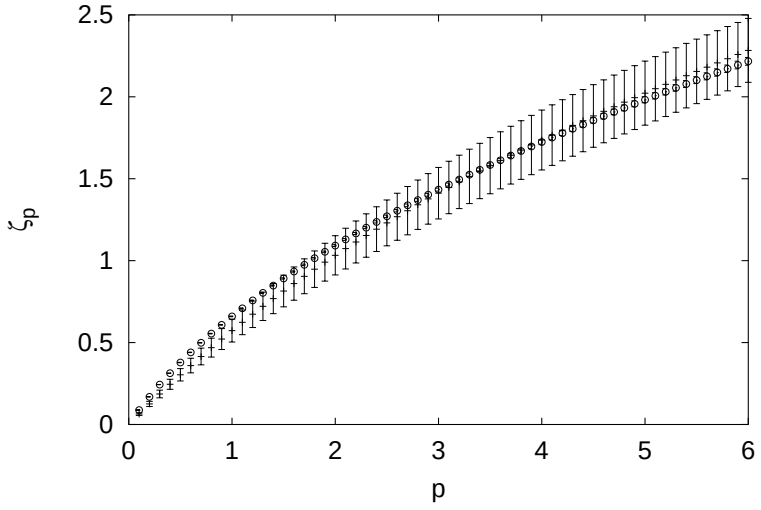

Figure 2.8: The scaling exponents of the passive scalar ζ_p^θ (+). We also show the exponents obtained from the exit times statistics ($\odot$) according to $\langle \exp[-\alpha p T_L(r)] \rangle \sim r^{\zeta_p^\theta}$ with average over about 2×10^5 couple of Lagrangian particles. The error-bars are estimated by the r.m.s. fluctuation of the local slope.

velocity field, with initial separation $d0$ between the two particles of each couple.

- A set of thresholds $\{r_i\}$ within the inertial range are fixed in geometric progression $r_i = r_0 \lambda^i$.
- The trajectories of Lagrangian particles are numerically computed according to $\dot{\boldsymbol{x}} = \boldsymbol{u}(\boldsymbol{x}, t)$ where the velocity field $\boldsymbol{u}$ has been obtained by parallel integration of Navier-Stokes equation.
- During the integration the distance between the two particles of each couple is measured, and the time T_i when it reaches the threshold r_i is stored.
- When the distance of a couple reaches the integral scale L at time T_L, the exit-times $T_L(r_i)$ are computed as

$$T_L(r_i) = T_L - T_i \ . \tag{2.39}$$

- The distance of the couple is then renormalized to $d0$ and the procedure is repeated.

Exit-times $T_L(r_i)$ provide an excellent tool for estimating the scaling exponent of the field. Since the thresholds can be chosen exactly within the inertial range, the scaling of Lagrangian structure function $\langle \exp[-\alpha p T_L(r)] \rangle \sim r^{\zeta_p}$ is not spoiled by contamination of the viscous range, and the excellent scaling allows for a precise measurement of the scaling exponents, which are in good agreement with those directly observed from the structure function of the passive field. Moreover, while the finite-time Lyapunov exponents are achievable only in numerical simulations, the measure of exit-times can be performed also in experiments by means of couple of Lagrangian tracers.

From the exit-time statistics it is also possible to recover the right tail of the Cramér function $S(\gamma)$ as the *inverse Legendre transform* [41] of the scaling exponents ζ_p:

$$\zeta_p = \min_{\gamma} \{p, [p\alpha + S(\gamma)]/\gamma\} \ . \tag{2.40}$$

which perfectly matches the Cramér function directly measured from the statistics of finite-time Lyapunov exponents (see Figure 2.9).

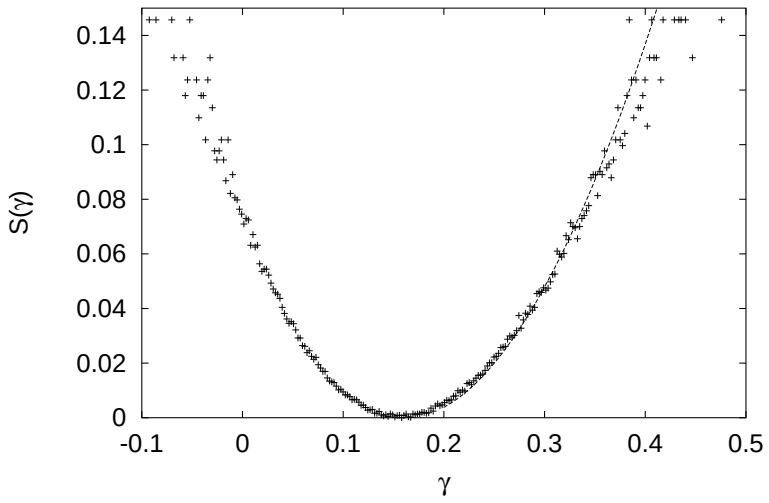

Figure 2.9: The Cramér function $S(\gamma)$ computed from finite time Lyapunov exponents (symbols) and exit-time statistics (line).

2.7 Summary

In this chapter we have analyzed the effects of linear friction on the enstrophy cascade in two-dimensional turbulence.

By means of theoretical arguments based on the Lagrangian description of fluid transport we have shown the analogy between the non-linear problem described by two-dimensional Navier-Stokes with friction and the linear one described by the advection-diffusion-reaction equation of a passive scalar with finite lifetime.

This analogy has allowed to obtain quantitative predictions for the steepening of the enstrophy spectrum and the intermittency of the small scale statistics, which have been tested by means of numerical simulations.

We have shown that intermittency arises from the competition between exponential separation of Lagrangian trajectories and exponential decay of fluctuations due to friction, and can be predicted in terms of exit-times statistics.

N	ν	k_f
512	$\nu = 5 \cdot 10^{-5}$	2
1024	$\nu = 1.5 \cdot 10^{-5}$	8
2048	$\nu = 5 \cdot 10^{-6}$	2

Table 2.1: Parameters of numerical simulations

Chapter 3

Polymer solutions: a brief introduction

The addition of small amounts of polymers to fluids produces a deep rheological change, which manifests itself in a wide range of spectacular phenomena. Because of their molecular structure, polymers have an elastic behavior, so that once they are added to a Newtonian fluid the resulting solution became a viscoelastic fluid. While for an ideal Newtonian fluid the stress is proportional to the deformation rate, for a perfectly elastic body the stress is proportional to the deformation itself. In the first case the proportionality constant is given by the viscosity in the second case by the Hook modulus. A viscoelastic solution can be thought of as a mixture of both these idealized situations.

The structural change in the dependence of the stress on the deformation properties is the origin of the different behavior of Newtonian and viscoelastic fluids. As an example, it is an everyday experience that rotating a teaspoon in a cup full of coffee, the fluids (which is roughly Newtonian) is pushed away from the rotating object by the centrifugal force, and a dip appears on the free surface. On the contrary when a rotating rod is inserted in a tank filled with viscoelastic fluid, the fluid moves in the opposite direction and climbs up the rod.

The effects produced by polymer addition to a Newtonian fluid cover a wide range: they can change the stability of laminar motion and the transition to turbulence, influence the formation or depletion of vortices, and modify the transport of heat, mass and momentum. The huge bibliography by Nadolink & Haigh [42] can give an idea of the number of papers devoted to the understanding of the behavior of viscoelastic fluids.

In this chapter I will introduce the basics of polymers dynamics in fluids and the simplest models which has been developed to describe viscoelas-

tic solutions. Finally I will briefly present the phenomenon of drag reduction [43], which characterize the turbulence of viscoelastic solutions in three dimension, in order to provide a comparison with the completely different two-dimensional behavior that will be the topic of next chapter.

3.1 Polymer dynamics in fluids

A polymeric molecule consists in a long chain formed by the repetition of a large number of single identical units, the monomers, linked by chemical bonds. For typical polymer used in drag reductions experiments the number of monomers is very large, $N = O(10^6 - 10^7)$ and the polymer can be considered, following Kuhn, as a *freely jointed chain* on n segments of length b, with independent relative orientation.

When a polymer molecule is put into an homogeneous flow, it assumes the aspect of a statistically spherical coil, because of the thermal agitation. The

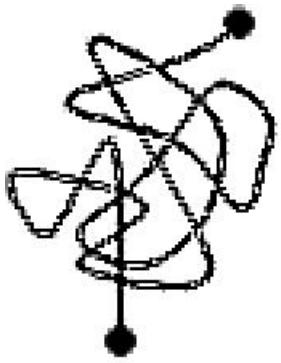

average size of the coil, which is also called *radius of gyration*, can be estimate as the length of the random walk formed by the n independent segments as $R_0 \sim n^{1/2}b$, in agreement with the results of light scattering experiments [44]. It is important to notice that the freely jointed segments do not correspond the single monomers, whose relative orientation is not independent because of the presence of chemical bonds. Indeed, for flexible linear molecules in good solvent, according to Flory[45] the radius of gyration is related to the number of monomers N as:

$$R_0 = N^{3/5}a \tag{3.1}$$

where a is the length of the single monomer. Typical value of R_0 are of order $0.1 - 0.2\mu m$. The coiled shape must be intended in a statistical sense: it correspond to the average of all the possible configurations assumed by a polymer in an homogeneous flow, but it doesn't mean that a given polymer at a given time looks like a sphere of radius R_0.

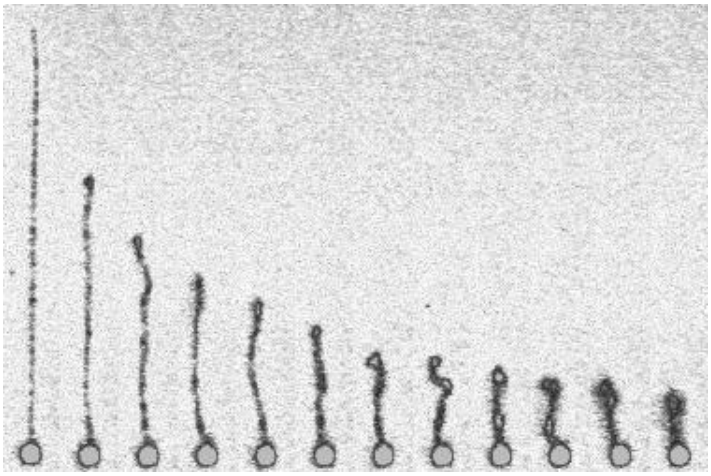

Figure 3.1: Images from Perkins Smith & Chu, *Science* 264, 819 (1994) of a single DNA molecule ($40\mu m$) tethered to a $1\mu m$ latex bead. The bead was trapped using optical tweezers and the DNA was labeled with a fluorescent dye. The DNA was stretched in a flow and its entropic relaxation was observed after the flow was turned off (left to right, 5 seconds intervals).

On the contrary, in a inhomogeneous flow the molecule is stretched into an elongated shape, that can be characterized by its end-to-end distance R, which can be significantly larger than R_0. The deformation of the molecules is the result of the competition between the stirring exercised by the gradients of velocity, and the relaxation of the polymer to its equilibrium configuration, as a result of Brownian bombardment. Experiments with DNA molecules [46, 47] show that this relaxation is linear provided that the elongation is smaller compared to the maximum extension $R \ll R_{max}$ (see Fig. 3.1).

This is consistent with the freely jointed chain model, where the equilibrium distribution for the end-to-end vector R resulting from the Brownian motion of the n elements of the chain has a Gaussian core:

$$P_{eq}(\boldsymbol{R}) = \left(\frac{3}{2\pi n b^2}\right)^{3/2} e^{-\frac{3}{2}\frac{R^2}{nb^2}} \tag{3.2}$$

with variance $< \boldsymbol{R}^2 >= nb^2 = 3R_0^2$. A quadratic entropy function for $\boldsymbol{R}$ leads, in the framework of the classical Fluctuation-Response theory [48] , to a linear relaxation $\dot{\boldsymbol{R}} = -R/\tau$.

A convenient measure on the relaxation time for the linear chain is that introduced by Zimm [49]:

$$\tau = \frac{\mu R_0^3}{k_B T} \tag{3.3}$$

where k_B is the Boltzmann constant, T is the solution temperature, μ is the solvent viscosity.

Indeed the relaxation process can be much more complex that the simple description given by Zimm model. Several microscopic model of the behavior of polymer molecule has been developed to characterize this process, from the *Rouse chain* to the *Reptation model*. An introduction to these models can be found in Doi & Edwards [50]. Nevertheless the simple linear relaxation is able to grasp, at least qualitatively, the basic features of polymer dynamics and feedback.

The relative strength between the relaxation of the polymer and stretching exerted by the flow is measured by the *Weissenberg number* Wi, defined as the product of the characteristic velocity gradient and τ. When $Wi \ll 1$ relaxation is fast compared with the stretching time, and the polymers remain in their coiled state. On the contrary, for $Wi \gg 1$ the polymers are stretched by the flow, and they became substantially elongated. This transition is known as the *coil-stretch transition*, and has been demonstrated to occur under general conditions in unsteady flow[51, 52] For the case of steady flow the transition is always present for purely elongational flow, while can be suppressed by rotation, because the polymers does not point always in the stretching direction[53].

In the case of turbulent flows polymers are stretched by a chaotic smooth flow, because their size is typically smaller than the viscous Kolmogorov scale of the fluid. The intensity of the stretching due to the gradients of a chaotic smooth velocity field can be measured by means of the Lyapunov exponent of Lagrangian trajectories λ that is the average logarithmic divergence rate of nearby fluid trajectories. The Weissenberg number for chaotic smooth flow thus reads:

$$Wi = \lambda\tau \tag{3.4}$$

For a turbulent flow the Lyapunov exponent gives an measure of the characteristic gradients of velocity which are determined by the smallest eddies of the turbulent cascade. By dimensional arguments it can be thought of as the inverse of the fastest eddy-turnover time. Within the Kolmogorov scaling the characteristic time at viscous scale $\eta \sim \epsilon^{-1/4}\nu^{3/4}$ is given by $\tau_\eta \sim \epsilon^{-1/3}\eta^{2/3} \sim \epsilon^{-1/2}\nu^{1/2}$, and consequently as the Reynolds number increases, the Lyapunov exponent grows as $\lambda \sim \sqrt{Re}$ as well as the the Weissenberg number $Wi \sim \sqrt{Re}$. Thus at a critical Re number the coil-stretch transition occurs.

The stretching of polymers is limited by their back reaction on the fluid. Indeed the stress tensor for a viscoelastic solution has an elastic component which is proportional to the polymer deformation tensor. When polymer are

substantially elongated the elastic stresses can become of the same order of the viscous stresses, and consequently polymers can modify the flow reducing the stretching and giving rise to a dynamical equilibrium state characterized by constant average elongation, which depends on the polymer concentration.

The reduction of the stretching due to polymers back reaction correspond to a strong reduction of the Lagrangian Lyapunov exponent of the viscoelastic fluid[54, 55], thus for the sake of clearness we will always define the Wi number a-priori as the product of the polymer relaxation time and the Lyapunov exponent of the Newtonian fluid $Wi \equiv \lambda_N \tau$.

3.2 Dumbbell model

The simplest model to describe the behavior of a molecule of polymer is the so called *Dumbbell model*. It consists in a couple of massless beads connected by a spring, which corresponds to the end-to-end vector of the polymer $\boldsymbol{R} = \boldsymbol{R}_1 - \boldsymbol{R}_2$. The evolution of $\boldsymbol{R}$ is determined by the sum of three forces: the hydrodynamic drag force acting on the molecule, the thermal noise, and the elastic force of the spring. In absence of external flow the equation for $\boldsymbol{R}$ reads:

$$\zeta \dot{\boldsymbol{R}} = -\frac{\partial E}{\partial \boldsymbol{R}} + \sqrt{2k_B T}\boldsymbol{\xi} \tag{3.5}$$

where ζ is the friction coefficient, E is the potential energy of the spring, and the thermal noise has been modeled by means of the zero average Brownian process $\boldsymbol{\xi}$ with correlation $\langle \xi_i(t)\xi_j(t')\rangle = \delta_{ij}\delta(t-t')$.

If the polymer is surrounded by a non homogeneous flow, we must add to Eq. (3.5) the stretching force determined by the difference of velocities of the external flow between the two beads:

$$\dot{\boldsymbol{R}} = \boldsymbol{v}(\boldsymbol{R}_1, t) - \boldsymbol{v}(\boldsymbol{R}_2, t) \tag{3.6}$$

Since the typical size of polymers (order $0.1 - 0.2\ \mu m$), is usually smaller than the viscous scale of turbulence $\eta \equiv (\nu^3/\epsilon)^{1/4}$, the velocity field is smooth on the scale $\boldsymbol{R}$ and the velocity difference can be estimate by the velocity gradient $v_i(\boldsymbol{R}_1, t) - v_i(\boldsymbol{R}_2, t) = \nabla_j v_i R_j + O(R^2)$.

With the addiction of the stretching term the equation (3.5) became:

$$\zeta \left[\dot{\boldsymbol{R}} - (\boldsymbol{R}\cdot\nabla)\boldsymbol{v}\right] = -\frac{\partial E}{\partial \boldsymbol{R}} + \sqrt{2k_B T}\boldsymbol{\xi} \tag{3.7}$$

As long as the elongation is smaller than the maximum length $R \ll R_{max}$, the polymer can be modeled by an elastic spring of Hook modulus K_0 so that $E = K_0 R^2/2$. The value of the elastic modulus is fixed by requiring

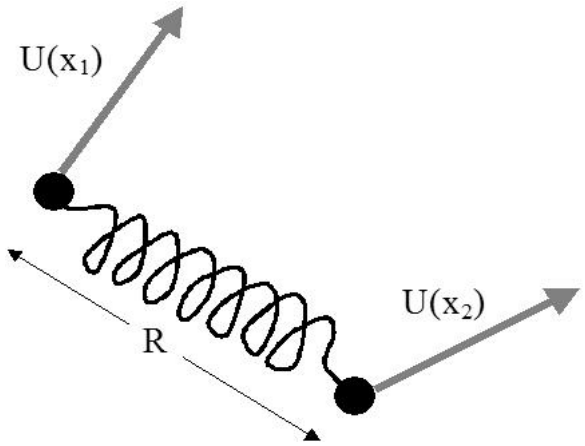

that the zero-shear equilibrium length, estimated from the balance between elastic end thermal energy $E \sim k_b T$, must be equal to the radius of gyration of the molecule R_0:

$$R_0 = \sqrt{k_B T / K_0} \tag{3.8}$$

The explicit expression for the Hook modulus $k_0 = K_B T / R_0^2$ points out the entropic origin of the "elastic" behavior of polymers.

Substituting the quadratic shape for potential energy into Eq. (3.7) we get the equation for the elongation $\boldsymbol{R}$ [56]:

$$\dot{\boldsymbol{R}} = (\boldsymbol{R} \cdot \nabla)\boldsymbol{v} - \frac{1}{\tau}\boldsymbol{R} + \sqrt{\frac{2R_0^2}{\tau}}\boldsymbol{\xi} \tag{3.9}$$

where has been introduced the polymer relaxation time τ

$$\tau = \frac{\zeta}{K_0} = \frac{\zeta R_0^2}{k_B T} \,. \tag{3.10}$$

The relaxation time τ in general is dependent on the elongation R, because the friction coefficient ζ changes with the size of the molecule, and when the elongation grows to values close to R_{max} the elastic potential is no longer quadratic, so the Hook modulus K_0 changes with R. To take in account these effects the *Finite Extendible Nonlinear Elastic model* (FENE model) [57] assumes $\tau \propto (R_{max}^2 - R^2)/(R_{max}^2 - R_0^2)$. Nevertheless, the linear model is supported by the experimental evidence of a constant relaxation time in the regime $R \ll R_{max}$.

In the Zimm model, considering the entraining of fluid within the coiled polymer, the friction coefficient is estimated as $\zeta = 4\pi R_0 \mu$, which substituted in (Eq (3.10) gives the Zimm relaxation time (Eq (3.3)).

The dumbbell model retains only the fundamental elastic mode of the polymer chain, with the slowest relaxation time. Although higher oscillatory modes, with faster relaxation times, have been observed experimentally [47] in DNA chains, they can be only weekly excited by the gradients of velocity in a turbulent flow, thus for a simplified rheological model it is sufficient to retain only the principal mode.

3.2.1 Coil-Stretch transition

The dumbbell model is able to reproduce the coil-stretch transition, which occurs when the stretching exerted by the flow overcomes the relaxation of polymer molecules.

The evolution of the polymer elongation can be obtained following the trajectories of polymer molecules, and Eq. (3.9) can be solved by characteristics as:

$$\boldsymbol{R}(t) = \int_0^t ds W(t,s)\sqrt{\frac{R_0^2}{\tau}}\boldsymbol{\xi}(s)e^{-(t-s)/\tau} + W(t,0)\boldsymbol{R}(0)e^{-t/\tau} \tag{3.11}$$

where $W(t_2,t_1)$ is the evolution matrix of the linearized flow along the fluid trajectory $\boldsymbol{X}(t)$ from time t_1 to time t_2.

We are interested in the tail of the probability distribution function of elongation R for $R \ll R_0$. Following Balkovsky *et al.* [52], at time large enough, when the initial condition is forgotten, the events contributing to the right tail of the pdf are those which have experienced large stretching. The gradients of velocity field tends to orientate the vector $\boldsymbol{R}$ in the direction of the leading Lyapunov vector, and its length is determined by the local value of the finite-time Lyapunov exponent $\gamma(s)$ as

$$R(t) \sim R_0 \int_0^\infty e^{\gamma s - s/\tau}\, ds \tag{3.12}$$

The values dominating the tail are those where $\gamma(s)s - s/\tau$ takes a sharp maximum at some s_* before relaxing to its typical negative values. The probability of those events is given by the asymptotic form of the finite-time Lyapunov exponents

$$P(\gamma(s_*)) \sim \exp^{S(\gamma(s_*))s_*} \tag{3.13}$$

where $S(\gamma)$ is the Cramér function (see Section 2.4). With logarithmic accuracy one can then replace $\gamma(s_*)s_* = \ln(R/R_0) + s_*/\tau$. The maximum value $X_* \equiv (s_*)^{-1}\ln(R/R_0)$ is fixed by the saddle-point condition that $S - X_*S'$ should vanish at $X_* + \tau^{-1} + \lambda$. The final answer for the pdf is:

$$P(R) \propto R_0^q R^{-1-q} \tag{3.14}$$

with

$$q = S'(X_* + \tau^{-1} + \lambda) \tag{3.15}$$

The convexity of the entropy function ensures that q is positive if $\lambda < 1/\tau$. In accordance with Eq. (3.15), the exponent q decreases when λ increases, and it tends to zero as $\lambda \to 1/\tau$. This means that when the value of the Weissenberg number $Wi = \lambda\tau$ exceeds unity the the integral of the pdf diverges at large R, and most of the polymer molecule are stretched. Below unity the pdf is stationary and only high moments of polymer elongation diverge. This is called "coil-stretch" transition.

The exponent q can be expressed via the equation $L_q = q/\tau$, where $L_q = \max_\gamma[q\gamma - S(\gamma)]$ is the generalized Lyapunov exponent of order q. Its value indicates the highest converging moment of polymer elongation.

In the coiled state, moments of polymer elongation $\langle R^n \rangle$ with $n < q$ reach stationary values, while high moments with $n > q$ diverge exponentially in time as:

$$< R^n > \sim e^{(L_n - \frac{n}{\tau})t} \tag{3.16}$$

In the Gaussian approximation of the Cramér function $S(\gamma)$, which holds near its minimum

$$S(\gamma) = \frac{(\gamma - \lambda)^2}{2\Delta} \tag{3.17}$$

the generalized Lyapunov exponents read

$$L_q = q\lambda + \frac{q^2}{2}\Delta \tag{3.18}$$

and the exponent q is $q = 2(1 - \lambda\tau)/(\tau\Delta)$.

3.3 Oldroyd-B model

In the dumbbell model the behavior of a single polymer molecule in a fluid is considered, but this microscopic model doesn't describe the feedback that polymers have on the flow. To include the feedback effect it is necessary to move to an hydro-dynamical description for the viscoelastic fluid. Oldroyd-B model [57] provides a simple linear viscoelastic model for dilute polymer solutions, based on the dumbbell model.

The passage from the microscopic behavior of the single molecule to a macroscopic hydro-dynamical description requires to get rid of the microscopic degrees of freedom such as the thermal noise. The macroscopic polymer behavior can be described in term of the *conformation tensor*:

$$\sigma_{ij} = R_0^{-2}\langle R_i R_j \rangle \tag{3.19}$$

where the average is taken over thermal noise, or equivalently over a small volume V containing a large number of molecules. By construction the tensor $\boldsymbol{\sigma}$ is symmetric, positive definite, and its trace tr$\boldsymbol{\sigma}$ is a measure of the square polymer elongation.

The equation for the conformation tensor follows from the linear equation (3.9) for the single molecule:

$$\partial_t \boldsymbol{\sigma} + (\boldsymbol{u} \cdot \boldsymbol{\nabla})\boldsymbol{\sigma} = (\boldsymbol{\nabla u})^T \cdot \boldsymbol{\sigma} + \boldsymbol{\sigma} \cdot (\boldsymbol{\nabla u}) - \frac{2}{\tau}(\boldsymbol{\sigma} - \mathbf{1}) \,, \tag{3.20}$$

where τ is the polymer relaxation time defined by Eq. (3.10), the matrix of velocity gradients is defined as $(\boldsymbol{\nabla u})_{ij} = \partial_i u_j$. The conformation tensor has been normalized with the equilibrium length R_0 such that in absence of external flow it relaxes isotropically to the unit tensor $\mathbf{1}$.

Equation (3.20) must be supplemented by the equation for the velocity field, which is derived from the momentum conservation law:

$$\frac{Du_i}{Dt} = f_i + \frac{1}{\rho}\frac{\partial \mathbb{T}_{ij}}{\partial x_j} \tag{3.21}$$

where $\boldsymbol{f}$ is sum of the body forces per unit mass, and $\mathbb{T}$ is the stress tensor of the fluid.

The stress tensor of a Newtonian fluid is linear in the deformation tensor $e_{ij} = 1/2(\nabla_j u_i + \nabla_i u_j)$, and is given by [4]:

$$\mathbb{T}^N_{ij} = -p\delta_{ij} + \mu\left[(\nabla_j u_i + \nabla_i u_j) - \frac{2}{3}\nabla_k u_k \delta_{ij}\right] \tag{3.22}$$

where μ is the dynamic viscosity and p the static pressure.

In the case of a viscoelastic solution, the stress tensor is given by the sum of the Newtonian stress tensor $\mathbb{T}^N$ and the elastic stress tensor $\mathbb{T}^P$, which takes into account the elastic forces of the polymers. While for a Newtonian fluid the stress tensor is proportional to the deformation rate tensor via the viscosity, in the Hookean approximation for the single polymer the elastic stress tensor is proportional via the Hook modulus to the deformation tensor $T_{ij} = K_0 R_i R_j$. The elastic stress tensor per unit volume of fluid is obtained summing the average contribution given by each polymer:

$$\mathbb{T}^P_{ij} = nK_0 < R_i R_j >= nK_0 R_0^2 \sigma_{ij} \tag{3.23}$$

where n is the concentration of polymer molecules.

For an incompressible fluid ($\nabla \cdot \boldsymbol{u} = 0$) with constant density ρ the equation obtained from the momentum conservation law (3.21) with the stress tensor $\mathbb{T} = \mathbb{T}^N + \mathbb{T}^P$ reads:

$$\partial_t \boldsymbol{u} + (\boldsymbol{u} \cdot \boldsymbol{\nabla})\boldsymbol{u} = -\boldsymbol{\nabla} p + \nu \Delta \boldsymbol{u} + \frac{2\eta\,\nu}{\tau}\boldsymbol{\nabla} \cdot \boldsymbol{\sigma} + \boldsymbol{f} \tag{3.24}$$

where p is the pressure, $\boldsymbol{f}$ is the external force (per unit mass) driving the flow. The solvent kinematic viscosity is denoted by $\nu = \mu/\rho$ and η is the zero-shear contribution of polymers to the total solution viscosity $\nu_t = \nu(1+\eta)$:

$$\eta = \frac{nK_0R_0^2\tau}{2\mu} \tag{3.25}$$

Eq. (3.24) is a generalization of Navier-Stokes equation for the viscoelastic solution and together with Eq. (3.20) fully determines the dynamics of Oldroyd-b model.

3.3.1 Newtonian limit: viscosity renormalization

In the limit $\tau \to 0$ the elastic force originated from the thermal motion keeps the molecules coiled near their equilibrium configuration, and the polymer solution is supposed to behave like a Newtonian fluid. Indeed, a perturbative expansion in τ for the conformation tensor

$$\sigma_{ij} = \sigma_{ij}^{(0)} + \tau\sigma_{ij}^{(1)} + O(\tau^2) \tag{3.26}$$

plugged in the equation Eq. (3.20) gives for the zeroth and first order terms:

$$\sigma_{ij}^{(0)} = \delta_{ij} \ , \sigma_{ij}^{(1)} = 1/2(\nabla_j u_i + \nabla_i u_j) = e_{ij} \tag{3.27}$$

We observe that at first order in τ the elastic stress tensor is proportional to the deformation tensor

$$\mathbb{T}_{ij}^P = nK_0R_0^2\tau e_{ij} + O(\tau^2) \ , \tag{3.28}$$

which means that the fluid is Newtonian up to higher order corrections $O(\tau^2)$. Anyway the presence of polymers changes the properties of the fluid also in the Newtonian limit, because the fluid is partially entrapped in the coiled polymers, producing a change in the total viscosity of the solution μ_t which is renormalized as:

$$\mu_t = \mu + \frac{1}{2}nK_0R_0^2\tau = \mu(1+\eta) \tag{3.29}$$

3.3.2 Energy balance

The free energy of the viscoelastic fluid is the sum of kinetic and elastic contributions:

$$\mathcal{F} = \int d^3r \left\{ \frac{1}{2}\rho u^2 + \frac{\eta\nu\rho}{\tau}[\mathrm{tr}\boldsymbol{\sigma} - \log\det\boldsymbol{\sigma}] \right\} \ . \tag{3.30}$$

where the last term represents the entropy of polymer molecules. The rate of change of the different components of the free energy can be obtained from Eqs. (3.24,3.20)

$$\frac{\partial}{\partial t}\frac{1}{2}u^2 = \boldsymbol{f}\cdot\boldsymbol{u} - \nu(\nabla_i u_j)^2 - \frac{\eta\nu}{\tau}[\sigma_{ij}\nabla_j \boldsymbol{u}_i + \sigma_{ij}\nabla_i \boldsymbol{u}_j] \tag{3.31}$$

$$\frac{\partial}{\partial t}\mathrm{tr}\boldsymbol{\sigma} = [\sigma_{ij}\nabla_j \boldsymbol{u}_i + \sigma_{ij}\nabla_i \boldsymbol{u}_j] - \frac{2}{\tau}\mathrm{tr}[\boldsymbol{\sigma} - \mathbf{1}] \tag{3.32}$$

$$\frac{\partial}{\partial t}\log\det\boldsymbol{\sigma} = \frac{2}{\tau}\mathrm{tr}[\boldsymbol{\sigma}^{-1} - \mathbf{1}]\ . \tag{3.33}$$

The forcing provides the input of kinetic energy which is then partially dissipated due to viscosity and relaxation of polymers. The term $\sigma_{ij}\nabla_j \boldsymbol{u}_i + \sigma_{ij}\nabla_i \boldsymbol{u}_j$ has not a definite sign, and represents the exchange between kinetic and elastic energy which can goes in both direction. Summing together the different contributions one obtain the rate of change of the free energy:

$$\frac{\partial \mathcal{F}}{\partial t} = \rho\int d^3r\left\{\boldsymbol{f}\cdot\boldsymbol{u} - \nu(\nabla_i u_j)^2 - \frac{2\eta\nu}{\tau^2}\mathrm{tr}[\boldsymbol{\sigma} - 2\mathbf{1} + \boldsymbol{\sigma}^{-1}]\right\}\ . \tag{3.34}$$

Since the conformation tensor $\boldsymbol{\sigma}$ is positive definite and symmetric, it can always be decomposed as the product of two symmetric matrices $\boldsymbol{S}$:

$$\sigma_{ij} = S_{ik}S_{kj} \tag{3.35}$$

so that the last term, which represent the energy dissipation rate due to polymers, can be rewritten as:

$$\mathrm{tr}[\boldsymbol{\sigma} - 2\mathbf{1} + \boldsymbol{\sigma}^{-1}] = \mathrm{tr}[(\boldsymbol{S} - \boldsymbol{S}^{-1})^2] \tag{3.36}$$

showing that it has a definite sign.

In the statistically steady state the average values of the free energy $\mathcal{F}$ is constant and the energy balance reads:

$$F = \nu\langle(\nabla_i u_j)^2\rangle + \frac{2\eta\nu}{\tau^2}(\langle\mathrm{tr}\boldsymbol{\sigma}\rangle - 2\mathrm{tr}\mathbf{1} + \langle\mathrm{tr}\boldsymbol{\sigma}^{-1}\rangle) \tag{3.37}$$

where F is the average energy input per unit mass. Assuming that the average kinetic energy and polymer elongation have statistically constant values, it follows that the average entropy production rate vanishes

$$\langle\mathrm{tr}\boldsymbol{\sigma}^{-1}\rangle - \mathrm{tr}\mathbf{1} = 0 \tag{3.38}$$

and the entropy of polymer molecule is conserved.

3.4 Fene-p

The linear Oldroyd-b model is based on the assumption that polymers can be modeled as Hookean springs, and consequently it allows for infinite extension of polymer molecules. This is clearly unphysical, because the polymer elongation is bounded by their total length R_{max}, moreover the assumption of linear relaxation is valid only when the polymer elongation is much smaller than R_{max}, while near R_{max} the Hook modulus is no more constant. To take in account these effects the *Finite Extendible Nonlinear Elastic model* (FENE model) [57] assumes that the Hook modulus diverges for $R \to R_{max}$:

$$K(R) = K_0 \frac{R_{max}^2 - R_0^2}{R_{max}^2 - R^2} \tag{3.39}$$

The elastic force is no more linear in the elongation and the resistance of the polymer to the stretching became infinite when it reaches its maximum elongation.

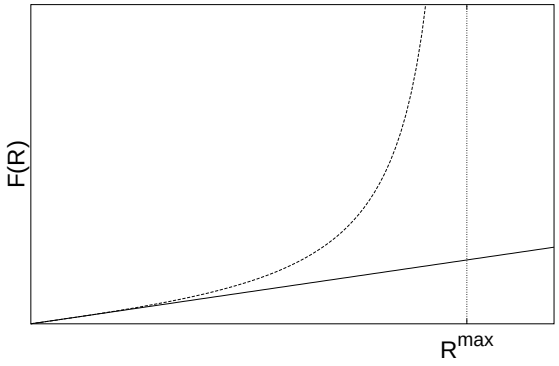

Figure 3.2: qualitative behavior of the elastic force $F(R)$ in the linear model (solid line) and FENE model (dashed)

Unfortunately the non linearity introduced in the equation for the single molecule does non allows to obtain a closed equation for the stress tensor $\langle R_i R_j \rangle$, since it involves higher order correlations $\langle R_i \cdots R_k \rangle$. A Gaussian closure was proposed by Peterlin, so that all correlations can be expressed in term of the second order one, and the equation for the conformation tensor can be closed. The FENE model with Peterlin's closure is referred to as *FENE-P* model. The Gaussian assumption is equivalent to a pre-averaging of the non linear function which modulates the elastic force in FENE model:

$$f(R^2) \to f(\langle R^2 \rangle) = \frac{R_{max}^2 - R_0^2}{R_{max}^2 - \langle R^2 \rangle} \tag{3.40}$$

The coupled equations for the conformation tensor and velocity field in the FENE-P model are:

$$\partial_t \boldsymbol{u} + (\boldsymbol{u}\cdot\boldsymbol{\nabla})\boldsymbol{u} = -\boldsymbol{\nabla} p + \nu\Delta\boldsymbol{u} + \frac{2\eta\,\nu}{\tau} f(\mathrm{tr}\boldsymbol{\sigma})\boldsymbol{\nabla}\cdot\boldsymbol{\sigma} + \boldsymbol{f} \tag{3.41}$$

$$\partial_t \boldsymbol{\sigma} + (\boldsymbol{u}\cdot\boldsymbol{\nabla})\boldsymbol{\sigma} = (\boldsymbol{\nabla}\boldsymbol{u})^T\cdot\boldsymbol{\sigma} + \boldsymbol{\sigma}\cdot(\boldsymbol{\nabla}\boldsymbol{u}) - \frac{2}{\tau}(f(\mathrm{tr}\boldsymbol{\sigma})\boldsymbol{\sigma} - \mathbf{1})\ , \tag{3.42}$$

where the non linear factor has been rewritten has:

$$f(\mathrm{tr}\boldsymbol{\sigma}) = \frac{\mathrm{tr}_{max} - \mathrm{tr}\mathbf{1}}{\mathrm{tr}_{max} - \mathrm{tr}\boldsymbol{\sigma}} \tag{3.43}$$

with $\mathrm{tr}_{max} = R^2_{max}/R^2_0$.

The FENE-P model provides an improvement of the simple linear model, because it is able to reproduce some features of polymer solutions like the shear thinning, i.e. the decrease of the viscosity at increasing shear rates, which are not included in Oldroyd-B model. Moreover in numerical simulations, a finite molecular extensibility reduces the onset of numerical instabilities associated with strong gradients of the conformation tensor field. For these reasons FENE-P model is usually adopted in numerical simulations of viscoelastic channel flows [61, 62].

3.5 Drag reduction

The phenomenon of drag reduction, reported for the first time by the British chemist Toms in 1949, is probably the effect produced by polymer addiction in fluids which has attracted the most attention, because of its relevance for applications. While performing experiments on the degradation of polymers, Toms observed that the addition of few parts per million of long chain polymers in turbulent flow produces a dramatic reduction of the friction drag.

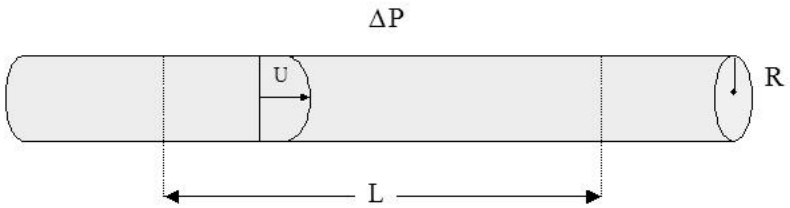

The adimensional quantity which is normally used to measure the friction drag in a pipe flow is the *Fanning friction factor* f defined as:

$$f = \frac{\Delta p}{\rho V^2}\frac{R}{L} \tag{3.44}$$

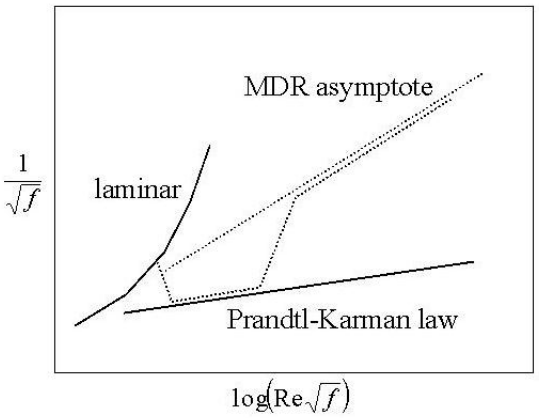

Figure 3.3: A schematic illustrating the onset of drag reduction and the MDR asymptote in the Prandtl-Karman coordinates. The Prandtl-Karman law correspond to the turbulent behavior of Newtonian fluids. The dotted line represent qualitatively the friction reduction in the viscoelastic case.

where R is the radius of the pipe, Δp is the pressure drop measured across a distance L in the pipe, ρ is the density of the fluid and V is the mean velocity over the section.

The physical meaning of the friction factor is the ratio between the input of energy provided by an external pressure difference and the kinetic energy of the resulting mean flow in the pipe, and essentially it gives a measure of the force that is required to sustain a certain mean flow. Rephrasing the drag reduction in this terms, it means that the force necessary to pump a fluid through a pipe can be reduced of a factor 80% with the simple addition of few ppm of polymers. The relevance for practical applications is thus enormous.

In Newtonian fluids the friction drag is a function of the Reynolds number, which for the pipe flow reads $Re = 2RV/\nu$ where ν is the kinematic viscosity. The dependence of the friction drag on the Re number is conventionally shown in the so-called Prandtl-Karman coordinates: $1/\sqrt{f}$ versus $\log(Re\sqrt{f})$ (see Figure (3.3)).

In the laminar regime the friction drag decrease as Re^{-1} until the critical Re number is reached. Transition to turbulence causes a sudden increase of the friction drag which for fully developed turbulence reaches an almost constant value with only a weak logarithmic dependence on Re described by the Prandtl-Karman (P-K) law (a straight line in P-K coordinates).

Dilute polymer solutions deviate from the P-K law: while for Re number smaller than a critical threshold their behavior is similar to the Newtonian fluid, for larger Re numbers the friction drag is drastically reduced with re-

spect to the Newtonian case and it finally reaches a universal asymptote which is independent on the kind of polymers or the concentration of the solution, and is known in literature as the *Maximum Drag Reduction asymptote* (MDR). A theory based on the elastic behavior of polymers was proposed by Tabor & de Gennes in 1986[58] to explain both the onset of the drag reduction and the presence of the universal upper bound, but its validity is still controversial. An overview of this theory can be found in Sreenivasan and White[59].

Recent works have provided new insights on the matter. A shell-model based on the Fene-P model has been proposed by Benzi *et al.* [64], which provides a simple and usefull tool for understanding the phenomenon of drag reduction. Numerical simulations of Oldroyd-B and Fene-P models are able to reproduce, at least qualitatively, the phenomenology of the problem [60, 62], and and have proved that drag reduction can occurs also in absence of boundaries [55]. Moreover, some experiments seems to indicate a peel off from the MDR asymptote at high Re numbers, opening new questions.

The interest for drag reduction is clearly amplified by its possible applications. Indeed nowadays it is widely applied in oil and water pipelines and specific polymers have been developed to reduce hydraulic friction for industrial and petrochemical applications.

3.6 Elastic turbulence

The phenomenon of elastic turbulence in viscoelastic solutions has been discovered very recently [65, 66]. While the drag reduction is a high Reynolds number phenomenon the elastic turbulence occurs at low Re numbers. The presence of polymer changes the stability of the laminar flow, and polymers with large elasticity (i.e. large relaxation time) can be stretched even by a weak primary shear flow, producing elastic instabilities which causes irregular secondary flow. This flow stretch further the polymer molecules, and because of their back reaction becomes increasingly turbulent, until a kind of saturated dynamic state is reached.

Transition to elastic turbulence has been observed at extremely small Re numbers (e.g. $Re \simeq 10^{-3}$, see [65]). Although the Re numbers can be arbitrarily small, the resulting flow displays all the main features of developed turbulence, as the enhancement of mixing and the power law spectrum of velocity fluctuations.

In some sense this phenomenon acts in the opposite direction of the drag reduction: at high Re numbers the polymers tend to suppress the small velocity fluctuations, reducing the turbulent drag, while at low Re number

they can destroy the laminar flow pumping energy to small scale motions through elastic instabilities.

Indeed, a linear stability analysis of Oldroyd-B model shows the presence of elastic instabilities in shear flows at small Re numbers and large Deborah numbers $De = U\tau/L$. For concentrations of polymer larger than the critical value $\eta* = 3/7$ it can be shown that the critical Re number for elastic instabilities vanishes at large enough De numbers, allowing for a possible transition to elastic turbulence at arbitrarily small Re number.

It seems thus that the simple Oldroyd-B model is able to reproduce, at least qualitatively, both the drag reduction and the elastic turbulence phenomena, and it constitutes an optimal tool for numerical and theoretical investigations.

Chapter 4

Two-dimensional turbulence of dilute polymer solutions

Since the discovery of the spectacular effect of drag reduction, most of the experimental and theoretical works have been devoted to the study of three-dimensional dilute polymer solution (see, e.g. Refs. [67, 42, 59]), while the two-dimensional case is remained quite unexplored.

Indeed, recent experiments on soap films [68] have shown that polymer addition in two-dimensional flow can give origin to completely different phenomena with respect to the three-dimensional case (see also Refs. [69, 70]).

At variance with the three-dimensional case, where thanks to the drag reduction effect, polymer addition allows to reduce the external force which is necessary to sustain a fixed mean kinetic energy in the pipe flow, in two-dimensional flows polymer injection causes a strong depletion of large-scale velocity.

It is thus questionable if simple models like Oldroyd-B are able to grasp also the two-dimensional phenomenology of viscoelastic flows.

In this chapter I will address this question, showing that Oldroyd-B model indeed describes also these new phenomena and moreover it provides a clear understanding of the physical origin of the different behavior between the 2d and 3d case.

I will then show that the presence of polymers causes a strong reduction of Lagrangian chaos, and influences the decay of two-dimensional turbulence as well as the the inverse energy cascade, which can be completely depleted for large enough polymer elasticity.

4.1 2D Oldroyd-B model

The study of two-dimensional viscoelastic solutions will be addressed by means of the two-dimensional version of Oldroyd-B model (3.12-3.16), which is described by the equations:

$$\partial_t \boldsymbol{u} + (\boldsymbol{u}\cdot\boldsymbol{\nabla})\boldsymbol{u} = -\boldsymbol{\nabla} p + \nu\Delta\boldsymbol{u} + \frac{2\eta\,\nu}{\tau}\boldsymbol{\nabla}\cdot\boldsymbol{\sigma} - \alpha\boldsymbol{u} + \boldsymbol{f} \tag{4.1}$$

$$\partial_t \boldsymbol{\sigma} + (\boldsymbol{u}\cdot\boldsymbol{\nabla})\boldsymbol{\sigma} = (\boldsymbol{\nabla}\boldsymbol{u})^T\cdot\boldsymbol{\sigma} + \boldsymbol{\sigma}\cdot(\boldsymbol{\nabla}\boldsymbol{u}) - \frac{2}{\tau}(\boldsymbol{\sigma}-\mathbf{1}) \tag{4.2}$$

The matrix $\boldsymbol{\sigma}$ is the conformation tensor of polymer molecules

$$\sigma_{ij} = R_0^{-2}\langle R_i R_j\rangle \tag{4.3}$$

and its trace tr$\boldsymbol{\sigma}$ is a measure of their square elongation. Because of its physical meaning the conformation tensor is symmetric and positive definite. The parameter τ is the (slowest) polymer relaxation time toward the equilibrium length R_0, therefore in absence of stretching the conformation tensor therefore relaxes to the the unit tensor $\mathbf{1}$. The matrix of velocity gradients which stretches the polymers is defined as $(\boldsymbol{\nabla}\boldsymbol{u})_{ij} = \partial_i u_j$. The solvent viscosity is denoted by ν and η is the zero-shear contribution of polymers to the total solution viscosity $\nu_t = \nu(1+\eta)$. The pressure term $-\boldsymbol{\nabla} p$ ensures incompressibility of the velocity field, which can be expressed in terms of the stream-function ψ as $\boldsymbol{u} = (\partial_y\psi, -\partial_x\psi)$. The dissipative term $-\alpha\boldsymbol{u}$ models the mechanical friction between the thin layer of fluid and the surrounding environment, and plays a prominent role in the energy budget of Newtonian two-dimensional turbulence [71]. The energy source is provided by the large-scale forcing $\boldsymbol{f}$, which is Gaussian, statistically homogeneous and isotropic, δ-correlated in time, with correlation length $L_f \approx 4$.

The numerical integration is performed by a fully dealiased pseudospectral code, with second-order Runge Kutta scheme, at different resolutions, $N^2 = 128^2, 256^2$ grid points, on a doubly periodic square box of size $L = 2\pi$. As customary, an artificial stress-diffusivity term $\kappa\Delta\boldsymbol{\sigma}$ is added to Eq.(4.2) to prevent numerical instabilities [72]. For the passive case we have adopted a Lagrangian code which explicitly which preserves the symmetries of the conformation tensor (see Appendix A).

4.2 Passive polymers

The feedback of polymers included in Oldroyd-B model is proportional to their concentration n through the parameter $\eta \propto n$ in Eq (4.1). In the limit

$\eta = 0$ polymers are passively transported and stretched by Newtonian two-dimensional turbulence. The flow is driven at the largest scales and develops an enstrophy cascade towards the small scales, while the inverse energy flux is immediately halted by friction. The ensuing velocity field is therefore everywhere smooth. According to Refs.[75, 52, 54] the statistics of stretched polymers in random smooth flows is expected to depend critically on the value of the Weissenberg number, here defined as

$$Wi = \lambda_N \tau \tag{4.4}$$

where λ_N is the maximum Lyapunov exponent of the Newtonian flow.

4.2.1 Coiled state

Below the coil-stretch transition, at $Wi < 1$ the polymer molecules spend most of the time in a coiled state, and stretch occasionally by a considerable amount with a strongly intermittent behavior (see Figure 4.1).

Following Balkovsky *et al* [54] Equation (4.2) for the conformation tensor can be written in the Lagrangian reference frame as:

$$\dot{\boldsymbol{\sigma}} = (\boldsymbol{\nabla u})^T \cdot \boldsymbol{\sigma} + \boldsymbol{\sigma} \cdot (\boldsymbol{\nabla u}) - \frac{2}{\tau}(\boldsymbol{\sigma} - \mathbf{1}) \ . \tag{4.5}$$

where conformation tensor $\boldsymbol{\sigma}$ and the velocity gradients $(\boldsymbol{\nabla u})_{ij} = \partial_i u_j$ are valued along the Lagrangian trajectory

$$\dot{\boldsymbol{X}}(s) = \boldsymbol{v}(\boldsymbol{X}(s), s). \tag{4.6}$$

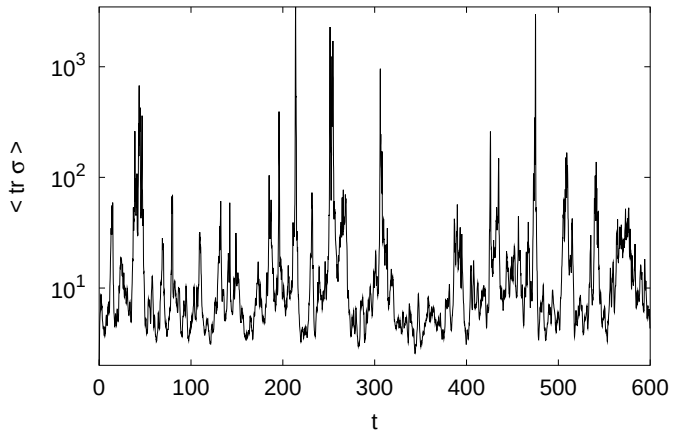

Figure 4.1: Mean square elongation $\int \mathrm{tr}\boldsymbol{\sigma}(\boldsymbol{x}, t)\, d\boldsymbol{x}$ of passive polymers as a function of time. Even in the coiled state ($Wi = \lambda_N \tau = 0.27$) polymers may experience strong elongations.

The value of the conformation tensor can be obtained following backward in time the Lagrangian trajectory which satisfies the condition $\boldsymbol{X}(t) = \boldsymbol{x}$ as:

$$\boldsymbol{\sigma}(\boldsymbol{x}, t) = \frac{2}{\tau} \int_{\infty}^{t} \boldsymbol{W}(t, s, \boldsymbol{x}) \boldsymbol{W}^T(t, s, \boldsymbol{x}) e^{-2(t-s)/\tau} \ , \tag{4.7}$$

The Lagrangian mapping matrix $\boldsymbol{W}$, defined by the relations

$$\partial_t \boldsymbol{W}(t, s) = (\boldsymbol{\nabla u}) \boldsymbol{W} \ , \boldsymbol{W}(s, s) = \mathbf{1} \tag{4.8}$$

describes the deformation of an infinitesimal fluid element along a given Lagrangian trajectory. The meaning of Eq. (4.7) is clear: the value of the conformation tensor at a given time is determined by the stretching due to velocity gradients that it has experienced during its past history, modulated by its exponential relaxation toward the equilibrium configuration.

The matrix $\boldsymbol{W}$ can be decomposed as

$$\boldsymbol{W}(t, s) = \boldsymbol{M} \boldsymbol{\Lambda} \boldsymbol{N} \tag{4.9}$$

where $\boldsymbol{M}$ and $\boldsymbol{N}$ are orthogonal matrices, and $\boldsymbol{\Lambda}$ is diagonal. Incompressibility of the flow imposes the condition $\det \boldsymbol{W} = 1$, and consequently the diagonal elements of $\boldsymbol{\Lambda}$ can be written as $e^{\gamma(t-s)}$ and $e^{-\gamma(t-s)}$, where γ is the finite-time Lyapunov exponent at time $t - s$. For time larger than the times correlation of velocity gradients the eigenvectors of the matrix $\boldsymbol{W}\boldsymbol{W}^T$ tend to the directions of the Lyapunov vectors, the matrix $\boldsymbol{M}$ became almost time-independent, and the finite-time Lyapunov exponents γ fluctuate around the value of the leading Lyapunov exponent λ. The trace of the conformation tensor can thus be written as

$$\mathrm{tr}\boldsymbol{\sigma}(\boldsymbol{x}, t) = \frac{2}{\tau} \int_{\infty}^{t} \mathrm{tr}\boldsymbol{\Lambda}^2(t, s, \boldsymbol{x}) e^{-2(t-s)/\tau} \ , \tag{4.10}$$

This allows to obtain a lower bound for the square polymer elongations. Since incompressibility imposes $\det \boldsymbol{\Lambda} = 1$ the eigenvalues of $\boldsymbol{\Lambda}^2$ can be written as e^{2x} and e^{-2x}. This leads to the inequality $\mathrm{tr}\boldsymbol{\Lambda}^2 = e^{2x} + e^{-2x} \geq 2$ which together with Eq. (4.10) gives the bound for the trace of the conformation tensor:

$$\mathrm{tr}\boldsymbol{\sigma} \geq \mathrm{tr}\mathbf{1} \tag{4.11}$$

Moreover Eq (4.10) allows to evaluate the statistics of polymer elongations in term of the statistics of finite-time Lyapunov exponents $P(\gamma, t) \propto \exp[-tS(\gamma)]$ as:

$$< (\mathrm{tr}\boldsymbol{\sigma})^q > \sim \int d\gamma e^{-t\left[S(\gamma) - 2q\left(\gamma - \frac{1}{\tau}\right)\right]} \tag{4.12}$$

where $S(\gamma)$ is the Cramér rate function (see, e.g., Ref. [73]). Intense stretching events give contributions to the right tail of the probability density function of $\mathrm{tr}\boldsymbol{\sigma}$ leading to the power law prediction:

$$p(\mathrm{tr}\boldsymbol{\sigma}) \sim (\mathrm{tr}\boldsymbol{\sigma})^{-1-q} \qquad \text{for} \qquad \mathrm{tr}\boldsymbol{\sigma} \gg \mathrm{tr}\mathbf{1} \; . \tag{4.13}$$

The exponent q is related to the probability of finite-time Lyapunov exponents via the equation

$$L_{2q} = 2q/\tau \tag{4.14}$$

where

$$L_{2q} = \max_{\gamma}[2q\gamma - S(\gamma)] \tag{4.15}$$

is the generalized Lyapunov exponent of order $2q$. The convexity of the Cramér rate function $S(\gamma)$ ensures the positivity of q for $Wi < 1$.

Since the distribution of polymer elongations is not accessible experimentally, in order to validate the theory it is necessary to resort to numerical simulations. Eckhardt et al. in Ref. [77] have given the first evidence of a power law tail for the probability distribution function of polymer elongation in three-dimensional shear turbulence. As shown in Fig. 4.2, in our two-dimensional simulations we observe a neat power law as well.

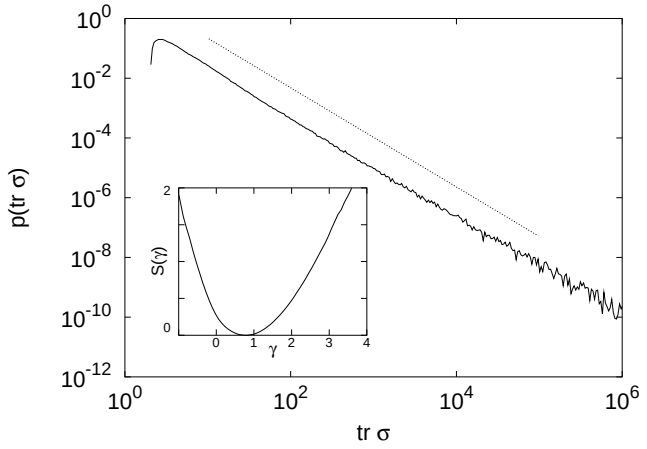

Figure 4.2: Power law tail of the probability density function of polymer square elongation, in the passive case $\eta = 0$. The Weissenberg number is $Wi = 0.4$, quite below the coil-stretch transition. The power law $(\mathrm{tr}\boldsymbol{\sigma})^{-1-q}$ with the value $q = 0.66$ (numerically obtained from the relation $L_{2q} = 2q/\tau$) is drawn for comparison. In the inset, the corresponding Cramér function $S(\gamma)$. Its minimum is $S(\lambda_N) = 0$, with $\lambda_N \simeq 0.8$.

In order to check whether the observed exponent coincides with the prediction (4.14) we have also performed direct numerical simulations of particle trajectories, and measured the probability distribution of finite-time Lyapunov exponents, thereby obtaining the expected q. The numerical result is in close agreement with theory.

4.2.2 Stretched state

As the Weissenberg number exceeds unity, the linear relaxation of polymers is no more able to overcome the average stretching of velocity gradients. On the contrary polymers start to elongate exponentially, and the statistics of the conformation tensor does not reach a steady state. The pdf of the trace of conformation tensor becomes unsteady, with a power-law tail which keeps moving to higher elongations (see Fig. 4.3). All the moments of conformation tensor statistics $\langle(\mathrm{tr}\boldsymbol{\sigma})^q\rangle$ grow exponentially in time, according to

$$< (\mathrm{tr}\boldsymbol{\sigma})^q > \sim e^{(L_{2q}-\frac{2q}{\tau})t} \tag{4.16}$$

In Figure (4.4) we show the exponential growth of the mean square elongation $< \mathrm{tr}\boldsymbol{\sigma} >$ for $Wi = \lambda_N \tau = 1.6$, compared with the prediction (4.16). Here $\tau = 2$, and the value of the generalized Lyapunov exponent $L_2 =\simeq 3.8$ has been obtained according to $L_{2q} = \max_\gamma[2q\gamma - S(\gamma)]$. For comparison we show also the steady state in a coiled case ($Wi = 0.27$).

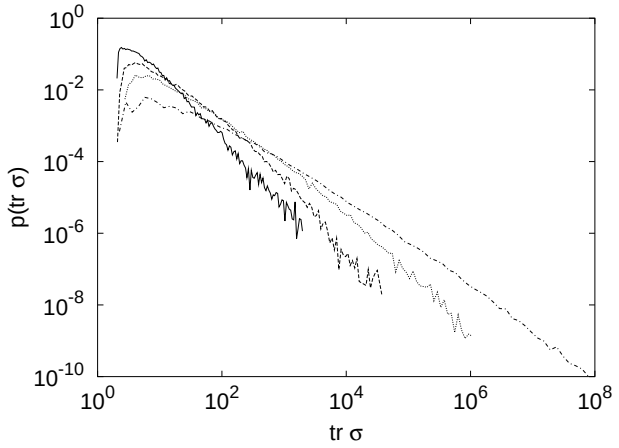

Figure 4.3: Pdfs of polymer square elongation for $Wi = \lambda_n \tau = 1.60$ at different times: $t = 1/2\tau$ (solid line), $t = \tau$ (dashed line), $t = 2\tau$ (dotted line), $t = 4\tau$ (dash-dotted line). Above the coil-stretch transition, the pdf of elongations becomes unsteady

This "coil-stretch" transition signals the breakdown of linear passive theory. Accounting for the nonlinear elastic modulus of polymer molecules allows to recover a stationary statistics and to develop a consistent theory of passive polymers at all Weissenberg numbers [78]. In the following we do not pursue that approach, but we rather focus on a different mechanism that limits polymer elongation: the feedback of polymers on the advecting flow.

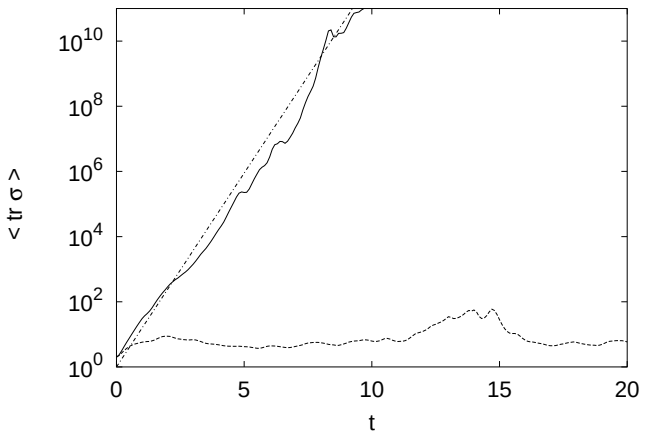

Figure 4.4: Mean square elongation $\int \mathrm{tr}\boldsymbol{\sigma}(\boldsymbol{x},t)\,d\boldsymbol{x}$ of passive polymers as a function of time. In the stretched case ($Wi = \lambda_N \tau = 1.6$ solid line) the mean square elongation grows exponentially according to Eq. (4.16) (dash dotted line), while in the coiled case ($Wi = 0.27$ dashed line) it reaches a statistically steady state.

4.3 Active polymers

At finite value of the concentration, when $\eta > 0$, the back reaction of polymers can not be neglected. Polymers can affect significantly the velocity dynamics, provided that they are sufficiently elongated – a condition that is met at $Wi > 1$. This strong feedback regime is characterized in two dimensions by a suppression of large-scale velocity fluctuations, an effect first observed in soap film experiments [68]. In Figure 4.5 are reported two images of soap film experiments from Amarouchene & Kellay. The large vortices in the polymer-free case are strongly reduced by polymer addition. The same behavior is observed in numerical simulations of 2D Oldroyd-B model (Figure 4.6).

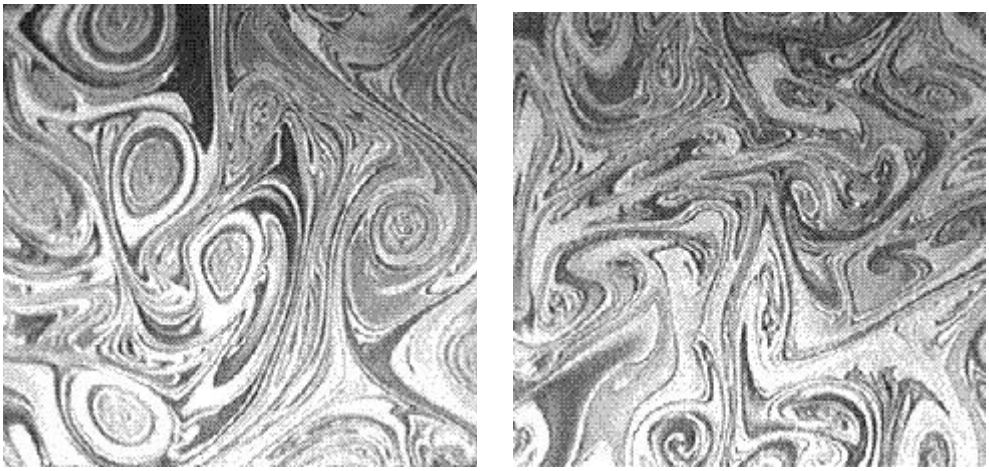

Figure 4.5: Interferograms of the thickness field of a soap film in the polymer-free case (left) and viscoelastic case (right). Y. Amarouchene, H. Kellay, Phys. Rev. Lett. **89**, 104502 (2002)

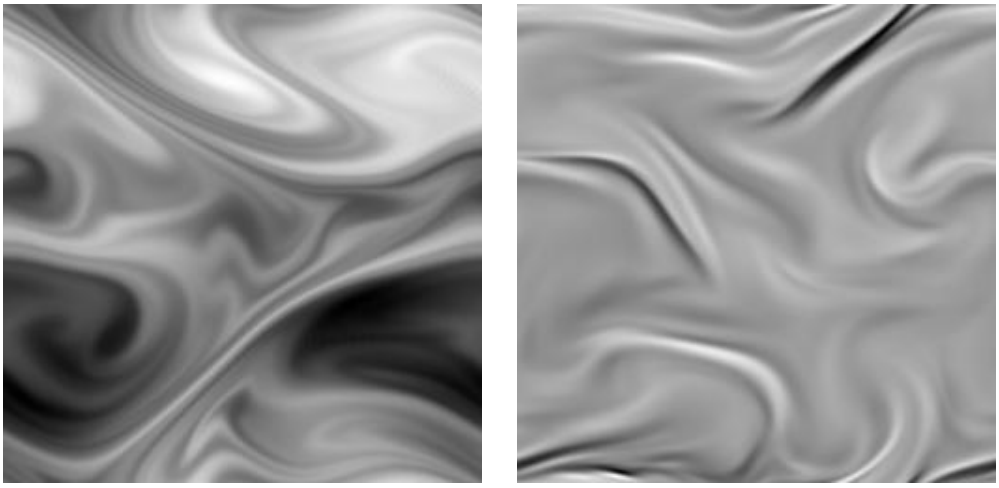

Figure 4.6: Snapshots of the vorticity field $\boldsymbol{\nabla} \times \boldsymbol{u}$ in the Newtonian (left) and in the viscoelastic case with strong feedback (right). Notice the suppression of large-scale structures in the latter case.

4.3.1 Depletion of kinetic energy

In Fig. 4.7 we present the time evolution of the total kinetic energy of the system in numerical simulations obtained by numerical integration of the viscoelastic model described by Eqs (4.1 - 4.2).

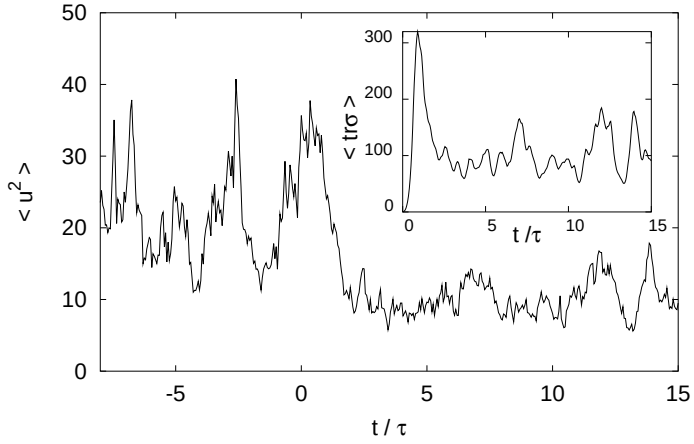

Figure 4.7: Dilute polymers reduce the level of velocity fluctuations $\int |\boldsymbol{u}(\boldsymbol{x},t)|^2\, d\boldsymbol{x}$. Polymers are introduced in the flow at $t = 0$. In the inset, the mean square elongation $\int \mathrm{tr}\boldsymbol{\sigma}(\boldsymbol{x},t)\, d\boldsymbol{x}$ as a function of time.

We fixed the relaxation time of polymer $\tau = 2$, such that the Weissenberg number $Wi = \lambda_N \tau = 1.6$ is above the coil-stretch transition. In the inset it is shown the corresponding evolution of the mean square elongation $\int \mathrm{tr}\boldsymbol{\sigma}(\boldsymbol{x},t)\, d\boldsymbol{x}$. At time $t = 0$ the polymer are injected in the zero-shear equilibrium state in the fluid, and they start to be stretched by the flow. In the initial stage, for time $t < \tau$, their elongation grows exponentially as in the passive case, but when the back-reaction switches on a drastic depletion of kinetic energy occurs, and the polymer elongation relaxes to a statistically steady state. Fluctuations of the mean square elongation are strongly correlated with the kinetic energy and follow its temporal evolution with a small time delay, revealing the continuous exchange between kinetic and elastic energy. The strong reduction of kinetic energy should be contrasted with the three-dimensional case where, on the opposite, velocity fluctuations are larger in the viscoelastic case than in the Newtonian one [61].

4.3.2 Energy balance

The suppression of velocity fluctuations by polymer additives in two-dimensional turbulence can be easily explained in the context of the randomly driven viscoelastic model. Indeed, the average kinetic energy balance in the statistically stationary state reads

$$F = \epsilon + \frac{2\eta\nu}{\tau^2}(\langle \mathrm{tr}\boldsymbol{\sigma}\rangle - \mathrm{tr}\mathbf{1}) + \alpha\langle|\boldsymbol{u}|^2\rangle \tag{4.17}$$

where $\epsilon = \nu\langle|\boldsymbol{\nabla u}|^2\rangle$ is the viscous dissipation and F is the average energy input, which is flow-independent for a Gaussian, δ-correlated random forcing $\boldsymbol{f}$. To obtain Eq. (4.17) we multiply Eq. (4.1) by $\boldsymbol{u}$, add to it the trace of Eq. (4.2) times $\eta\nu/\tau$, and average over space and time. Since in two dimensions kinetic energy flows towards large scales, it is mainly drained by friction, and viscous dissipation is vanishingly small in the limit of very large Reynolds numbers [71]. Neglecting ϵ and observing that in the Newtonian case ($\eta = 0$) the balance (4.8) yields $F = \alpha\langle|\boldsymbol{u}|^2\rangle_N$, we obtain

$$\langle|\boldsymbol{u}|^2\rangle = \langle|\boldsymbol{u}|^2\rangle_N - \frac{2\eta\nu}{\alpha\tau^2}(\langle \mathrm{tr}\boldsymbol{\sigma}\rangle - \mathrm{tr}\mathbf{1})\,. \tag{4.18}$$

According to Eq (4.11), incompressibility of the flow ensures that $\mathrm{tr}\boldsymbol{\sigma} \geq \mathrm{tr}\mathbf{1}$, and we finally have $\langle|\boldsymbol{u}|^2\rangle \leq \langle|\boldsymbol{u}|^2\rangle_N$, in agreement with numerical results. This simple energy balance argument can be generalized to nonlinear elastic models. As viscosity tends to zero, the average polymer elongation increases so as to compensate for the factor ν in eq. (4.18), resulting in a finite effect also in the infinite Re limit. Since energy is essentially dissipated by linear friction, the depletion of $\langle|\boldsymbol{u}|^2\rangle$ entails immediately the reduction of energy dissipation. The main difference between two-dimensional "friction reduction" and three-dimensional drag reduction resides in the lengthscales involved in the energy drain, i.e. large scales in 2D *vs* small scales in 3D.

4.3.3 Statistics of velocity fluctuations

The effect of polymer additives cannot be merely represented by a rescaling of velocity fluctuations by a given factor. In Fig. 4.8 we show the probability distribution of a velocity component, u_x. The choice of the x direction is immaterial by virtue of statistical isotropy. In the Newtonian case the distribution is remarkably close to the sub-Gaussian density $N\exp(-c|u_x|^3)$ stemming from the balance between forcing and nonlinear terms in the Navier-Stokes equation, in agreement with the prediction by Falkovich and Lebedev [79]. On the contrary, the distribution in the viscoelastic case is markedly super-Gaussian, with approximately exponential tails. This strong intermittency

in the velocity dynamics is due to the alternation of quiescent low-velocity phases ruled by polymer feedback and bursting events where inertial nonlinearities take over.

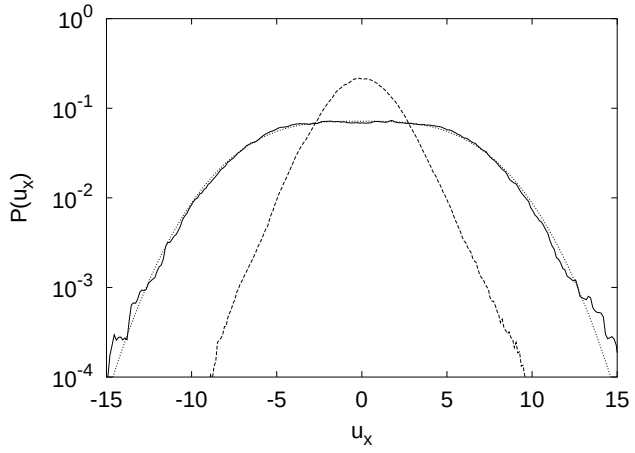

Figure 4.8: Intermittency of velocity fluctuations induced by polymer additives. The probability density function $P(u_x)$ of the velocity component u_x for the Newtonian (solid line) and for the viscoelastic case with strong feedback (dashed line). Same parameters as in Fig. 4.6. Also shown the distribution $\Gamma(2/3)3^{3/2}\exp(-c|u_x|^3)/(4\pi c)$ with $c = 2.1 \cdot 10^{-3}$ (dotted line).

The sub-Gaussian shape of the pdf of velocities in the Newtonian case can be predicted from the statistics of the forcing with the following dimensional argument. The values of velocity can be considered as the result of summation of forcing contributions during one large-eddy turnover time $t_L \sim L/V$.

In the case of a *slow forcing*, with a decorrelation time τ_f longer that the large-eddy turnover time $\tau_f > t_L$, those contributions are correlated, producing a ballistic growth of velocity $V(t) \sim ft$ up to the time $t_L \sim L/V$ when the non-linear term starts to transfer energy down in the cascade. Thus we obtain the dimensional estimate $V \sim ft_L \sim fL/V$, or equivalently $V^2 \sim Lf$, which can be used to link the pdf of the forcing to the pdf of velocities. If the statistics of forcing is Gaussian $P(f) = Ne^{-f^2/2F_0}$, the resulting pdf for velocities is $P(V) = Ne^{-\beta V^4}$

Since we are using a Gaussian, δ-correlated in time forcing, we are in the opposite limit of *fast forcing*, with $\tau_f < t_L$. In this case the different contributions are independent, producing a diffusive growth $V^2(t) \sim f^2\tau_f t$ for $t \leq t_L \sim L/V$. Substituting the resulting dimensional estimate $V^3 \sim f^2\tau_f L$ in the Gaussian pdf of forcing we end with the prediction for the pdf of single

point velocities:

$$P(V) = Ne^{-\beta V^3} \tag{4.19}$$

which is consistent with our measurement.

4.3.4 Lagrangian chaos reduction

Dilute polymers also alter significantly the distribution of finite-time Lyapunov exponents $P(\gamma, t)$. In Fig. 4.9 the Cramér rate function $S(\gamma) \propto t^{-1} \ln P(\gamma, t)$ is shown for the Newtonian and for the viscoelastic case.

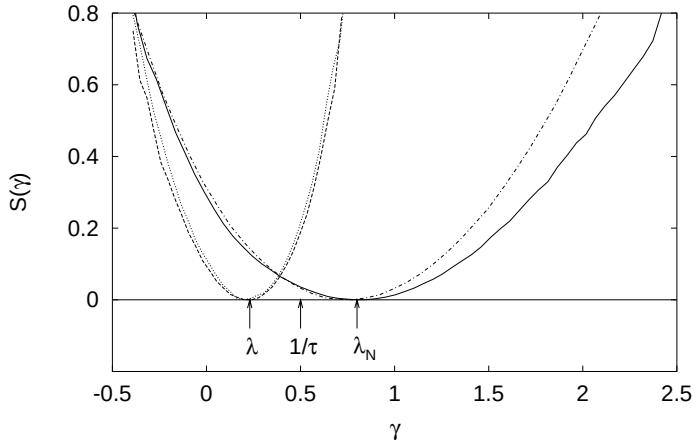

Figure 4.9: Finite-time Lyapunov exponents decrease in presence of polymers. The Cramér rate function $S(\gamma)$ for the Newtonian (solid line) and for the viscoelastic case with strong feedback ($Wi = \lambda_N \tau = 1.6$, dashed line). Viscosity $\nu = 6 \cdot 10^{-3}$, relaxation time $\tau = 2$, $\eta = 0.2$ (dashed), $\eta = 2$ (dotted). For sake of completeness, we also show $S(\gamma)$ for a mild feedback case ($Wi = 0.4$, $\eta = 0.2$, dash-dotted line). In the latter case, the Lyapunov exponent is practically identical to the Newtonian value, and polymers affect only the right tail of $S(\gamma)$ reducing appreciably the probability of large stretching events $\gamma \gg \lambda_N$.

Since in the former situation the Lyapunov exponent λ_N is greater than $1/\tau$, were the polymers passive all moments of elongation would grow exponentially fast. However, the feedback can damp stretching so effectively that after polymer addition λ lies below $1/\tau$. This implies a strong reduction of Lagrangian chaos and a decreased mixing efficiency. Moreover, we find that L_n is smaller than n/τ for all n, a result which guarantees the stationarity of the statistics of tr$\boldsymbol{\sigma}$ in presence of feedback, while imposing a less restrictive condition on $S(\gamma)$ than the one proposed in Ref. [54]. The lowering of

$\lambda\tau$ below unity would seem to contradict the statement that strong feedback takes place only at $Wi > 1$. Actually there is no inconsistency, since the critical value $Wi = 1$ holds for passive polymers only. For active polymers, the presence of correlations between the conformation tensor and the stretching exponents can indeed lower significantly the threshold. For a discussion of the differences between active and passive transport, see Ref. [80]

4.3.5 Decaying turbulence

The organization into coherent vortices, starting from from a disordered background is a characteristic feature of decaying two-dimensional turbulence (see Chapter 1). This complex and interesting phenomenology is suppressed by the presence of a strong friction which halts the flux of energy toward large scales. Since in this case the energy is mainly dissipated by the linear friction, the decay of total energy trivially display an exponential behavior $E(t) \simeq E(0)e^{2\alpha t}$ where α is the friction coefficient. (see Fig. 4.10).

The coupling with polymer dynamics changes in a different way the decay of two-dimensional turbulence. Starting from different configuration randomly chosen from the statistically steady state above the coil-stretch tran-

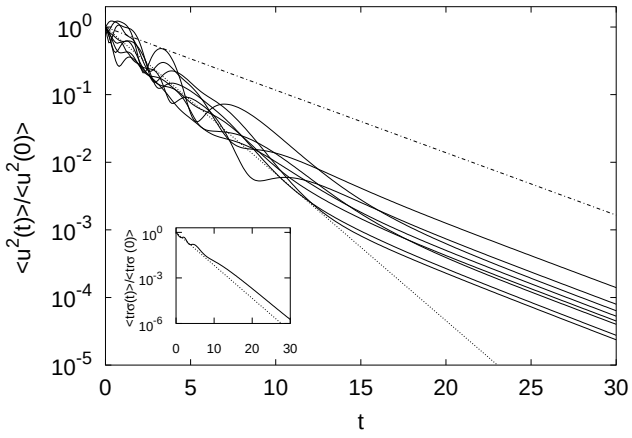

Figure 4.10: Decay of mean velocity fluctuation $\langle u^2(t)\rangle$. While in the Newtonian case (dashed line) the decay is exponential with a rate fixed by the friction coefficient $\langle u^2(t)\rangle = \langle u^2(0)\rangle e^{-2\alpha t}$ the viscoelastic solution shows an oscillatory behavior with an exponential trend fixed by the polymer relaxation time. The oscillations are anti-correlated with those of the mean elastic energy (see inset). At late stage there is a sharp decoupling of the polymer and velocity fields which recovers the Newtonian behavior.

sition $Wi \simeq 3.2$ we turned off the forcing on the velocity field and let the coupled system decay. In the first stage the balance is dominated by polymer contribution. An oscillatory decay of the kinetic energy is observable (see Fig. 4.10), with an exponential trend fixed by the polymer relaxation time, while the friction term in the energy balance seems to be sub-dominant. Thus the mean square elongation of polymers decay exponentially as $tr(\boldsymbol{\sigma}) \sim e^{2t/\tau}$, with over-imposed strong oscillations which are anti-correlated to those of the kinetic energy. In this stage there is a continuous exchange of energy between the velocity field and polymers and the decay of the two fields is strongly coupled. Since the trend of decay imposed by the polymers is steeper than the exponential decay predicted by the friction, at a certain moment the feedback term which slaves the kinetic energy decay becomes smaller than friction one. From this point there is a sharp decoupling of the dynamics of the two fields: the oscillations disappear and each field decays exponentially with his own characteristic time: τ for polymers and $\frac{1}{\alpha}$ for velocity, which in this late stage recovers the Newtonian behavior.

4.3.6 Inverse energy cascade

The strong influence of polymers on the energy balance pose the intriguing question of the possible effects on the inverse energy cascade which occurs in the Newtonian case. Indeed, in absence of friction, the growth rate of kinetic energy $E(t) = 1/2\langle|\boldsymbol{u}(t)|^2\rangle$ can be obtained repeating the derivation of the energy balance (4.17) but averaging only over space and over the statistics of the random forcing $\boldsymbol{f}$:

$$\frac{dE}{dt} = F - \epsilon - \frac{2\eta\nu}{\tau^2}(\langle \mathrm{tr}\boldsymbol{\sigma}(t)\rangle - \mathrm{tr}\mathbf{1}) \tag{4.20}$$

As already shown, the polymer contribution has a definite sign, acting as a dissipative term. Neglecting the viscous dissipation ϵ, which in the limit of infinite Reynolds number is vanishingly small, it is clear from Eq. (4.20) that the energy growth rate in the viscoelastic case is reduced with respect to the Newtonian case where it is essentially given by the input of the random forcing.

In order to measure the energy growth rate, I performed numerical simulations of the viscoelastic model using a slightly different configuration: I turned off the friction term and put the forcing on a smaller scale, allowing the energy to give origin to an inverse cascade. After an initial growth, the polymer elongation reaches indeed a statistically steady state, and consequently the energy growth rate is reduced of a constant fraction depending

on the concentration and the Weissenberg number of the polymer solution, in quantitative agreement with Eq. (4.20) (see Fig. (4.11)).

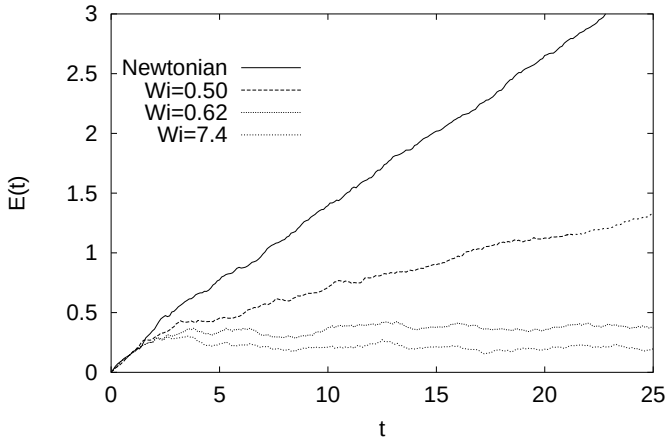

Figure 4.11: Linear growth of kinetic energy growth in absence of friction. The energy growth rate is reduced by the polymer feedback at increasing Wi number. If the Weissenberg number is large enough the energy growth can be completely stopped.

We remark the striking fact that at sufficiently high Wi numbers, the energy growth rate in the viscoelastic case can be reduced to zero when the polymer dissipation balances exactly the forcing input. This means that the inverse cascade can be completely suppressed by the polymer feedback even in absence of friction.

The feedback of polymers reacts on the fluid in order to reduce its velocity gradients. In the case of two-dimensional turbulence the power spectrum of velocity gradients is peaked at the forcing length-scale, thus is reasonable to assume that polymer feedback is essentially localized at the scale of forcing and does not entail the inertial range. Thus we expect to observe also for the viscoelastic two-dimensional solution the development of the inverse cascade, with a constant flux $\Pi(k) \simeq \epsilon$ reduced of a fraction depending on the elongation of the polymers:

$$\epsilon_{Viscoelastic} = \epsilon_{Newtonian} - \frac{2\eta\nu}{\tau^2}(\langle \mathrm{tr}\boldsymbol{\sigma}(t)\rangle - \mathrm{tr}\mathbf{1}) \tag{4.21}$$

A direct measurement of the energy flux requires a large scaling range in the inverse energy cascade, but at the same time it is necessary to resolve also the direct enstrophy cascade whose smooth flow is responsible of the polymer stretching. Unfortunately this task is unaffordable with actual

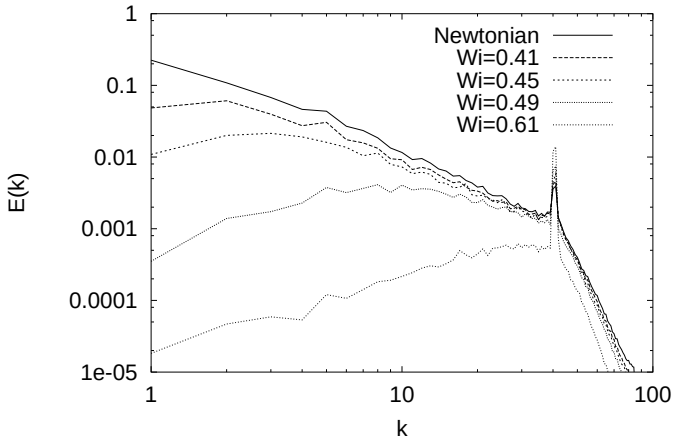

Figure 4.12: Inverse energy cascade in viscoelastic simulations. Increasing the Wi number the energy flux in the cascade is reduced and consequently the friction term stops the cascade at smaller scale.

computational resource. Nevertheless it is possible to have an indirect check of our prediction. The hypothesis of an inverse cascade with constant energy flux, leads to a Kolmogorov-like scaling law for the velocity fluctuations $u_\ell = \epsilon^{1/3}\ell^{1/3}$ with the reduced flux given by Eq. (4.21). The friction length scale ℓ_f where the friction term balance the nonlinear term responsible for the energy transfer, can be estimated by dimensional arguments (see Chapter 1) as $\ell_f \sim \epsilon^{1/2}\alpha^{-3/2}$. The reduction of the energy flux in the viscoelastic case should then reflect in a reduction of the friction length-scale. Restoring the friction term in our simulations, we checked that at increasing values of Wi number the inverse energy cascade is indeed stopped by friction at smaller scale as shown in Figure (4.12).

While the mean square polymer elongation $\langle \mathrm{tr}\boldsymbol{\sigma}(t)\rangle$ quickly reaches statistically constant values depending on the value of Wi, the kinetic energy grows up with different rates until it reaches the steady state fixed by the energy balance (4.17) (see Figure (4.13))

4.4 Summary

In this chapter it has been presented a theoretical and numerical investigation of the effects of polymer additives on two-dimensional turbulence by means of Oldroyd-B viscoelastic model.

In the passive case, i.e. neglecting the polymer feedback, I showed that for values of the Wi number below the *coil-stretch* transition the polymer

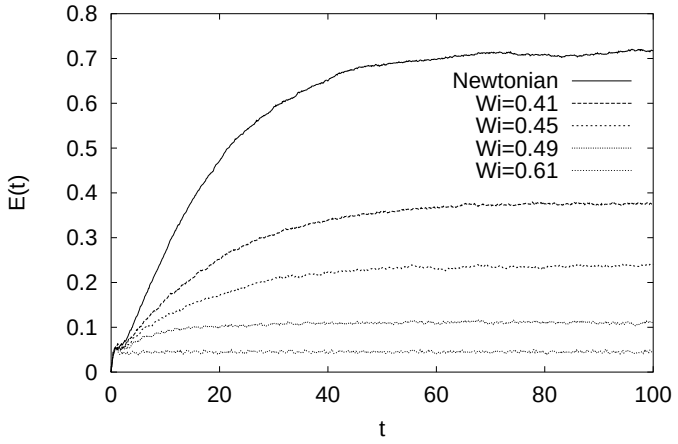

Figure 4.13: Average kinetic energy in viscoelastic simulations of the inverse energy cascade. In the initial stage the energy grows linearly with smaller rates at larger Wi numbers then it is stopped by the friction term at values determined by the energy balance (4.17)

elongations reaches a steady probability distribution functions with power-law tail. Its slope is related to the statistics of finite-time Lyapunov exponents of the flow, in quantitative agreement with theoretical predictions. Above the coil-stretch transition the statistics became unsteady.

Restoring the polymer feedback I showed that the kinetic energy of the fluid is drastically reduced in the viscoelastic case, as observed in soap film experiments. Oldroyd-B model provides a clear explanations of this phenomenon: part of the energy is converted into elastic energy of polymers, and consequently dissipated by their relaxation.

I showed that polymers cause a strong reduction of Lagrangian chaos, a phenomenon which is probably independent on the dimension of the space.

Finally I studied the effects of polymers on the inverse energy cascade, showing that for large enough elasticity the inverse cascade can be completely suppressed by the polymer feedback even in absence of friction.

Conclusions

In this thesis I have presented a numerical and theoretical study of the effects of friction and polymer additives on two-dimensional turbulence.

The Lagrangian description of turbulent transport has been used to demonstrate the equivalence between the statistics of small-scale fluctuations of vorticity in presence of friction and that of a passive scalar field with finite lifetime transported by the same velocity field. This allowed to obtain quantitative predictions for the steepening of the energy spectrum and the scaling exponents of the structure functions of vorticity, in terms of the statistics of finite-time Lyapunov exponents. These results have been validated by means of parallel integration of Navier-Stokes equation in two dimensions, supplemented by a linear fiction term, and of the advection-reaction-diffusion equation for the passive scalar with finite lifetime.

The effects of polymers have been studied by means of the linear viscoelastic model Oldroyd-B. A Lagrangian numerical code, which preserves the symmetries of the model has been developed to obtain accurate measurements of the probability distribution function of polymer elongation, which validate the predictions obtained within the Lagrangian approach. A strong reduction of kinetic energy as a consequence of polymer addition has been observed in numerical simulations of two-dimensional Oldroyd-B model, in agreement with results of soap film experiments. I showed that this phenomenon can be explained and predicted by means of the energy balance of Oldroyd-B model.

I have then studied the effects of polymers on the statistics of finite-time Lyapunov exponents, showing that a strong reduction of Lagrangian chaos occurs. This phenomenon seems to be independent on the dimensionality of the flow.

Finally I considered the effects of polymers on the inverse energy cascade, showing that for large enough elasticity it can be completely suppressed by polymer feedback.

Appendix A

Lagrangian code for polymer dynamics

The numerical integration of viscoelastic models is rather challenging, since it is necessary to solve at the same time the modified Navier-stokes equation and the equation for the components of the conformation tensor. As a consequence, the CPU time and memory required by standard pseudospectral simulation of the viscoelastic model are about 5 times larger in 2D than the Newtonian case with the same resolution.

Moreover the linear viscoelastic model Oldroyd-B model allows for infinite elongation, and consequently the stretching exerted by velocity gradients can generate singularities in the conformation tensor. Indeed the eigenvectors of the conformation tensor tend to align in the directions of the Lyapunov vectors, and the eigenvalues can experience exponential growth, leading to the formation of sharp fronts with diverging gradients which are involved in the feedback on the velocity fields. The consequence is a sudden rise of numerical instabilities in the simulations, which typically blow up after a short time.

Another critical aspect is the fact that the conformation tensor must remain positive definite because of its physical meaning: its eigenvalues represent the square axes of the inertia tensor. Since the smaller eigenvalues can became arbitrarily close to zero, infinitesimal errors arising from the integration scheme can bring it below zero, producing a new source of numerical instabilities.

The adoption of finite extensibility of the polymer is not sufficient to solve these problems. One of the standard trick to avoid the formation of singularities in viscoelastic simulations is the addiction of an artificial diffusivity in the equation for the conformation tensor [72]. In this way the sharp gradients are regularized, and simulations can be performed. Nevertheless

this solution is not completely satisfactory, because the values of diffusivity that must be used are unrealistic, especially for passive simulations where the formation of sharp gradients is not prevented by feedback of polymers.

In order to perform accurate simulation of the passive limit for Oldroyd-B model we developed a numerical code which explicitly preserves the positive definiteness of the conformation tensor.

In two dimension the symmetric conformation tensor reads:

$$\boldsymbol{\sigma} = \begin{pmatrix} \sigma_{xx} & \sigma_{xy} \\ \sigma_{xy} & \sigma_{yy} \end{pmatrix} \tag{A.1}$$

Its evolution along a Lagrangian trajectory $\boldsymbol{X}(s)$ is determined by the equation

$$\dot{\boldsymbol{\sigma}}(\boldsymbol{X}(t)) = (\boldsymbol{\nabla u})^T \cdot \boldsymbol{\sigma} + \boldsymbol{\sigma} \cdot (\boldsymbol{\nabla u}) - \frac{2}{\tau}(\boldsymbol{\sigma} - \mathbf{1}) \, . \tag{A.2}$$

The velocity gradients $(\boldsymbol{\nabla u})_{ij} = \partial_i u_j$ are valued along the Lagrangian trajectory

$$\dot{\boldsymbol{X}}(s) = \boldsymbol{v}(\boldsymbol{X}(s), s) \, , \tag{A.3}$$

by means of standard second order interpolation of the velocity gradient fields obtained by parallel integration of Navier-Stokes equation, in which the polymer feedback has been turned off.

Let us write the evolution of the three components of the conformation tensor along the Lagrangian trajectory in the vectorial form:

$$\dot{\bar{\boldsymbol{\sigma}}} = \boldsymbol{A}\bar{\boldsymbol{\sigma}} + \bar{\boldsymbol{b}} \tag{A.4}$$

with:

$$\bar{\boldsymbol{\sigma}} = \begin{pmatrix} \sigma_{xx} \\ \sigma_{xy} \\ \sigma_{yy} \end{pmatrix} \tag{A.5}$$

$$\bar{\boldsymbol{b}} = \begin{pmatrix} \frac{2}{\tau} \\ 0 \\ \frac{2}{\tau} \end{pmatrix} \tag{A.6}$$

$$\boldsymbol{A} = \begin{pmatrix} 2\partial_x u_x - \frac{2}{\tau} & 2\partial_y u_x & 0 \\ \partial_x u_y & -\frac{2}{\tau} & \partial_y u_x \\ 0 & 2\partial_x u_y & 2\partial_y u_y - \frac{2}{\tau} \end{pmatrix} \tag{A.7}$$

The discrete evolution at first order accuracy in dt can be obtained as:

$$\bar{\boldsymbol{\sigma}}(t + dt) = e^{\boldsymbol{A}(t)dt} \left(\bar{\boldsymbol{\sigma}}(t) + \boldsymbol{A}^{-1}(t)\bar{\boldsymbol{b}} \right) - \boldsymbol{A}^{-1}(t)\bar{\boldsymbol{b}} \tag{A.8}$$

which explicitly preserves the positive definiteness of the conformation tensor. This procedure can be immediately extended to higher order integration schemes. In our simulation we have adopted a Runge Kutta second order scheme which requires a further evaluation of the matrix $\boldsymbol{A}$ in the mid-point $\boldsymbol{X}(t + dt/2)$.

To obtain an explicit form for the exponential matrix $e^{\boldsymbol{A}(t)dt}$ it is necessary to distinguish the case in which the predominant effect of velocity gradients on the conformation tensor is either the stretching or the rotation, depending on the sign of the determinant of velocity gradients:

$$\det(\boldsymbol{\nabla u}) = \partial_x u_x \partial_y u_y - \partial_y u_x \partial_x u_y \tag{A.9}$$

Indeed since the trace of the velocity gradients tensor vanishes because of incompressibility, the two eigenvalues must be opposite and either real, when $\det(\boldsymbol{\nabla u}) < 0$ or pure imaginary when $\det(\boldsymbol{\nabla u}) > 0$. In the first case, which corresponds to regions of intense stretching, the linearized flow is hyperbolic, while the second case corresponds to elliptic regions where rotation is the predominant effect.

Introducing the *Weiss function* Q defined as [81]

$$Q = S^2 - \omega^2 = -4 \det(\boldsymbol{\nabla u}) \tag{A.10}$$

where ω is the vorticity and

$$S^2 = \frac{1}{2} \sum_{i,j=1,2} \left(\frac{\partial u_i}{\partial x_j} + \frac{\partial u_j}{\partial x_i} \right)^2 \tag{A.11}$$

the three cases can be distinguished according to the sign of Q:

hyperbolic regions where $Q > 0$

elliptic regions where $Q < 0$

neutral regions where $Q = 0$

A.0.1 Hyperbolic regions

In hyperbolic regions, where the predominant effect of velocity gradients is the stretching, using the incompressibility $\partial_x u_x = -\partial_y u_y$ and defining

$$\lambda = \sqrt{-\det(\boldsymbol{\nabla u})} \tag{A.12}$$

the matrix $\boldsymbol{A}$ can be diagonalized as

$$\boldsymbol{A} = \boldsymbol{N D N}^{-1} \tag{A.13}$$

where

$$\boldsymbol{D} = \begin{pmatrix} -\frac{2}{\tau} + 2\lambda & 0 & 0 \\ 0 & -\frac{2}{\tau} & 0 \\ 0 & 0 & -\frac{2}{\tau} - 2\lambda \end{pmatrix} \tag{A.14}$$

and the eigenvectors matrix $\boldsymbol{N} = (\bar{u}_1, \bar{u}_2, \bar{u}_3)$ is

$$\boldsymbol{N} = \begin{pmatrix} \partial_y u_x(\partial_x u_x + \lambda) & \partial_y u_x \partial_x u_x & \partial_y u_x(\partial_x u_x - \lambda) \\ \partial_x u_x \partial_y u_y + \lambda^2 & \partial_x u_x \partial_y u_y & \partial_x u_x \partial_y u_y + \lambda^2 \\ \partial_x u_y(\partial_y u_y + \lambda) & \partial_x u_y \partial_y u_y & \partial_x u_y(\partial_y u_y - \lambda) \end{pmatrix} \tag{A.15}$$

The exponential matrix is thus valued as

$$e^{\boldsymbol{A}(t)dt} = e^{-\frac{2}{\tau}dt} \boldsymbol{N} \begin{pmatrix} e^{2\lambda dt} & 0 & 0 \\ 0 & 1 & 0 \\ 0 & 0 & e^{-2\lambda dt} \end{pmatrix} \boldsymbol{N}^{-1} \tag{A.16}$$

A.0.2 Elliptic regions

In elliptic regions, using again the incompressibility $\partial_y u_y = -\partial_x u_x$ and defining

$$\theta = \sqrt{\det(\boldsymbol{\nabla u})} \tag{A.17}$$

the matrix $\boldsymbol{A}$ can be decomposed in a diagonal part and a pure rotational part:

$$\boldsymbol{A} = \boldsymbol{N}(\boldsymbol{D} + \boldsymbol{R})\boldsymbol{N}^{-1} \tag{A.18}$$

where

$$\boldsymbol{D} + \boldsymbol{R} = \begin{pmatrix} -\frac{2}{\tau} & 0 & -2\theta \\ 0 & -\frac{2}{\tau} & 0 \\ 2\theta & 0 & -\frac{2}{\tau} \end{pmatrix} \tag{A.19}$$

The eigenvectors matrix $\boldsymbol{N} = (\bar{u}_1, \bar{u}_2, \bar{u}_3)$ is

$$\boldsymbol{N} = \begin{pmatrix} \partial_y u_x(\partial_x u_x + \theta) & \partial_y u_x \partial_x u_x & \partial_y u_x(\partial_x u_x - \theta) \\ \partial_x u_x \partial_y u_y - \theta^2 & \partial_x u_x \partial_y u_y & \partial_x u_x \partial_y u_y - \theta^2 \\ \partial_x u_y(\partial_y u_y + \theta) & \partial_x u_y \partial_y u_y & \partial_x u_y(\partial_y u_y - \theta) \end{pmatrix} \tag{A.20}$$

and the exponential matrix reads

$$e^{\boldsymbol{A}(t)dt} = e^{-\frac{2}{\tau}dt} \boldsymbol{N} \begin{pmatrix} \cos(2\theta dt) & 0 & -\sin(2\theta dt) \\ 0 & 1 & 0 \\ \sin(2\theta dt) & 0 & \cos(2\theta dt) \end{pmatrix} \boldsymbol{N}^{-1} \tag{A.21}$$

A.0.3 Neutral regions

In regions where the relative intensity of rotation and stretching are equal (e.g. in the case of shear flows) the determinant of the velocity gradients vanishes. In this case the matrix $\boldsymbol{A}$ has a single eigenvector with multiplicity 3 and its exponential can be evaluated as:

$$e^{\boldsymbol{A}(t)dt} = e^{-\frac{2}{\tau}dt}\left(\mathbf{1} + (\boldsymbol{A} + \frac{2}{\tau}\mathbf{1})dt + \frac{1}{2}(\boldsymbol{A} + \frac{2}{\tau}\mathbf{1})^2 dt^2\right) \tag{A.22}$$

This numerical scheme allows to perform accurate simulations of the passive limit of Oldroyd-B model, which are non achievable with standard Eulerian codes.

In principle it is possible to include the feedback of polymers on the velocity field, by reconstructing at each time step the Eulerian conformation tensor field on a regular grid from the Lagrangian values obtained along n simultaneously integrated fluid trajectories.

Unfortunately this mixed Eulerian-Lagrangian code does not solve the problem of numerical instabilities of Oldroyd-B model, because Lagrangian particles with different values of the conformation tensor are transported arbitrarily close to each other during the simulation, and thus the Eulerian field reconstructed from the Lagrangian one still have diverging gradients, which are involved in the feedback and cannot be resolved by the Eulerian part of the code.

Bibliography

[1] A. S. Monin, A. M. Yaglom, *Statistical Fluids Mechanics*, The Mit Press (1979).

[2] A. S. Monin, A. M. Yaglom, *Statistical Fluids Mechanics II*, The Mit Press (1981).

[3] G. K. Batchelor, *The theory of homogeneous turbulence*, Cambridge University Press (1953).

[4] G. K. Batchelor, *An introduction to fluid dynamics*, Cambridge University Press (1967).

[5] U. Frisch, *Turbulence*, Cambridge University Press (1995).

[6] M. Lesieur, *Turbulence in Fluids*, Kluwer Academic Publishers (1997).

[7] K. R. Sreenivasan, Phys. Fluids **27**, 1048-1051 (1984).

[8] S. A. Orszag, J. Fluid Mech. **41**, 363-386 (1970).

[9] L. F. Richardson, *Weather Prediction by Numerical Process*, Cambridge University Press (1922).

[10] H. L. Grant, R. W. Stewart and A. Moilliet, J. Fluid Mech. **12**, 241-263 (1962).

[11] F. Anselmet, Y. Gagne, E. J. Hopfinger, R. A. Antonia, J. Fluid Mech. **140**, 63-89 (1984).

[12] B. Castaing, Y. Gagne, E. J. Hopfinger, Physica D, **46**, 177-200 (1990).

[13] J. Herweijer, W. van de Water Phys. Rev. Lett. **74**, 4651 (1995).

[14] R. Benzi, G. Paladin, G. Parisi, A. Vulpiani, J. Phys. A **17**, 3521-3531 (1984).

[15] D. Biskamp, *Nonlinear Magnetohydrodynamics*, Cambridge University Press (1993).

[16] R. H. Kraichnan, Phys. Fluids **10** 1417-1423 (1967).

[17] G. K. Batchelor, Phys. Fluids Suppl. **12** 233-239 (1969).

[18] R. H. Kraichnan, D. Montgomery, Rep. Prog. Phys **43** 548-619 (1980).

[19] M. Chertkov, Phys. of Fluids, **10**, 3017 (1998).

[20] L. M. Smith, V. Yakhot, Phys. Rev. Lett. **71**, 352-355 (1993).

[21] G. Boffetta, A. Celani, M. Vergassola, Phys. Rev. E **61** R29 (2000).

[22] P. Tabeling, S. Burkhart, O. Cardoso, H. Willaime Phys. Rev. Lett. **67** 3772-3775 (1991).

[23] J. C. McWilliams, J. Fluid Mech. **146** 21-43 (1984).

[24] C. Basdevant, B. Legras, R. Sadourny, M. Beland, J. Atmos. Sci. **38**, 2305-2326 (1981).

[25] J. C. McWilliams, J. Fluid Mech. **219** 361-385 (1990).

[26] G. F. Carvevale, J. C. McWilliams, Y. Pomeau, J. B. Weiss, W. R. Young, Phys. Rev. Lett. **66** 2735-2738 (1991).

[27] R. Salmon, *Geophysical Fluid Dynamics*, Oxford University Press, New York, USA (1998).

[28] J. Sommeria, J. Fluid Mech. **170**, 139 (1986).

[29] M. Rivera and X. L. Wu, Phys. Rev. Lett. **85**, 976 (2000).

[30] K. Nam, E. Ott, T.M. Antonsen, P.N. Guzdar, Phys. Rev. Lett. **84**, 5134 (2000).

[31] J. Paret, D. Marteau, O. Paireau and P. Tabeling, Phys. Fluids **9**, 3102 (1997).

[32] J. Paret, M. C. Jullien and P. Tabeling, Phis. Rev. Lett. **83**, 3418 (1999).

[33] D. Bernard, Europhys. Lett. **50**, 333 (2000).

[34] S.'Corrsin, J. Fluid Mech. **11**, 407 (1961).

[35] K. Nam, T. M. Antonsen, P. N. Guzdar, E. Ott, Phys. Rev. Lett. **83**, 3426 (1999).

[36] Z. Neufeld, C. Lopez, E. Hernandez-Garcia, T. Tel, Phys. Rev. E.,**61**, 3857 (2000).

[37] M. R. Maxey, J. Riley, Phys. Fluids, **26**, 883-889 (1983).

[38] E. Ott, *Chaos in Dynamical Systems*, Cambridge University Press, Cambridge, UK (1993).

[39] T. Bohr, M. H. Jensen, G. Paladin and A. Vulpiani, *Dynamical Systems Approach to Turbulence*, Cambridge University Press, Cambridge, UK (1998).

[40] G. Falovich, K. Gawedzki, M. Vergassola, Rev. Mod. Phys. **73**, 913-975 (2001).

[41] M. J. Sewell, *Maximum and Minimum Principles*, Cambridge University Press (1987).

[42] R. H. Nadolink and W. W. Haigh, ASME Appl. Mech. Rev. **48**, 351 (1995).

[43] B. A. Toms, Proceedings of the International Congress of rheology Amsterdam, Vol. 2, 0.135-141 (North Holland 1949).

[44] P. S. Virk, AIChE j. **21** 625-656 (1975).

[45] P. J. Flory, *Statistical Mechanics of Chain Molecules* (Hanser Publisher, New York, 1989).

[46] T. T. Perkins, D. E. Smith, and S. Chu, Science **264**, 819 (1994).

[47] S.R. Quake, H. Babcock, and S. Chu, Nature **388**, 151 (1997).

[48] R. Kubo, M. Toda and N. Hashitsume, *Statistical Physics 2* (Springer, Berlin 1985).

[49] B. H. Zimm, J. Chem. Phys. **2**4, 269-278, (1956).

[50] M. Doi, S. F. Edwards, *The theory of polymer dynamics*, Clarendon Press, Oxford (1986).

[51] J. L. Lumley, J. Polym. Sci., Part D: Macromol.Rev. **7**, 263 (1973).

[52] E. Balkovsky, A. Fouxon, and V. Lebedev, Phys. Rev. Lett. **84**, 4765 (2000)

[53] J. L. Lumley, Symp Math, **9**. 315 (1972).

[54] E. Balkovsky, A. Fouxon, and V. Lebedev, Phys. Rev. E, **64**, 056301 (2001)

[55] G. Boffetta, A. Celani, S. Musacchio Phys. Rev. Lett. **91**, 034501 (2003)

[56] E. J. Hinch, Phys. Fluids **20**, S22 (1977).

[57] R. B. Bird, C. F. Curtiss, R. C. Armstrong, and O. Hassager, *Dynamics of polymeric fluids* Vol.2, Wiley, New York (1987).

[58] M. Tabor, and P. G. de Gennes, Europhys. Lett. **2**, 519-522 (1986).

[59] K. R. Sreenivasan and C. M. White, J.Fluid Mech. **409**, 149-164 (2000).

[60] R. Sureshkumar, A. N. Beris, and R. A. Handler, Phys. Fluids **9**, 743 (1997).

[61] E. De Angelis, C. M. Casciola, R. Benzi, and R. Piva, Phys. Fluids, submitted (2002); see also http://arxiv.org/abs/nlin.CD/0208016.

[62] E. De Angelis, C. M. Casciola, V. S.L'vov, and R. Piva, Phys. Rev. E **67**, 056312 (2003).

[63] G. Boffetta, A. Celani and A. Mazzino, http://arxiv/abs/nlin.CD/0309036 (2003).

[64] R. Benzi, E. De Angelis, R. Govindarajan, I. Procaccia, Phys. Rev. E **68** 016308 (2003).

[65] A. Groisman and V. Steinberg, Nature **405**, 53 (2000).

[66] A. Groisman and V. Steinberg, Nature **410**, 905 (2001).

[67] J. Lumley, Annu. Rev. Fluid Mech. **1**, 367 (1969).

[68] Y. Amarouchene and H. Kellay, Phys. Rev. Lett. **89**, 104502 (2002).

[69] J. R. Cressman, Q. Bailey, and W. Goldburg, Phys. Fluids **13**, 867 (2001).

[70] O. Paireau and D. Bonn, Phys. Rev. Lett. **83**, 5591 (1999).

[71] G. Boffetta, A. Celani, S. Musacchio, and M. Vergassola, Phys. Rev. E **66**, 026304 (2002).

[72] R. Sureshkumar and A. N. Beris, J. Non-Newtonian Fluid Mech. **60**, 53 (1995).

[73] G. Paladin, and A. Vulpiani , Phys. Rep. **156**, 147 (1987).

[74] R. H. Kraichnan and D. Montgomery, Rep. Prog. Phys. **43**, 547 (1980).

[75] M. Chertkov, Phys. Rev. Lett. **84**, 4761 (2000).

[76] P. Halin, G. Lielens, R. Keunings, and V. Legat, J. Non-Newtonian Fluid Mech. **79**, 387 (1998).

[77] B. Eckhardt, J. Kronjäger, and J. Schumacher, Comp. Phys. Comm. **147**, 538 (2002).

[78] J.-L. Thiffeault, Phys. Lett. A **308**, 445-450 (2003).

[79] G. Falkovich and V. Lebedev, Phys. Rev. Lett **79**, 4159 (1997).

[80] A. Celani, M. Cencini, A. Mazzino, M. Vergassola, Phys. Rev. Lett. **89**, 234502 (2002).

[81] J. Weiss, La Jolla Instutute preprint LJ1-TN-81-121 (1981).

Acknowledgments

I would like to thank my supervisor, G. Boffetta for his friendship and for the huge support he has given me during my degree thesis and my Ph.D.

I would also like to thank A. Celani, M. Vergassola, A. Vulpiani, A. Mazzino, M. Cencini and F. De Lillo for all the work they have done with me during these years.

I am gratefull to everybody at the "Istituto di Scienze dell'Atmosfera e del Clima e del Clima", Torino, for their kind hospitality.